FAKULTÄT FÜR MEDIZIN DER TECHNISCHEN UNIVERSITÄT MÜNCHEN

DEUTSCHES ZENTRUM FÜR NEURODEGENERATIVE ERKRANKUNGEN E.V. (DZNE)

siRNA AS THERAPEUTIC STRATEGY FOR A NEURODEGENERATIVE TAUOPATHY

HONG XU

Vollständiger Abdruck der von der Fakultät für Medizin der Technischen Universität München zur Erlangung des akademischen Grades eines

Doktors der Naturwissenschaften (Dr.rer.nat.)

genehmigten Dissertation.

Vorsitzender: Univ.-Prof. Dr. Thomas Misgeld

Prüfer der Dissertation:

1. Univ.-Prof. Dr. Günter Höglinger
2. Univ.-Prof. Dr. Michael Schemann

Die Dissertation wurde am 23.12.2014 bei der Technischen Universität München eingereicht und durch die Fakultät für Medizin am 11.03.2015 angenommen.

To my wife and our parents

0 INDEX

A. TABLE OF CONTENTS

0 Index 1
1 Abstract 5
2 Introduction 6
2.1 Microtubule-associated Protein Tau 6
2.1.1 The Gene 6
2.1.2 The Protein 7
2.1.3 Post-translational Modifications 8
2.1.4 Tau Function 11
2.2 Major Tauopathies 11
2.2.1 Alzheimer's Disease 12
2.2.2 Corticobasal Degeneration 12
2.2.3 Pick's Disease 13
2.2.4 Progressive Supranuclear Palsy 13
2.3 Tau as Therapeutic Target for Tauopathies 13
2.4 P301S Mouse Model 14
2.4.1 Tauopathy in P301S Mouse 14
2.4.2 Behavioral Characteristics 16
2.5 RNA Interference and Small Interfering RNAs 16
3 Aim of Study 18
4 Material and Methods 19
4.1 Animals 19

4.2 Behavioral Baseline Tests 19
4.2.1 Rotarod 19
4.2.2 Novel Open Field 19
4.2.3 Morris Water Maze 20
4.3 Tau Pathology in P301S Mice 20
4.3.1 Immunohistology 20
4.3.2 Immunoblot 21
4.3.3 Golgi Staining and Dendritic Spine Quantification 21
4.4 Tau Suppression *in Vitro* 22
4.4.1 Primary Cortical Neuron Culture 22
4.4.2 LUHMES Cell Cultures 22
4.4.3 siRNA Delivery 22
4.4.4 Cell Toxicity Test 22
4.4.5 Semi-quantitative Reverse Transcription-PCR (RT-PCR) 23
4.4.6 Quantitative PCR (qPCR) 23
4.4.7 Immunoblot 23
4.5 Tau Suppression *In vivo* 24
4.5.1 siRNAs Delivery 24
4.5.2 Stereology 24
4.5.3 Suppression Area Calculation 25
4.5.4 TUNEL Assay 25
4.6 Optical Density Measurement 25
4.7 Statistics 25
5 Results 27
5.1 Aim One: 27

5.2 Aim Two: 28
6 Discussion 29
6.1 Aim One 29
6.2 Aim Two 31
6.3 Conclusion 33
7 Acknowledgement 34
8 Summary of Contributions 35
9 References 36
10 Appendix 44
10.1 Experimental Materials 44
10.1.1 Chemicals and Kits 44
10.1.2 Buffers and Solutions 47
10.1.3 Primer for RT-PCR 53
10.1.4 Primer for qPCR 53
10.1.5 Antibodies 55
10.1.6 Devices and Software 56
10.2 Curriculum Vitea 59
10.3 List of publications 61

B. TABLES

Table 1.1. Chemicals, solutions and materials 44

Table 1.2. Buffers and solutions 47

Table 1.3. Primers and programs for RT-PCR 53

Table 1.4. Primers for qPCR 53

Table 1.5. Accell siRNAs 54

Table 1.6. First antibodies 55

Table 1.7. Secondary antibodies 56

Table 1.8. Software 56

Table 1.9. Devices 57

C. FIGURES

Figure 1.1. Alternative splicing of *MAPT* gene and isoforms of tau. 7

Figure 1.2. Hypothetical secondary structure of 4R tau. 8

Figure 1.3. Phosphorylation sites of tau 9

Figure 1.4. Tau protein in the brain and spinal cord of 5 month-old P301S mouse. 15

Figure 1.5. Schematic structure of siRNA duplex 16

Figure 1.6. Schematic pathway of siRNA guided RNAi. 17

1 ABSTRACT

Tauopathies are neurodegenerative disorders characterized by the intraneural aggregation of the microtubule-associated protein tau. Reducing tau expression might be a promising way to cure human tauopathies. RNA interference, induced by small interfering RNAs, is an endogenous mechanism to silence the expression of specific genes. So far, there is very little experience using the siRNA method in the living brain.

The purpose of this study was firstly, to identify the behavioral deficits of transgenic mice overexpressing human P301S-mutated tau, secondly, to correlate the behavioral deficits with the cerebral tau pathology using biochemical and immunohistological methods, and thirdly to suppress the transgenic tau expression *in vivo* in an attempt to reverse the tau pathology.

We found memory deficits to precede the onset of motor dysfunction in the P301S-tau mice. Onset of the memory deficits coincided with the appearance of conformationally changed, S202-phosphorylated tau and reduced dendritic spine density in the hippocampus in the absence of neuronal cell loss. In addition, one commercially available siRNA against the tau gene effectively suppressed tau expression *in vitro* and *in vivo* with no need of a delivery agent. After single injection, the siRNA showed moderate distribution in the hippocampus of mice without any disturbance to other regions of the mouse brain. Analysis of NeuN, GFAP, Iba-1 and MHC II antibodies indicated neither neurotoxicity nor neuroinflammation. No sign of apoptosis was found in the neurons containing siRNA.

The data suggest that siRNAs may be a useful therapeutic tool for treating tauopathies.

2 INTRODUCTION

The microtubule associated protein tau (*MAPT*) gene was first described in 1975 by Marc Kirshner. It is located on chromosome 17 q21-22 (1, 2) and encodes the tau protein. Abnormalities of tau have been linked to the pathology of several neurodegenerative diseases, jointly termed tauopathies.

2.1 Microtubule-associated Protein Tau

Tau is expressed in the central nervous system and participates in the stabilization and assembly of microtubules (3). Due to the association of tau and tauopathies, tau was intensively studied in the last decades. However, the full physiological function of tau remains to be disclosed.

2.1.1 **The Gene**

The *MAPT* gene contains 16 exons in total, of which 11 are constitutive to the protein (E1, E2, E3, E4, E5, E7, E9, E10, E11, E12, and E13) (4). Various splicing variants of *MAPT* are found before transcription, of which 6 are usually present in the adult human central nervous system, leading to 6 isoforms of the tau protein. The differences of these 6 isoforms lie in the alternative splicing of exons 2, 3 and 10, encoding 29-aminoacids or 31-amino acids, respectively. Among them, the appearance of exon 3 is always accompanied by exon 2, leading to the following combinations: 2+3+10+, 2+3+10-, 2+3-10+, 2+3-10-, 2-3-10+, and 2-3-10-.

The *MAPT* gene exists in 2 haplotypes, haplotype 1 (H1) and haplotype 2 (H2). H1, with direct orientation was functionally associated with higher transcriptional activity of the *MAPT* gene, which was further linked to higher risk of tauopathies. H2 has an inverse orientation and is mainly found in European populations, which is much more conserved, showing less recombination compared to H1 (5).

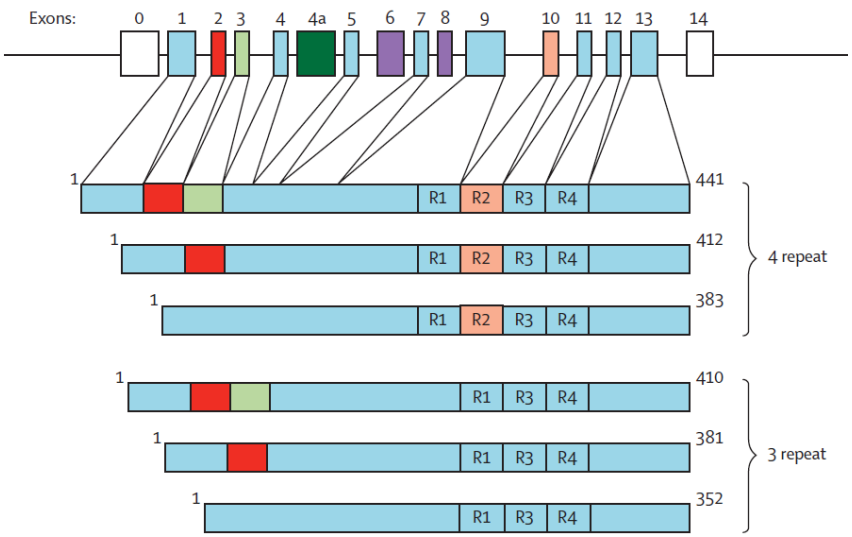

Figure 1.1. Alternative splicing of the *MAPT* gene and isoforms of tau protein. The human *MAPT* gene is more than 100kb large and consists of 16 exons. In the central nervous system only exons 1, 2, 3, 4, 5, 7, 9, 10, 11, 12 and 13 are transcribed into six different isoforms of tau protein. Due to the difference at the tandem repeated domain (microtubule-binding domain) they are sub-divided into 4 repeat (4R) and 3 repeat (3R) groups (6).

2.1.2 **The Protein**

Six splicing variants result in 6 isoforms of tau, which are, depending on the presence or absence of exon 10 and the number of tandem repeats (microtubule-binding domains), further divided into 3 repeat (3R) and 4 repeat (4R) groups (Fig. 1.1). In the human fetal brain, only the shortest 3R tau isoform (2-3-10-) is expressed. In contrast, six isoforms of tau are present in the adult brain ranging from 352 to 441 amino acids (60 -74 kDa).

Tau starts with the acidic N-terminus (exons 1-5), followed by a proline-rich region (exon 7 and 9), and ends with the C-terminus (exon 13). The functionally relevant microtubule-binding domain is encoded by exons 9-12.

Tau is a soluble protein exhibiting highly dynamic conformations according to its physiological and functional requirement (7, 8). Various secondary structures of tau have been described. Generally, tau starts as an unfolded protein after transcription (9). The protein quickly undergoes post-transcriptional modifications, such as phosphorylation, in

in order to form the secondary structures. A short alpha-helical structure was reported in the microtubule-binding domain (Thr245-Ser324) after phosphorylation (10). In addition, a so-called paperclip structure was discovered in the same region, where the C-terminus of tau turns over to interact with the microtubule-binding domains and the N-terminus overlaps with the C-terminus (11) (Fig. 1.2). Such a dynamic pattern of tau conformation indicates multiple functions in accordance with the complex activity of microtubules.

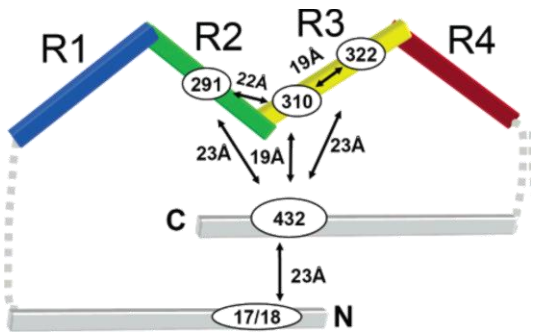

Figure 1.2. Hypothetical secondary structure of 4R tau. The residues 17/18 on the N-terminus of tau overlap with the residue 432 at the C-terminus. Four tandem repeats (R1, R2, R3, and R4) are fully exposed to microtubules. The structure appears to be a paperclip-like shape (11).

2.1.3 **Post-translational Modifications**

In order to fulfill the complex activities of microtubules, tau needs to regulate its activity and conformation. Post-translational modifications of tau, including truncation, acetylation, phosphorylation, glycosylation, ubiquitination, polyamination, sumoylation, and others play key roles in such regulations

2.1.3.1 Phosphorylation

The most intensively studied post-translational modification of tau is phosphorylation, which is associated with several neurodegenerative diseases. The phosphorylation sites of tau mainly locate on serine, threonine and tyrosine residues. In total, 85 phosphorylation sites were reported, of which more than half are located on serines (45 serines, 35 threonines and 5 tyrosines) (Fig. 1.3) (12). Normally, the phosphorylated sites of tau are

equally distributed throughout the whole protein with an average ratio of 2-3 moles phosphates per mole of tau (13).

In general, phosphorylation decreases the affinity of tau to microtubules. The phosphorylation in the tandem repeat domains, especially at S262 and S356, detaches tau from microtubules (14), whereas phosphorylation at S214 and T231 of tau only decreases the binding ability of tau, leading to the instability of the neuronal cytoskeleton (15). The change of tau phosphorylation is also involved in regulation of synaptic plasticity (16).

Kinases and phosphatases regulate the phosphorylation of tau. Up to now more than 20 kinases were identified as involved in the phosphorylation of tau, such as glycogen synthase kinase 3 beta (GSK3β), cyclin-dependent kinase 5 (CDK5), protein kinase A (PKA), Ca2+/calmodulin-dependent protein kinase II (CaMKII). Abnormal activation of the kinases leads to hyperphosphorylation of tau and ultimately tau pathologies. On the other hand, inhibition of tau kinases ameliorate tau pathologies by down-regulation of the phosphorylation. Infusion of lithium, an inhibitor of GSK3β, reversed the behavioral deficits in the rodent tauopathy models (17, 18). In addition, activation of phosphatases attenuates the phosphorylation (19).

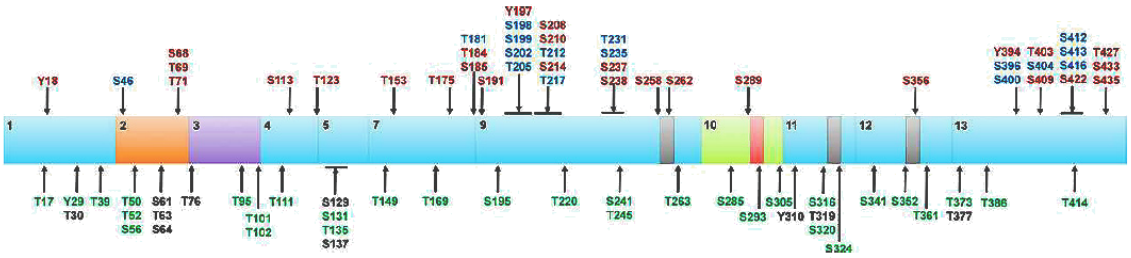

Figure 1.3. Phosphorylation sites of tau. Different colors indicate different phosphorylation situations: green represents phosphorylation sites in the normal brain; brown represents sites found in the Alzheimer's disease brains; blue represents sites found both in the normal and the Alzheimer's disease brain; black represents putative phosphorylation sites (20).

2.1.3.2 Other Modifications

Glycosylation refers to the process that enzymatically attaches glycans to proteins. Eleven putative glycosylation sites of tau were described previously (21). Depending on

the attached sites of oligosaccharides, glycosylation of tau was sub-divided into two types: N-glycosylation (on serine) and O-glycosylation (on threonine). Glycosylation of tau shows a negative effect to the phosphorylation of tau (22, 23), which is believed to be caused by the competitive occupancy of sites on tau. Abnormal glycosylation of tau was previously reported in AD patients' brains (24). The inhibition of O-glycosylation hydrolyzing enzyme (O-GlcNAcase, OGA) can enhance the glycosylation of tau and further reduce tau phosphorylation, tau aggregation and slow neurodegeneration (25, 26). However, an acute dose of an OGA inhibitor showed a differential effect on tau phosphorylation on different sites (27).

Non-enzymatic glycosylation, or glycation, is also found on tau protein. It is usually believed to be an irreversible protein modification caused by aging, which prohibits the protein from normal degradation. Therefore, it is also considered as a detrimental process to the target proteins since glycation disrupts normal protein functions, sensitizes them to oxidative stress and increases free radicals (28). In the case of tau, glycation decreases the affinity of tau to microtubules and enhances its aggregation; indirectly, the increased sensitivity to free radicals up-regulates tau phosphorylation and further causes hyperphosphorylation (29).

Ubiquitination binds ubiquitin to the protein, which regulates degradation of proteins by the ubiquitin proteasome system (UPS). Ubiquitination of tau was observed during the formation of paired helical filaments (PHFs) and increased along with the aggregation process (30, 31). The ubiquitination sites on tau mainly locate in the microtubule-binding domain at K254, K311 and K353 (32). Increased ubiquitination of tau was found in the Alzheimer's disease (AD) patient (31). Experimentally, up-regulation of ubiquitination caused by lithium treatment attenuated tau pathology in a mouse model (33).

Prolyl-isomerization changes the *cis/trans* isomerism of disulfide bonds in tau. Thus, prolyl-isomerization regulates the conformation of tau. Moreover, change of conformation affects the exposure of phosphorylation sites on tau to phosphatase (34) and, further the affinity of tau to microtubule. Only one prolyl-isomerization site on tau was reported, located at T231. The same site is also an important phosphorylation site regulated by peptidyl-prolyl *cis/trans* isomerase NIMA-interacting-1 (Pin1) (35) .

Polyamination is regulated by trans-glutaminases, when an acyl is transferred from a glutamine (acyl donor) to a lysine (acyl acceptor). Tau has in total eight acceptor sites and ten donor sites (36). The trans-glutaminase was shown to be over-activated in AD patient brains (37). Furthermore, increased polyamination of tau was found in the neuronal filament tangles (NFT) composed of tau aggregates (38). In addition, the polyamination of tau is associated with the formation and stabilization of NFT in a P301L mutated-tau mouse model (39).

Nitration adds nitrogen dioxide on tyrosine residues. Tau has four nitration sites that are also phosphorylation sites. *In vitro* and *in vivo* studies showed that the nitration antagonizes tau aggregation (40, 41).

2.1.4 **Tau Function**

Tau binds to microtubules with the microtubule-binding domain at the C-terminus (1, 42). It stabilizes them and facilitates their assembly. Micro-injected tau binds to cytoplasmic microtubules and stabilizes them against the depolymerization induced by nocadazole in fibroblasts (43).

The binding affinity of tau depends on the number of repeat regions in the microtubule-binding domain and the level of post-translational modifications. 4R tau has one more repeat region compared with 3R tau and exhibits higher binding affinity to microtubules (44). Phosphorylation, especially on the repeat regions, reduces the affinity of tau. In normal neurons, the ratio of 3R: 4R tau in the adult brain is close to 1:1 in a homeostatic balance (45). Tau usually is located in axons where microtubules are very dense and compact.

The function of the N-terminal projection domain is not fully understood. However, it may function as a spacer to maintain order between the microtubules.

2.2 Major Tauopathies

The term tauopathy refers to a series of neurodegenerative diseases, which are commonly characterized by the intraneuronal aggregation of tau protein. They include, but are not limited to Alzheimer's disease (AD), Pick's disease (PiD), progressive supranuclear palsy

(PSP), frontotemporal dementia and parkinsonism linked to chromosome 17 with tau pathology (FTDP-17-tau) (6). Although tauopathies exhibit distinct clinical features, from cognitive impairments to behavioral or motor dysfunctions, they share similar pathological abnormalities of tau. Form and morphology of pathological tau inclusions may vary from one taupathy to another.

2.2.1 **Alzheimer's Disease**

In 1907, the link between the presence of abnormal protein inclusions and dementia was simultaneously described by Alois Alzheimer in Munich and Oskar Fisher in Prague. Both of them described abundance of argyrophilic extracellular plaques (β-amyloid deposits) and intracellular neurofibrillary tangles (tau deposits) in the cerebral cortex of patients (46). The disease was named after Alzheimer later by Emil Kraepelin. In the 1970s, researchers reported that most of the patients with senile dementia had similar pathological changes in their brains to patients with Alzheimer's disease (AD), and the finding consequently led senile dementia to be categorized as AD (47). Nowadays, AD affects 10% of the global population over 65 years old (48). It is considered to be the most common neurodegenerative disease. In AD, neurofibrillary tangles are formed by aggregates of hyperphosphorylated tau consisting of all six isoforms (49). Although the involvement of tau hyperphosphorylation and aggregation in neurotoxicity is still controversial, the abnormality of tau are taken as one pathological hallmark of AD. In addition, changes in tau kinases and phosphatases are also described in Alzheimer's disease. For example, up-regulation of cdk5, one of the major tau kinases (50), and down-regulation of PP2A, a tau phosphatase (51, 52), were reported in AD brains.

2.2.2 **Corticobasal Degeneration**

Corticobasal degeneration (CBD) was first described by Rebeiz in 1967 (53). It is a neurodegenerative disease resulting in neuron loss or depigmentation in the substantia nigra and further impairing the basal ganglia (54). The onset of CBD occurs at around 60 years of age and patients share a profile of motor and motor-associated cortical dysfunctions including Parkinsonism, alien limb syndrome, apraxia and aphasia. Postmortem studies of CBD brains showed ballooned neurons, gliosis and tauopathy (55).

The tau inclusions in CBD brains are found as neuropil threads in gray and white matter and in neurofibrillary tangles (56).

2.2.3 **Pick's Disease**

Pick's disease (PiD) was named after Arnold Pick who firstly described the disease in 1892. PiD causes neurodegeneration predominantly in the frontotemporal lobes. Multiple symptoms of PiD were reported ranging from behavioral changes to cognitive dysfunctions (57). A unique hallmark of PiD is the presence of huge, dark-staining aggregates of tau and ubiquitin in ballooned neurons, called Pick cells (58). The round aggregated tau inclusions within Picks cells, known as Pick bodies, contain only one or two isoforms of hyperphosphorylated 3R tau and can be found in many regions of the brain (59, 60).

2.2.4 **Progressive Supranuclear Palsy**

Progressive supranuclear palsy (PSP) is a rare neurodegenerative disease with an incidence of 6/100000 (61). The disease causes the death of neurons in the cerebral cortex, basal ganglia, cerebellum, brain stem and spinal cord. It results in deficits in balance, movement, change of personality and dementia (62). The pathological hallmark of PSP is the accumulation of tau inclusions in the neural cells. PSP patients show a predominantly 4R tau accumulation in specific brain regions (61). Four risk genes have been identified and associated with the disease, i.e. *MAPT, STX6, EIF2A3,* and *MOBP* (63).

2.3 Tau as Therapeutic Target for Tauopathies

An abnormality of tau function and metabolism is involved in all the tauopathies. Mutations on the *MAPT* gene, conformational changes or hyperphosphorylation of tau are associated with tauopathies, leading to various forms of tau inclusions. For instance, tau forms the filamentous core of the neurofibrillary tangles (NFTs) in AD, but argyrophilic Pick bodies in PiD (6). The presence of tau species also varies in different stages of tauopathies. Very recently, *in vitro* and *in vivo* studies revealed that several tau

species could spread and seed tauopathies in a prion-like manner (64, 65). Reduction of tau by suppressing tau expression with controllable promoters of the *MAPT* gene led to a reversal of behavioral deficits in mouse models (66-68). Besides, tau knockout mice showed no crucial changes compared with wild-type mice (69) indicating high tolerance to tau reduction *in vivo*. Such a tolerance makes the suppression of tau *in vivo* for therapeutic purposes possible. For the development of therapeutic strategies aiming at suppressing endogenous human tau in the central nerve system, high efficiency and safety are strictly needed. Ribonucleic acid interference (RNAi) shows promising potential in this regard. As a tool to induce RNAi, small interfering RNA (siRNA) displayed highly specific suppression with limited off-target effects in previous studies and relatively short half-life *in vivo* (70). Previous studies reported promising effects of therapeutic RNAi in mouse models of neuronal diseases (71, 72). However, limitations of these studies were present, such as the use of viral vectors for siRNA delivery, low delivery efficiency, high neuronal toxicity and inflammatory responses. For tauopathies, a previous study suppressed tau phosphorylation by targeting at the cyclin-dependent kinase 5 (*CDK5*) (73). Nonetheless, directly silencing tau by RNAi had not been attempted so far.

2.4 P301S Mouse Model

The hereditary tauopathy FTDP-17-tau is caused by *MAPT* mutations. It is clinically characterized by behavioral disturbances, cognitive impairment and parkinsonism. The P301S mutation was found in early onset FTDP-17-tau patients (74). For studying the effects of the mutation, P301S mice were generated to overexpress the 0N4R human tau with the P301S mutation controlled by the murine thy1 promoter (75).

2.4.1 **Tauopathy in P301S Mouse**

Abundant hyperphosphorylated tau and tau filaments are found in neurons and neuropils of the P301S mouse brains and spinal cords (Figure 1.4.). Hyperphosphorylated tau co-localizes with activated MAP kinase family members, suggesting a possible tau pathology (75). Ultrastructurally, both tau aggregates are found in the form of half-twisted ribbons (FTDP-17-related) and PHFs (AD-related) (75). About 49% of motor

neuron loss are found in the spinal cord at 6 months of age (75). In summary, the model develops pathological hallmarks similar to human tauopathies (75, 76).

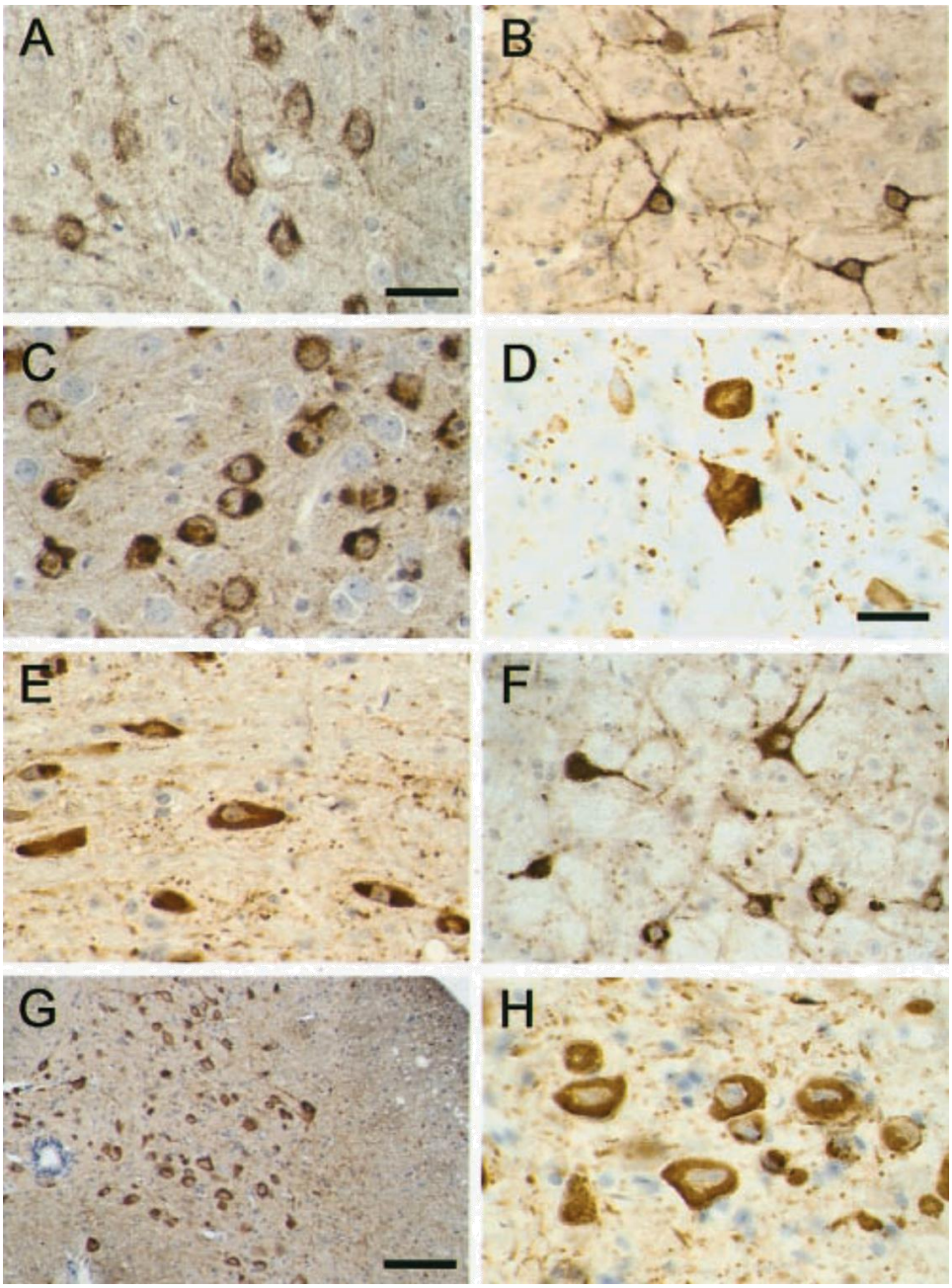

Figure 1.4. Tau protein in the brain and spinal cord of 5 month-old P301S mice. Immunoreactivity of tau (brown) was found in nerve cell bodies in the cerebral cortex (A, B), amygdala (C), dentate nucleus of the cerebellum (D), brainstem (E, F), and spinal cord (G, H). Scale bars: A = 40 µm (A–C, E, F); D = 60 µm (D, H); G = 250 µm (75).

2.4.2 **Behavioral Characteristics**

Behaviorally, P301S pups produced more ultrasound vocalisations than control pups, when they were away from the mother (77). P301S mice showed a decline of the balancing ability starting at 3 months of age (77). The model also showed a decreased exploration behaviour starting at 5 months of age (77). The appearance of sarkosyl-insoluble tau and neuron loss in the anterior horn of the spinal cord of the mouse correlated with the onset of hind limb motor phenotype at 5 months of age (77).

2.5 RNA Interference and Small Interfering RNAs

RNAi is a cellular gene regulation system that digests redundant endogenous mRNAs and protects cell from the invasion of viruses (78, 79). There are two pathways of RNAi, which are guided respectively by exogenous small interfering RNA (siRNA) or endogenous microRNA (miRNA). During RNAi, an mRNA sequence is used as a template to specifically silence the corresponding target genes. This pathway drew intensive scientific attention, because of its designable guiding sequence yielding specificity against target genes.

siRNA is a double-stranded RNA with an overhanging structure formed by the phosphorylated 5’ ends and hydroxylated 3’ ends. It usually contains 19 - 20 base pair nucleotides (Figure. 1.5.) (80).

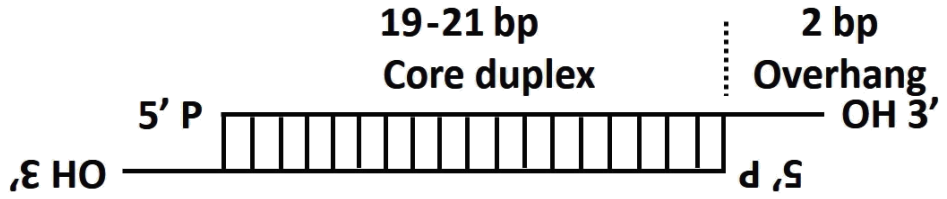

Figure 1.5. Schematic structure of siRNA duplex (81)

In the siRNA pathway, exogenous double strand RNAs are first cleaved into small RNAs. The endoribonuclease Dicer further cleaves small RNAs into siRNAs. These siRNAs bind to the RNA-induced silencing complex (RISC) and activate the complex. With the

bound siRNA, the activated complexes are guided to the target mRNAs and digest them to silence the target genes (82) (Figure. 1.6.).

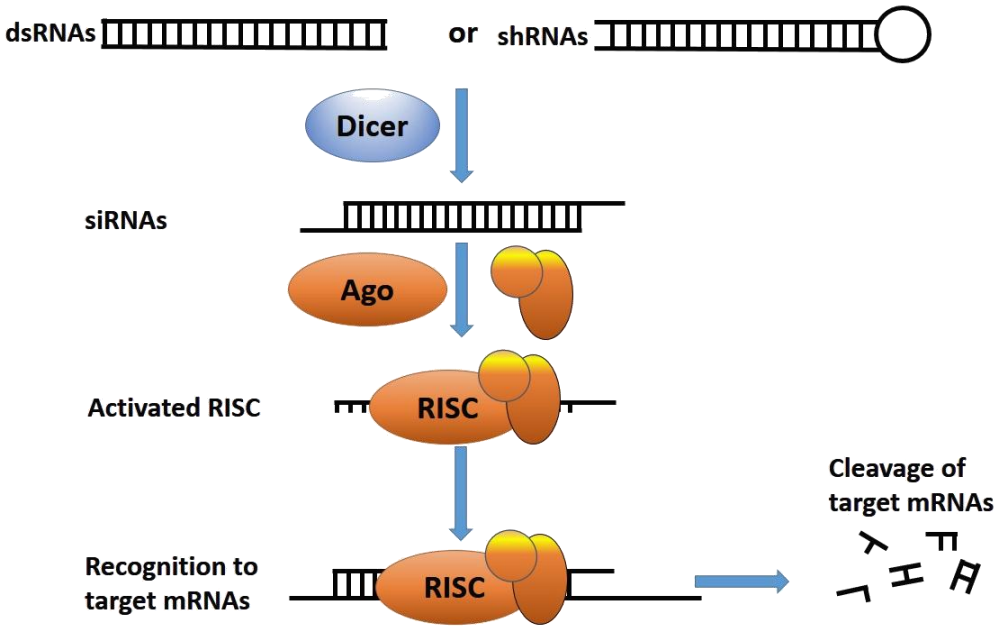

Figure 1.6. Schematic pathway of siRNA guided RNAi. Double strand RNAs (dsRNAs) or short hairpin RNAs (shRNAs) are first cleaved into siRNAs by the Dicer complex. siRNAs then incorporate the argonaute protein (AGO) and form the RNAi-induced silencing complex (RISC). By the sequence of incorporated siRNA, the activated RISC is guided to target mRNAs, which will then be cleaved by the catalytic domain of AGO. (81)

siRNA demonstrates silencing efficiency, specificity toward target genes, easiness of applying the treatment as well as low safety concerns for the clearance after the treatment. Nevertheless, several key elements of using siRNA *in vivo* as a therapeutic approach have to be taken into consideration. The siRNA has to specifically and locally suppress target genes in target regions. The off-target effect needs to be reduced as much as possible (83). In addition, the side effects caused by the application of the siRNA treatment, such as an unwanted immune response should be reduced to an unnoticeable level (84). At last, the biological half-life of siRNA *in vivo* should be well-characterized in regards to the condition of therapy and safety (85).

3 AIM OF STUDY

Aim one: P301S mouse is a widely used model of frontotemporal dementia and parkinsonism linked to chromosome 17 with tau pathology (FTDP-17-Tau). We aimed to search for hippocampal structural deficits and to correlate these to the onset of behavioral deficits, as well as relating the occurrence of different tau species (phosphorylated, conformationally changed) to the onset of structural neuronal alterations and behavioral deficits.

Aim two: Suppression of tau expression in conditional transgenic mice improved behavioral deficits in mouse models of tauopathies. Therefore, the aim of the study was to evaluate the effectiveness of small interference RNAs and their cerebral delivery to suppress human tau expression *in vivo* on the P301S mouse model, which might be a therapeutic option for human tauopathies.

4 MATERIAL AND METHODS

4.1 Animals

Transgenic mice with C57BL/6 background were developed by Michel Goedert, Cambridge, UK, to overexpress human P301S-mutant 4R tau (E2-E3-E10+) (75). They were backcrossed more than 10 times into the C57BL/6 background. Wild type C57BL/6 mice were used as controls. Only male mice were used for the tests. Animals were kept under a normal 12 h day/night cycle at 23 ± 1 °C in the animal cabinet with free access to food and water. All animals were handled according to the EU Council Directive 2010/63/EU, the Guide for the Care and Use of Laboratory Animals (National Research Council 2011) and the guidelines of the local institutional committee.

4.2 Behavioral Baseline Tests

The behavioral study was carried out as shown in Figure 3.1. Fifteen P301S mice underwent monthly the novel open field test from 2-6 months of age and the Morris water maze test at 2.5 and 5.5 months of age; nineteen P301S mice underwent monthly the rotarod test from 2-6 months of age; the same numbers of the wild-type mice were studied as controls.

4.2.1 **Rotarod**

The balancing ability of animals was tested at 2, 3, 4, 5 and 6 months of age using a rotarod system. Each mouse (n = 19 per group) was placed on a rod (diameter = 30 mm), rotating at a constant speed (10 rpm). Mice were allowed to stay on the rod up to 2 min. The latency to fall was recorded by the software when a mouse fell down to the bottom and interrupted the light beam. Mice were allowed to have four training trials in order to familiarize themselves with the task one day before the test.

4.2.2 **Novel Open Field**

Locomotor and exploration abilities of mice (n = 15 per group) were investigated monthly form 2-6 months of age. The test was carried out in boxes (32 cm × 32 cm) under dim light (2.0 lux) for 30 min. A video tracking system (Viewer^2) recorded moving

tracks and its length. Rearing was detected by light beams placed at 8 cm high from the bottom of the boxes and recorded by the Viewer^2 software.

4.2.3 **Morris Water Maze**

The Morris water maze test was performed to analyze spatial learning and memory at 2.5 and 5.5 months of age (n = 15 per group). A cylindrical water basin (diameter 120 cm) filled with water (height 31 cm) was used for the test. Four signs were placed on walls of the room as visual cues. The basin was equally divided into four quadrants and a platform (diameter 12 cm) was hidden under the water. The water was paled with non-dairy creamer. Three days pre-training, four days training and one day probe trial were sequentially performed in the test. At pre-training day one, mice were given six trials with a visible platform in the basin. At pre-training day two and three, six trials were given each day with a hidden platform. Each trial maximally lasted two min and the position of the platform was randomized in different days. During the four-days training, mice were given one trial per day to search for a hidden platform within one min. The position of the platform was fixed within one test session but differed at 2.5 and 5.5 months of age. Probe trial followed 24 h later, during which mice were given a free searching chance within one min without the platform under the water. The Viewer^2 system was used to record swimming tracks and latency to find the platform.

4.3 Tau Pathology in P301S Mice

4.3.1 **Immunohistology**

For histology, to identify tau pathology in P301S mouse brains, mice were sacrificed at 2, 3, 4, 5, or 6 months of age ($n \geq 3$ per group and time-point). Mouse brains were post-fixed in 4% paraformaldehyde (PFA) for 48 h at 4°C and cryo-protected in 30% sucrose solution thereafter. Fixed brains were cut into 30 µm thick coronal sections with a cryostat. Each brain was divided into equally spaced series separated in ten vials. Sections were stained by the free-floating method with the following antibodies: AT180 for PHF-tau phosphorylated at threonine 231; MC1 for conformationally changed tau and CP13 for serine 202-phosphorylated tau; anti-NeuN antibody for neuronal nuclei. Primary antibodies were diluted in 0.1 M PB buffer with 0.3% Triton 100 and 5% normal

donkey serum, incubated overnight at 4°C, and revealed with biotinylated secondary antibodies and 3, 3'-diaminobenzidine. siRNAs treated mice were sacrificed 7, 14, 21 and 28 days after injection. Free floating sections were immunostained with the following antibodies: AT180; MC1; CP13; anti-GFAP for astrocytes; anti-Iba-1 for microglia and macrophages; anti-MHC II for major histocompatibility complex class II molecules; anti-NeuN. Immunofluorescent staining was performed with the following antibodies: AT180; anti-NeuN. Secondary antibodies were goat anti-mouse Alexa 488 and donkey anti-rabbit Cy5. 4',6-diamidino-2-phenylindole (DAPI) was used as nuclear counter staining.

4.3.2 **Immunoblot**

For immnuoblots, mice (n = 3 per group) were sacrificed at 2 and 6 months of age by cervical dislocation. The brains were removed. The hippocampi were dissected under a dissection microscope and homogenized in T-PER tissue protein extraction reagent, 1% (v/v) protease inhibitor and phosphatase inhibitor cocktails. The extracts were centrifuged for 30 min at 80,000 x g. Supernatants were collected as the soluble fraction. Pellets were further extracted using a protocol for sarkoysl-insoluble fractions (76). Both fractions were separated were separated in a Bio-Rad electrophoresis system with 10% Tris-HCl SDS-PAGE gel. Gels were blotted using polyvinylidene fluoride (PVDF) membranes at 75 V for 1 h. After blotting, membranes were blocked with a solution of skim milk powder (0.5%) + TBST (0.1% tween-20) and incubated over night with the primary antibodies. Tau species were detected by AT180, CP13, and MC1 antibodies. Primary antibodies were revealed by peroxidase conjugated anti-mouse IgG secondary antibody and ECL prime solution. Blots were imaged using a Gel Doc™ XR system and analyzed by the Imagelab™ software. The optical densities were normalized to actin. Six month values were scaled to 2 month values (set as 1).

4.3.3 **Golgi Staining and Dendritic Spine Quantification**

After sacrifice by cervical dislocation (n = 4 per group), brains were quickly removed and rinsed with Millipore water. The impregnation was performed using the GolgiStain™ kit following the manufacturer's guidelines. After impregnation, brains were cut on a cryostat into 200-µm-thick coronal sections and covered with Corbit-Balsam for imaging. Secondary to quaternary branches of dendrites within a distance range of 30 - 120 µm

from the pyramidal body and two to three basal and apical dendrites from each neuron (n = 10 per brain) were analyzed. Dendrites (≥ 10 μm in length) were first reconstructed into 3D images, from which spine density, length, cross-sectional area, and volume were quantified using the Imaris software.

4.4 Tau Suppression *in Vitro*

4.4.1 Primary Cortical Neuron Culture

After decapitation, the embryos were removed at embryonic day 15. Brains of embryos were quickly dissected and cortices were removed from the brains under a dissecting microscope. After trypsinizing (trypsin 0.25%), cells were resuspended in Hank's Balanced Salt Solution (HBSS) and plated at a density of 30,000 cells/cm^2 in polyethyleneimine coated 24-well plates with 500 μL neurobasal medium. The cells were kept in a humidified incubator at 37 °C with an atmosphere of 5% CO_2. Cytosine arabinoside (10μM) was added into the medium 48 h after plating to eliminate proliferating glial cells. Under these conditions, the percentage of neurons is more than 95% on 7-8 days old cultures (86).

4.4.2 LUHMES Cell Cultures

The immortalized neurons were proliferated in the growth media in poly-L-lysine (PLL) coated plates. After the culture reached a confluence of 80%, the cells were trypsinized and plated in PLL and fibronectin double-coated plates in differentiation media at a density of 130,000 cells/cm^2 (87).

4.4.3 siRNA Delivery

siRNAs were diluted with neurobasal medium or differentiation medium into different concentrations. 48 h after plating, the old medium was replaced by fresh medium containing siRNAs.

4.4.4 Cell Toxicity Test

The medium was removed after incubation with siRNA and a phosphate buffered saline solution with 0.5 mg/mL 3-(4, 5-dimethylthiazol-2-yl)-2, 5-diphenyltetrazolium bromide

(MTT) was added. After incubation at 37 °C for 1 h, the solution was completely removed and the plates were allowed to stay in a freezer at -80 °C for more than 1 h. Dimethyl sulfoxide (DMSO) was added to the plates before analyzing on a plate reader at a wave length of 590 nm.

4.4.5 **Semi-quantitative Reverse Transcription-PCR (RT-PCR)**

Total mRNA was extracted from neurons using Nucleospin® RNA II kit. RT-PCRs were performed with respective programs with primers against human *MAPT* and Mouse *Gapdh*. The RT-PCR products were separated by electrophoresis in 1.5% agarose gels and revealed with SYBR® Safe dye. Images were taken by a Gel Doc™ XR System. The optical density was quantified with Imagelab™ software and all the target genes were normalized to the housekeeping gene (*Gapdh*). All data were collected from at least 3 independent experimental repeats.

4.4.6 **Quantitative PCR (qPCR)**

After mRNA extraction, 1000 ng of total mRNA was reversely transcripted into cDNA using the iScript cDNA synthesis kit. The qRCR analysis was accomplished with the SteponePlus™ real-time PCR system, Tagman® Universal Master Mix II with UNG and Tagman® gene expression assay kit using the comparative threshold cycle (Ct) method. The Ct values of target genes were determined by four reference genes. Primers against following genes were used: *MAPT*, *OAS1*, *PPiA*, *PPiB*, *GAPDH*, *PSMC1*. Relative quantities of target mRNAs were normalized to the level of non-treated control (set as 1). All data were collected from three independent biological repeats.

4.4.7 **Immunoblot**

Primary cells were harvested and extracted in protein extraction buffer. Samples were centrifuged at 13,000 g at 4 °C for 15 min and pellets were discarded. The supernatants were separated in a Bio-Rad electrophoresis system with 10% Tris-HCl SDS-PAGE gel. Proteins were blotted using polyvinylidene fluoride (PVDF) membranes at 75 V for 1 h. After blotting, membranes were blocked with a solution of skim milk powder (0.5%) + TBST (0.1% tween-20) and incubated over night with the primary antibodies. After that, blots were incubated with peroxidase conjugated secondary antibodies for 1 h following

visualization with an enhanced chemi-luminescence solution (ECL solution). Images were taken by a Gel Doc™ XR System. Optical density measurements were performed by Imagelab™ software and results were normalized to the housekeeping gene (GAPDH). All data were collected from at least three independent experimental repeats.

4.5 Tau Suppression *In vivo*

4.5.1 **siRNAs Delivery**

After anaesthetization with rompun® (0.2% xylazine) and 1 mg/ml ketamine, mice were fixed onto a stereotactic frame. The intracerebral delivery of siRNA were performed with a microinjection syringe placed at the coordinates relative to the surface of dura (88). siRNAs were desolved in 0.9% NaCl solution and a volume of 2 µL solutions was injected at a rate of 0.2 µL/min. In the *MAPT* siRNA treated groups, the right hippocampus was injected with *MAPT* siRNA and left with the same doses of non-targeting siRNA. In the sham control mice group (n = 4), left hippocampus was injected with 0.4 nmol non-targeting siRNA, right side untreated, and sacrificed 14 days later. Four groups of mice ($n \geq 4$ per group) were bilaterally injected with 0.4 nmol of *MAPT* and non-targeting siRNAs, and sacrificed respectively at post injection day 7, 14, 21 and 28. Three groups of mice ($n \geq 5$ per group) were bilaterally injected with 0.1 nmol, 0.2 nmol, and 0.4 nmol of the two siRNAs and sacrificed 14 days later.

4.5.2 **Stereology**

The hippocampi of the sham control and *MAPT* siRNA treated animals (n = 3 per group) were analysed with a stereo-investigator microscope. Sections (n = 5) of each hippocampus ranging from -1.34 to -2.3 mm posterior to the bregma were analysed using the optical fractionator method. NeuN-labelled neurons were counted in a counting frame of 20 x 20 µm under a 63 x oil objective. Only cells with the presence of nuclei were counted and total cell number was estimated by integration along the rostrocaudal extent of the structures. The sampling strategy gave a coefficient of error less than 0.09 with Gundersen method (m = 1). The estimated cell numbers were normalized to the contralateral non-targeting siRNA treated side for comparisons. The analysis was performed blinding the labels of the slices.

4.5.3 **Suppression Area Calculation**

Three adjacent sections (0.4 nmol *MAPT* siRNA treated, 14 days post injection, n = 7) showed suppression on AT180 immunoreactivity were chosen for the quantification. The affected areas "S" were delineated on the sections "I" and measured by the ImageJ software. The effected volume was calculated as $\text{Section Thickness (30 µm)} * \text{Sectioning Intervall (10)} * \sum_i^n (S_i)$

4.5.4 **TUNEL Assay**

Click-iT® TUNEL assay kit was used to perform the TUNEL assay. 4% paraformaldehyde-fixed sections were first hydrated in 100% xylene and a series of ethanol solutions (100% - 50%) following 10 min pretreatment at 99℃ in sodium citrate solution (10mM sodium citrate, 0.05% Tween 20, pH = 6.0). After cooling down, the sections were incubated with PBS containing 0.25% TritonX-100 for 20 min at room temperature and then washed twice with deionized water. Control sections were treated with DNase I solution. The treatment was carried out following the user guideline of the kit.

4.6 Optical Density Measurement

Histologically stained brain sections were imaged under an E-330 Olympus camera. The grey scale of the interested areas from 3 sections per mouse brain were measured by ImageJ software (http://rsb.info.nih.gov/ij). Either medial globus pallidus or corpus callosum was used as control for background, which showed no immunoreactivity with the used antibodies. The results were scaled to the values of contralateral sides (non-targeting siRNA injected side, set as 1).

4.7 Statistics

All data are presented as mean + standard error (SE). Comparisons between groups were performed by two-sided t-tests. Multiple comparisons were performed by one-way ANOVA or repeated measures (RM) ANOVA, followed by Student-Newman-Keuls's

post hoc test. Calculations were made with the Sigmaplot Standard Statistical Software Package. A p-value < 0.05 was considered to be significant.

The detailed information of all chemicals, reagents, kits, solutions and devices are listed in the appendix.

5 RESULTS

5.1 Aim One:

In the first study, we identified hippocampus-dependent visuospatial memory deficits in P301S mice with an onset prior to the locomotor dysfunction, at an early age of 2.5 months. Pathologically, conformationally changed tau, the S202-phosphorylated tau and the PHF-tau were all found in the soluble fraction of the brain homogenates at this age, but not in the sarkosyl-insoluble fraction. Histologically, we also observed tau immunoreactivity with the pathological conformation (MC1 antibody) and the S202-phosphorylation (CP13 antibody), but no PHF-tau (AT180 antibody) in the hippocampus. The pathology was not associated with neuronal loss in the hippocampus, but a reduction of dendritic spines.

The detailed results were published in the article: Xu H, Roesler TW, Carlsson T, de Andrade A, Bruch J, Hoellerhage M, Oertel WH, Hoeglinger GU. Memory Deficits Correlate with Tau and Spine Pathology in P301S MAPT Transgenic Mice. Neuropathology and applied neurobiology. 2014 Dec; 40 (7):833-43. doi: 10.1111/nan.12160. Full article attached in the appendix.

5.2 Aim Two:

We identified a commercially available siRNA can be applied in vivo by intracerebral injection without the use of a delivery reagent to suppress tau expression. We show a significant knock-down without any detectable neurotoxicity, inflammation or apoptosis in the hippocampus, where tau pathology is prominent and which correlates with behavioral read-outs of the P301S tauopathy mouse model. A single injection resulted in moderate distribution, spatially confined to the area surrounding the injection site, and transiently in a well-defined period of time; suppression of intracellular tau occurred very specifically in these neurons, in which the siRNA molecules had entered.

The detailed results were published in the article: Xu H, Roesler TW, Carlsson T, de Andrade A, Fiala O, Hoellerhage M, Oertel WH, Goedert M, Aigner A, Hoeglinger GU. Tau Silencing by siRNA in the P301S Mouse Model of Tauopathy. Current Gene Therapy. 2014b: in press. Full article attached in the appendix.

6 DISCUSSION

6.1 Aim One

The balancing ability of the P301S mice abruptly decreased at 5 months of age in the rotarod test and deteriorated sharply at 6 months. The results were matched with the exploring activity of P301S mice in the novel open field test. The deficit was likely caused by the previously reported loss of neurons in the brain and spinal cord (75). Such a locomotor deficit seems to be a common phenotype of the human-tau-transgenic mice since it also had been previously reported in the same mouse model (77) as well as another mouse models of FTDP-17-tau (89, 90).

At both young and old ages (2.5 and 5 months), the P301S mice showed a poor learning curve compared with the wild-type mice in the Morris water maze test. A lack of preference to the target quadrant in the probe trial was only found in young mice, indicating an early onset of memory deficit. The memory deficits were not previously reported in the same mouse model at 2 months of age (77). In another heterozygous P301S-tau transgenic mouse line, a trend of increased time in Morris water maze was described at 10 months of age (91). The data suggest that transgenic tau is a likely cause for the memory deficits in these mouse models.

The nature of toxicity of tau is still in debate, mainly due to the existence of variants of tau species. We assumed conformationally changed tau (MC1 antibody), threonine 231-phosphorylated PHF-tau (AT180 antibody), and serine 202-phosphorylated tau (CP13 antibody) to be the toxic species since they are characteristically present at early stages of tauopathies. The hippocampus was studied histologically and biochemically since it is the anatomical substrate of visuospatial memorization.

Immunoblots showed a general increase of all the three tau species, however with differential patterns. An increase of PHF-tau (AT180 positive) was found in the sarkosyl-insoluble brain fractions, but not in the soluble ones, which partly confirmed the results of a previous study (76). A similar pattern was also found with S202-phosphorylated tau (CP13 positive). These data suggest a possible progressive tau pathology in the P301S

mouse brain, switching from soluble to insoluble pathology. The increase in conformationally altered tau (MC1 positive) was restricted to the soluble fraction. The increase of soluble MC1 positive tau and insoluble AT180 and CP13 positive tau correlated with the onset of motor deficits at the older age of 5 months. On the other hand, all three pathological tau species were present in the soluble fraction in the 2 month-old P301S mouse brains, which coincides with the onset of memory deficits in the Morris water maze test, indicating a possible link between soluble tau species and memory deficits.

Histologically, an age-dependent increase of all three tau species was also observed in the hippocampus of P301S mice. The immunoreactivities of these three antibodies showed a diffuse distribution rather than a condensed pattern. The hippocampal region was free of thioflavin-S staining from two to six months of age suggesting an absence of tau inclusions or lack of tau aggregates with beta-sheet structure. At the earlier age, we also found tau in somato-dendritic localisation, while tau is normally only found in axons, indicating a missorting of tau species in the hippocampal neurons (92). A similar pattern was also reported in a transgenic mouse model of FTDP-17-tau with the deletion of lysine 280 on human tau (93, 94), which was reported showing a phenotype of disruption in postsynaptic function of Fyn (proto-oncogene tyrosine-protein kinase Fyn) (95). In addition, there was also evidence that such somato-dendritic missorting was associated with the development of memory deficits (67), which could also contribute to the memory deficit we observed in P301S mice.

Neuronal cell loss was reported neither in previous studies nor in the present study in the hippocampus of P301S mice. To identify a possible structural substrate of the behaviour deficits, we investigated therefore the dendritic spines of pyramidal neurons in the hippocampus region. Across genotypes, the present study identified a decrease of the average spine density, length, area and volume in P301S mouse hippocampi at an early age. The decrease in spine density paralleled the attenuated learning curve of P301S mouse. Dendritic spines are protrusions on the dendrites of neurons, receiving inputs from axons via synapses (96), regulating the acquisition of new memory as well as maintaining old memory by their dynamic alterations (97). Changes in the size and

number of dendritic spines have been associated with memory deficit and memory dysfunction of several different mouse models of tauopathies (98-101). According to the current theory, smaller spines seed new memories, while larger spines maintain old memories that could last lifelong (102, 103). A reduction in spine density and size could worsen the memory formation.

Within the group of P301S mice, spine densities did not differ at older age from younger age, but they were larger in size (area and volume) at older age. Such a pattern was not found in wild-type mouse brains, which had an increase in spine density and smaller spines with aging. A reduced spine density and larger spine size in P301S mice might be an indication of dysfunctional synaptogenesis or synapse elimination, which can impair the acquisition of new memories (97).

The first part of the study suggests that a tauopathy-induced impairment of synaptic connectivity in the hippocampus leads to memory deficits in P301S mice at an early age. The behavioural deficit and the assumed patho-anatomical substrate may be helpful as a target and read-out for the development of future therapeutic treatments.

6.2 Aim Two

One previous study described that shutting down the expression of mutant tau in a conditional transgenic mouse model at an adult age reversed the already established neuronal tau-aggregates and corresponding behavioural impairments (66). However, it is still an unresolved research question, how one could efficiently and safely suppress the tau expression in human patients for therapeutic purposes. RNAi was chosen as a candidate in the present study because of its high specificity and efficiency to silence target genes (104). Although there is first evidence suggesting feasibility of cerebral administration and therapeutic efficacy in a mouse model of neurodegeneration (105), the concern of the safety and effective delivery of siRNA to the central nervous system is still an unresolved matter of intense research (104, 106, 107). Major obstacles include the necessity to overcome the blood-brain barrier, the need for long-lasting and widespread delivery, the risk of raising inflammation and neurotoxicity, as well as the wish for a reversible system to terminate the effect in case of adverse events.

For chronic neurodegenerative disorders, the specific treatment requires an enduring therapy. Although viral-based delivery systems for siRNA (by encoding shRNAs) could fulfil that requirement (105, 108, 109), the intracerebral delivery of virus bears the risk to induce adverse effects, for lentiviral vectors, which irreversibly integrates exogenous DNA into the host genome, and for adeno-associated viruses, which may trigger an immune response.

Compared to viral-based systems, non-viral based siRNA delivery is a relatively safe system since it is reversible and less prone to immune response. A previous study achieved an allele specific suppression of tau in Cos-7 and HeLa cells using Lipofectamine® Plus to deliver shRNA (110). In our study, lipofectamine mixed with siRNA *in vivo* gave a high toxicity to neurons and limited distribution. We also tested polyethyleneimine (PEI)- complexed siRNA (1.5 µg/µL) (111) *in vivo* that also showed high neurotoxicity in our experimental setting. G2-5 dendrimer (112) as transfection agent only achieved a very limited intracerebral distribution in our hands. Hence, the transfection agents commonly used *in vitro* did not prove to be properly working *in vivo*.

The chemically modified Accell™ siRNAs can penetrate cell membranes without additional transfection agents and have been widely used *in vitro* so far (113, 114). One previous study suppressed cyclophilin-B and GAPDH by single intracerebroventricular injection of the same siRNAs in the rat brain (115). In our study, a single injection of *MAPT* siRNA into the lateral ventricular in P301S mice could not achieve any suppressive effect on the tau expression in the hippocampus. This may be due to the high copy level of human mutant tau in the P301S mouse brain. Efficacy of intracerebroventricular injection might possible be achieved using an osmotic pump infusion over a prolonged period of time. Nonetheless, after a single injection into the hippocampal parenchyma, a moderate distribution and a neuron-specific and siRNA-dependent knock-down was achieved in our hands.

A dose-dependent suppression of human tau was observed by the use of siRNA *in vitro* as well as suppression of 45% of tau expression *in vivo*. Results of time course experiments proved that the suppression effect after a single administration of siRNA lasted for a maximum of 14 days. The neurotoxicity and inflammation level was tested

using different antibodies. It was clearly observed that the entrance of siRNA did not induce any discernible inflammation or apoptotic neurons within the region, where a suppression of tau was found.

Thus, the second part of our study showed the safety of this method and provided a realistic delineation of the efficacy of a siRNA treatment in the brain parenchyma in the temporal and spatial dimension.

6.3 Conclusion

Tau pathology is prominent in the hippocampus of the P301S mouse model (75, 77, 116) and was shown to correlate with several behavioural read-outs. A commercially available siRNA was identified, which could be applied *in vivo* by intracerebral injection without the use of a delivery reagent to suppress tau expression. A single injection resulted in moderate distribution of the silencing effect, spatially confined to the injected region, and a transient silencing effect in a well-defined period; suppression of intracellular tau that occurred specifically in neurons. The suppression was achieved *in vivo* without any detectable neurotoxicity, inflammation or apoptosis in the hippocampus. In summary, the present study provided first evidence that Accell™ siRNAs can be administered *in vivo* to achieve suppression of the tau protein in a tau-overexpression mouse model with good efficacy and safety. The work supports further development of this method for therapeutic purposes in brain disorders.

7 ACKNOWLEDGEMENT

First of all, I want to give my greatest gratitude to my parents for their never ending support both to my life and study with demanding nothing for return. Second, I want to thank my wife for the sacrifice that she made for me and the family. Especially I want to thank Dr. Lixia Lv, who introduced me to Prof. Günter Höglinger after my master study. I thank greatly to Prof. Günter Höglinger as my first professor for his countless help, who made my doctoral study in Germany possible and nicely guided me into the academic world. At the same time, I thank my second professor, Prof. Michael Schemann and mentor, Prof. Stefan Lichtenthaler for their thoughtful enlightenment and patient guidance with my doctoral project. I also owe my gratitude to Dr. Thomas Rölser and Dr. Thomas Carlson for their great efforts of lecturing and enlightening me with their advanced experiments and manuscript writing skills. I give my gratitude to Dr. Wei-Hua Chiu, Dr. Anderson de Andrade, Dr. Thomas Koeglsperger, and especially Dr. Julius Bruch, for their nice collaboration and thoughtful discussion in all the experimental projects. I also thank Ms. Tasnim Chakroun, Ms. Elisabeth Findeiss and Ms. Natasha Fussi for proofreading my thesis. I especially thank Dr. Sigrid Schwarz for the nice coaching of my scientific side projects as well as valuable suggestions she has offered for my career and family. In addition, I want to make a great acknowledgement to Mr. Robin Konhaeuser and Ms. Magda Baba for the excellent technical assistance, as well as Ms. Carolin Nierwetberg for her kind help with my contract and experimental orderings. I owe my great gratitude to Mr. Johannes Melms for his great help of looking for an apartment for me which actually saved my small family from sleeping on the street. In the end, I will take this opportunity to express my deepest thanks to all the people who have ever offered me any kind help which makes my life and study possible in Germany.

8 SUMMARY OF CONTRIBUTIONS

In the publication entitled "Memory Deficits Correlate with Tau and Spine Pathology in P301S MAPT Transgenic Mice", I found that memory deficits and dendritic spine pathology of P301S-tau transgenic mice coincide at a relatively early age. The pre-described motor deficits were found after the onset of memory deficits together, coinciding with the increase of tau in the sarkosyl-insoluble protein fraction. This newly recognized behavioral deficit and the suggested patho-anatomical substrate could serve as a useful read-out for the development of new therapeutic tau-targeting interventions. I carried out all the experimental work and wrote the manuscript under the supervising of Prof. Dr. Günter Höglinger. The manuscript was revised together with my colleagues and supervisor, including Dr. Thomas Rösler, Dr. Thomas Carlson, Dr, Matthias Höllerhage and Prof. Günter Höglinger and submitted to the journal by myself with the approval of the co-authors and supervisor.

In the publication entitled "Tau Silencing by siRNA in the P301S Mouse Model of Tauopathy", I demonstrated the safety and provided a realistic delineation of the efficacy in the temporal and spatial dimension of a single injection of siRNA into the brain parenchyma of P301S mouse. The work could provide a stable basis for the further development of this method for therapeutic purposes in brain disorders. Apart from the siRNAs delivery work done by the help of transfection agents, which was done by my former colleagues Dr. Thomas Carlson and Dr. Ondrej Fiala, all the other results were collected from my own experiments. The manuscript was drafted by myself, which was revised and proof read together with my colleagues, Dr. Thomas Roesler, Dr. Thomas Carlson, Dr, Matthias Höllerhage and Prof. Dr. Günter Höglinger.

9 REFERENCES

1. Weingarten MD, Lockwood AH, Hwo SY, Kirschner MW. A protein factor essential for microtubule assembly. Proceedings of the National Academy of Sciences of the United States of America. 1975;72(5):1858-62.
2. Wilhelmsen KC, Lynch T, Pavlou E, Higgins M, Nygaard TG. Localization of disinhibition-dementia-parkinsonism-amyotrophy complex to 17q21-22. American journal of human genetics. 1994;55(6):1159-65.
3. Gotz J, Xia D, Leinenga G, Chew YL, Nicholas H. What Renders TAU Toxic. Frontiers in neurology. 2013;4:72.
4. Neve RL, Harris P, Kosik KS, Kurnit DM, Donlon TA. Identification of cDNA clones for the human microtubule-associated protein tau and chromosomal localization of the genes for tau and microtubule-associated protein 2. Brain Res. 1986;387(3):271-80.
5. Caffrey TM, Wade-Martins R. The role of MAPT sequence variation in mechanisms of disease susceptibility. Biochem Soc Trans. 2012;40(4):687-92.
6. Spillantini MG, Goedert M. Tau pathology and neurodegeneration. Lancet neurology. 2013;12(6):609-22.
7. Minoura K, Mizushima F, Tokimasa M, Hiraoka S, Tomoo K, Sumida M, et al. Structural evaluation of conformational transition state responsible for self-assembly of tau microtubule-binding domain. Biochemical and biophysical research communications. 2005;327(4):1100-4.
8. Mukrasch MD, Bibow S, Korukottu J, Jeganathan S, Biernat J, Griesinger C, et al. Structural polymorphism of 441-residue tau at single residue resolution. PLoS biology. 2009;7(2):e34.
9. Schweers O, Schonbrunn-Hanebeck E, Marx A, Mandelkow E. Structural studies of tau protein and Alzheimer paired helical filaments show no evidence for beta-structure. The Journal of biological chemistry. 1994;269(39):24290-7.
10. Mendieta J, Fuertes MA, Kunjishapatham R, Santa-Maria I, Moreno FJ, Alonso C, et al. Phosphorylation modulates the alpha-helical structure and polymerization of a peptide from the third tau microtubule-binding repeat. Biochimica et biophysica acta. 2005;1721(1-3):16-26.
11. Jeganathan S, von Bergen M, Brutlach H, Steinhoff HJ, Mandelkow E. Global hairpin folding of tau in solution. Biochemistry. 2006;45(7):2283-93.
12. Hanger DP, Byers HL, Wray S, Leung KY, Saxton MJ, Seereeram A, et al. Novel phosphorylation sites in tau from Alzheimer brain support a role for casein kinase 1 in disease pathogenesis. The Journal of biological chemistry. 2007;282(32):23645-54.
13. Kopke E, Tung YC, Shaikh S, Alonso AC, Iqbal K, Grundke-Iqbal I. Microtubule-associated protein tau. Abnormal phosphorylation of a non-paired helical filament pool in Alzheimer disease. The Journal of biological chemistry. 1993;268(32):24374-84.
14. Buee L, Bussiere T, Buee-Scherrer V, Delacourte A, Hof PR. Tau protein isoforms, phosphorylation and role in neurodegenerative disorders. Brain research Brain research reviews. 2000;33(1):95-130.

15. Cho JH, Johnson GV. Glycogen synthase kinase 3beta phosphorylates tau at both primed and unprimed sites. Differential impact on microtubule binding. The Journal of biological chemistry. 2003;278(1):187-93.
16. Hanger DP, Anderton BH, Noble W. Tau phosphorylation: the therapeutic challenge for neurodegenerative disease. Trends in molecular medicine. 2009;15(3):112-9.
17. O'Brien WT, Klein PS. Validating GSK3 as an in vivo target of lithium action. Biochem Soc Trans. 2009;37(Pt 5):1133-8.
18. O'Donnell KC, Gould TD. The behavioral actions of lithium in rodent models: leads to develop novel therapeutics. Neuroscience and biobehavioral reviews. 2007;31(6):932-62.
19. Chohan MO, Khatoon S, Iqbal IG, Iqbal K. Involvement of I2PP2A in the abnormal hyperphosphorylation of tau and its reversal by Memantine. FEBS letters. 2006;580(16):3973-9.
20. Martin L, Latypova X, Wilson CM, Magnaudeix A, Perrin ML, Terro F. Tau protein phosphatases in Alzheimer's disease: the leading role of PP2A. Ageing research reviews. 2013;12(1):39-49.
21. Martin L, Latypova X, Terro F. Post-translational modifications of tau protein: implications for Alzheimer's disease. Neurochemistry international. 2011;58(4):458-71.
22. Yuzwa SA, Macauley MS, Heinonen JE, Shan X, Dennis RJ, He Y, et al. A potent mechanism-inspired O-GlcNAcase inhibitor that blocks phosphorylation of tau in vivo. Nature chemical biology. 2008;4(8):483-90.
23. Liu F, Iqbal K, Grundke-Iqbal I, Gong CX. Involvement of aberrant glycosylation in phosphorylation of tau by cdk5 and GSK-3beta. FEBS letters. 2002;530(1-3):209-14.
24. Takahashi M, Tsujioka Y, Yamada T, Tsuboi Y, Okada H, Yamamoto T, et al. Glycosylation of microtubule-associated protein tau in Alzheimer's disease brain. Acta Neuropathol. 1999;97(6):635-41.
25. Lefebvre T. Neurodegeneration: Recall sugars, forget Alzheimer's. Nature chemical biology. 2012;8(4):325-6.
26. Yuzwa SA, Shan X, Macauley MS, Clark T, Skorobogatko Y, Vosseller K, et al. Increasing O-GlcNAc slows neurodegeneration and stabilizes tau against aggregation. Nature chemical biology. 2012;8(4):393-9.
27. Yu Y, Zhang L, Li X, Run X, Liang Z, Li Y, et al. Differential Effects of an O-GlcNAcase Inhibitor on Tau Phosphorylation. PLoS ONE. 2012;7(4):e35277.
28. Yan SD, Chen X, Schmidt AM, Brett J, Godman G, Zou YS, et al. Glycated tau protein in Alzheimer disease: a mechanism for induction of oxidant stress. Proceedings of the National Academy of Sciences of the United States of America. 1994;91(16):7787-91.
29. Su B, Wang X, Lee HG, Tabaton M, Perry G, Smith MA, et al. Chronic oxidative stress causes increased tau phosphorylation in M17 neuroblastoma cells. Neurosci Lett. 2010;468(3):267-71.
30. Arnaud LT, Myeku N, Figueiredo-Pereira ME. Proteasome-caspase-cathepsin sequence leading to tau pathology induced by prostaglandin J2 in neuronal cells. J Neurochem. 2009;110(1):328-42.

31. Iqbal K, Liu F, Gong CX, Alonso Adel C, Grundke-Iqbal I. Mechanisms of tau-induced neurodegeneration. Acta Neuropathol. 2009;118(1):53-69.
32. Cripps D, Thomas SN, Jeng Y, Yang F, Davies P, Yang AJ. Alzheimer disease-specific conformation of hyperphosphorylated paired helical filament-Tau is polyubiquitinated through Lys-48, Lys-11, and Lys-6 ubiquitin conjugation. The Journal of biological chemistry. 2006;281(16):10825-38.
33. Nakashima H, Ishihara T, Suguimoto P, Yokota O, Oshima E, Kugo A, et al. Chronic lithium treatment decreases tau lesions by promoting ubiquitination in a mouse model of tauopathies. Acta Neuropathol. 2005;110(6):547-56.
34. Koren J, 3rd, Jinwal UK, Davey Z, Kiray J, Arulselvam K, Dickey CA. Bending tau into shape: the emerging role of peptidyl-prolyl isomerases in tauopathies. Molecular neurobiology. 2011;44(1):65-70.
35. Zhou XZ, Kops O, Werner A, Lu PJ, Shen M, Stoller G, et al. Pin1-dependent prolyl isomerization regulates dephosphorylation of Cdc25C and tau proteins. Molecular cell. 2000;6(4):873-83.
36. Murthy SN, Wilson JH, Lukas TJ, Kuret J, Lorand L. Cross-linking sites of the human tau protein, probed by reactions with human transglutaminase. J Neurochem. 1998;71(6):2607-14.
37. Citron BA, SantaCruz KS, Davies PJ, Festoff BW. Intron-exon swapping of transglutaminase mRNA and neuronal Tau aggregation in Alzheimer's disease. The Journal of biological chemistry. 2001;276(5):3295-301.
38. Wilhelmus MM, Grunberg SC, Bol JG, van Dam AM, Hoozemans JJ, Rozemuller AJ, et al. Transglutaminases and transglutaminase-catalyzed cross-links colocalize with the pathological lesions in Alzheimer's disease brain. Brain pathology. 2009;19(4):612-22.
39. Halverson RA, Lewis J, Frausto S, Hutton M, Muma NA. Tau protein is cross-linked by transglutaminase in P301L tau transgenic mice. The Journal of neuroscience : the official journal of the Society for Neuroscience. 2005;25(5):1226-33.
40. Zhang YJ, Xu YF, Chen XQ, Wang XC, Wang JZ. Nitration and oligomerization of tau induced by peroxynitrite inhibit its microtubule-binding activity. FEBS letters. 2005;579(11):2421-7.
41. Reynolds MR, Berry RW, Binder LI. Site-specific nitration and oxidative dityrosine bridging of the tau protein by peroxynitrite: implications for Alzheimer's disease. Biochemistry. 2005;44(5):1690-700.
42. Fellous A, Francon J, Lennon AM, Nunez J. Microtubule assembly in vitro. Purification of assembly-promoting factors. European journal of biochemistry / FEBS. 1977;78(1):167-74.
43. Drubin D, Kobayashi S, Kirschner M. Association of tau protein with microtubules in living cells. Annals of the New York Academy of Sciences. 1986;466:257-68.
44. Butner KA, Kirschner MW. Tau protein binds to microtubules through a flexible array of distributed weak sites. The Journal of cell biology. 1991;115(3):717-30.
45. Chen S, Townsend K, Goldberg TE, Davies P, Conejero-Goldberg C. MAPT isoforms: differential transcriptional profiles related to 3R and 4R splice variants. Journal of Alzheimer's disease : JAD. 2010;22(4):1313-29.

46. Goedert M, Ghetti B. Alois Alzheimer: his life and times. Brain pathology. 2007;17(1):57-62.
47. Katzman R. The prevalence and malignancy of Alzheimer disease: a major killer. Alzheimer's & dementia : the journal of the Alzheimer's Association. 2008;4(6):378-80.
48. Rocca WA, Hofman A, Brayne C, Breteler MM, Clarke M, Copeland JR, et al. Frequency and distribution of Alzheimer's disease in Europe: a collaborative study of 1980-1990 prevalence findings. The EURODEM-Prevalence Research Group. Annals of neurology. 1991;30(3):381-90.
49. Goedert M, Jakes R, Crowther RA, Cohen P, Vanmechelen E, Vandermeeren M, et al. Epitope mapping of monoclonal antibodies to the paired helical filaments of Alzheimer's disease: identification of phosphorylation sites in tau protein. The Biochemical journal. 1994;301 (Pt 3):871-7.
50. Patrick GN, Zukerberg L, Nikolic M, de la Monte S, Dikkes P, Tsai LH. Conversion of p35 to p25 deregulates Cdk5 activity and promotes neurodegeneration. Nature. 1999;402(6762):615-22.
51. Vogelsberg-Ragaglia V, Schuck T, Trojanowski JQ, Lee VM. PP2A mRNA expression is quantitatively decreased in Alzheimer's disease hippocampus. Experimental neurology. 2001;168(2):402-12.
52. Sontag E, Hladik C, Montgomery L, Luangpirom A, Mudrak I, Ogris E, et al. Downregulation of protein phosphatase 2A carboxyl methylation and methyltransferase may contribute to Alzheimer disease pathogenesis. Journal of neuropathology and experimental neurology. 2004;63(10):1080-91.
53. Rebeiz JJ, Kolodny EH, Richardson EP, Jr. Corticodentatonigral degeneration with neuronal achromasia: a progressive disorder of late adult life. Transactions of the American Neurological Association. 1967;92:23-6.
54. Iwatsubo T, Hasegawa M, Ihara Y. Neuronal and glial tau-positive inclusions in diverse neurologic diseases share common phosphorylation characteristics. Acta Neuropathol. 1994;88(2):129-36.
55. Scaravilli T, Tolosa E, Ferrer I. Progressive supranuclear palsy and corticobasal degeneration: lumping versus splitting. Movement disorders : official journal of the Movement Disorder Society. 2005;20 Suppl 12:S21-8.
56. Feany MB, Dickson DW. Widespread cytoskeletal pathology characterizes corticobasal degeneration. Am J Pathol. 1995;146(6):1388-96.
57. Takeda N, Kishimoto Y, Yokota O. Pick's disease. Advances in experimental medicine and biology. 2012;724:300-16.
58. Yamakawa K, Takanashi M, Watanabe M, Nakamura N, Kobayashi T, Hasegawa M, et al. Pathological and biochemical studies on a case of Pick disease with severe white matter atrophy. Neuropathology : official journal of the Japanese Society of Neuropathology. 2006;26(6):586-91.
59. Reig S, Buee-Scherrer V, Mourton-Gilles C, Defossez A, Delacourte A, Beauvillain JC, et al. Immunogold labelling of paired helical filaments and amyloid fibrils by specific monoclonal and polyclonal antibodies. Acta Neuropathol. 1995;90(5):441-7.
60. Ferrer I, Lopez-Gonzalez I, Carmona M, Arregui L, Dalfo E, Torrejon-Escribano B, et al. Glial and neuronal tau pathology in tauopathies: characterization of disease-

specific phenotypes and tau pathology progression. Journal of neuropathology and experimental neurology. 2014;73(1):81-97.
61. Barsottini OG, Felicio AC, Aquino CC, Pedroso JL. Progressive supranuclear palsy: new concepts. Arquivos de neuro-psiquiatria. 2010;68(6):938-46.
62. Gerstenecker A, Duff K, Mast B, Litvan I. Behavioral abnormalities in progressive supranuclear palsy. Psychiatry research. 2013;210(3):1205-10.
63. Hoglinger GU, Melhem NM, Dickson DW, Sleiman PM, Wang LS, Klei L, et al. Identification of common variants influencing risk of the tauopathy progressive supranuclear palsy. Nature genetics. 2011;43(7):699-705.
64. Clavaguera F, Akatsu H, Fraser G, Crowther RA, Frank S, Hench J, et al. Brain homogenates from human tauopathies induce tau inclusions in mouse brain. Proceedings of the National Academy of Sciences. 2013;110(23):9535-40.
65. Iba M, Guo JL, McBride JD, Zhang B, Trojanowski JQ, Lee VM. Synthetic tau fibrils mediate transmission of neurofibrillary tangles in a transgenic mouse model of Alzheimer's-like tauopathy. The Journal of neuroscience : the official journal of the Society for Neuroscience. 2013;33(3):1024-37.
66. SantaCruz K. Tau Suppression in a Neurodegenerative Mouse Model Improves Memory Function. Science. 2005;309(5733):476-81.
67. Hochgrafe K, Sydow A, Mandelkow EM. Regulatable transgenic mouse models of Alzheimer disease: onset, reversibility and spreading of Tau pathology. The FEBS journal. 2013;280(18):4371-81.
68. Engel T, Hernandez F, Avila J, Lucas JJ. Full reversal of Alzheimer's disease-like phenotype in a mouse model with conditional overexpression of glycogen synthase kinase-3. The Journal of neuroscience : the official journal of the Society for Neuroscience. 2006;26(19):5083-90.
69. Morris M, Hamto P, Adame A, Devidze N, Masliah E, Mucke L. Age-appropriate cognition and subtle dopamine-independent motor deficits in aged Tau knockout mice. Neurobiology of aging. 2013;34(6):1523-9.
70. de Fougerolles AR. Delivery vehicles for small interfering RNA in vivo. Human gene therapy. 2008;19(2):125-32.
71. Dorn G, Patel S, Wotherspoon G, Hemmings-Mieszczak M, Barclay J, Natt FJ, et al. siRNA relieves chronic neuropathic pain. Nucleic acids research. 2004;32(5):e49.
72. Thakker DR, Natt F, Husken D, Maier R, Muller M, van der Putten H, et al. Neurochemical and behavioral consequences of widespread gene knockdown in the adult mouse brain by using nonviral RNA interference. Proceedings of the National Academy of Sciences of the United States of America. 2004;101(49):17270-5.
73. Piedrahita D, Hernandez I, Lopez-Tobon A, Fedorov D, Obara B, Manjunath BS, et al. Silencing of CDK5 reduces neurofibrillary tangles in transgenic alzheimer's mice. The Journal of neuroscience : the official journal of the Society for Neuroscience. 2010;30(42):13966-76.
74. Bugiani O, Murrell JR, Giaccone G, Hasegawa M, Ghigo G, Tabaton M, et al. Frontotemporal dementia and corticobasal degeneration in a family with a P301S mutation in tau. Journal of neuropathology and experimental neurology. 1999;58(6):667-77.

75. Allen B, Ingram E, Takao M, Smith MJ, Jakes R, Virdee K, et al. Abundant tau filaments and nonapoptotic neurodegeneration in transgenic mice expressing human P301S tau protein. The Journal of neuroscience : the official journal of the Society for Neuroscience. 2002;22(21):9340-51.
76. Delobel P, Lavenir I, Fraser G, Ingram E, Holzer M, Ghetti B, et al. Analysis of tau phosphorylation and truncation in a mouse model of human tauopathy. Am J Pathol. 2008;172(1):123-31.
77. Scattoni ML, Gasparini L, Alleva E, Goedert M, Calamandrei G, Spillantini MG. Early behavioural markers of disease in P301S tau transgenic mice. Behav Brain Res. 2010;208(1):250-7.
78. Krol J, Loedige I, Filipowicz W. The widespread regulation of microRNA biogenesis, function and decay. Nature reviews Genetics. 2010;11(9):597-610.
79. Carrington JC, Ambros V. Role of microRNAs in plant and animal development. Science. 2003;301(5631):336-8.
80. Chang CI, Yoo JW, Hong SW, Lee SE, Kang HS, Sun X, et al. Asymmetric shorter-duplex siRNA structures trigger efficient gene silencing with reduced nonspecific effects. Molecular therapy : the journal of the American Society of Gene Therapy. 2009;17(4):725-32.
81. Kurreck J. siRNA efficiency: structure or sequence-that is the question. Journal of biomedicine & biotechnology. 2006;2006(4):83757.
82. Ramachandran PS, Keiser MS, Davidson BL. Recent advances in RNA interference therapeutics for CNS diseases. Neurotherapeutics : the journal of the American Society for Experimental NeuroTherapeutics. 2013;10(3):473-85.
83. Walton SP, Wu M, Gredell JA, Chan C. Designing highly active siRNAs for therapeutic applications. The FEBS journal. 2010;277(23):4806-13.
84. Alexopoulou L, Holt AC, Medzhitov R, Flavell RA. Recognition of double-stranded RNA and activation of NF-kappaB by Toll-like receptor 3. Nature. 2001;413(6857):732-8.
85. Whitehead KA, Langer R, Anderson DG. Knocking down barriers: advances in siRNA delivery. Nature reviews Drug discovery. 2009;8(2):129-38.
86. Culmsee C, Gerling N, Lehmann M, Nikolova-Karakashian M, Prehn JH, Mattson MP, et al. Nerve growth factor survival signaling in cultured hippocampal neurons is mediated through TrkA and requires the common neurotrophin receptor P75. Neuroscience. 2002;115(4):1089-108.
87. Hollerhage M, Goebel JN, de Andrade A, Hildebrandt T, Dolga A, Culmsee C, et al. Trifluoperazine rescues human dopaminergic cells from wild-type alpha-synuclein-induced toxicity. Neurobiology of aging. 2014;35(7):1700-11.
88. Franklin KBJ PG. The mouse brain in stereotaxic coordinates. 2nd ed. San Diego, CA: Academic Press; 1997.
89. Boekhoorn K, Terwel D, Biemans B, Borghgraef P, Wiegert O, Ramakers GJ, et al. Improved long-term potentiation and memory in young tau-P301L transgenic mice before onset of hyperphosphorylation and tauopathy. The Journal of neuroscience : the official journal of the Society for Neuroscience. 2006;26(13):3514-23.

90. Ikeda M, Shoji M, Kawarai T, Kawarabayashi T, Matsubara E, Murakami T, et al. Accumulation of filamentous tau in the cerebral cortex of human tau R406W transgenic mice. Am J Pathol. 2005;166(2):521-31.
91. Dumont M, Stack C, Elipenahli C, Jainuddin S, Gerges M, Starkova NN, et al. Behavioral deficit, oxidative stress, and mitochondrial dysfunction precede tau pathology in P301S transgenic mice. FASEB journal : official publication of the Federation of American Societies for Experimental Biology. 2011;25(11):4063-72.
92. Li X, Kumar Y, Zempel H, Mandelkow EM, Biernat J, Mandelkow E. Novel diffusion barrier for axonal retention of Tau in neurons and its failure in neurodegeneration. The EMBO journal. 2011;30(23):4825-37.
93. Eckermann K, Mocanu MM, Khlistunova I, Biernat J, Nissen A, Hofmann A, et al. The beta-propensity of Tau determines aggregation and synaptic loss in inducible mouse models of tauopathy. The Journal of biological chemistry. 2007;282(43):31755-65.
94. Mocanu MM, Nissen A, Eckermann K, Khlistunova I, Biernat J, Drexler D, et al. The potential for beta-structure in the repeat domain of tau protein determines aggregation, synaptic decay, neuronal loss, and coassembly with endogenous Tau in inducible mouse models of tauopathy. The Journal of neuroscience : the official journal of the Society for Neuroscience. 2008;28(3):737-48.
95. Ittner LM, Ke YD, Delerue F, Bi M, Gladbach A, van Eersel J, et al. Dendritic function of tau mediates amyloid-beta toxicity in Alzheimer's disease mouse models. Cell. 2010;142(3):387-97.
96. Zito K, Scheuss V, Knott G, Hill T, Svoboda K. Rapid functional maturation of nascent dendritic spines. Neuron. 2009;61(2):247-58.
97. Kasai H, Fukuda M, Watanabe S, Hayashi-Takagi A, Noguchi J. Structural dynamics of dendritic spines in memory and cognition. Trends in neurosciences. 2010;33(3):121-9.
98. Zempel H, Thies E, Mandelkow E, Mandelkow EM. Abeta oligomers cause localized Ca(2+) elevation, missorting of endogenous Tau into dendrites, Tau phosphorylation, and destruction of microtubules and spines. The Journal of neuroscience : the official journal of the Society for Neuroscience. 2010;30(36):11938-50.
99. Perez-Cruz C, Nolte MW, van Gaalen MM, Rustay NR, Termont A, Tanghe A, et al. Reduced Spine Density in Specific Regions of CA1 Pyramidal Neurons in Two Transgenic Mouse Models of Alzheimer's Disease. Journal of Neuroscience. 2011;31(10):3926-34.
100. Kremer A, Maurin H, Demedts D, Devijver H, Borghgraef P, Van Leuven F. Early improved and late defective cognition is reflected by dendritic spines in Tau.P301L mice. The Journal of neuroscience : the official journal of the Society for Neuroscience. 2011;31(49):18036-47.
101. Ricobaraza A, Cuadrado-Tejedor M, Marco S, Pérez-Otaño I, García-Osta A. Phenylbutyrate rescues dendritic spine loss associated with memory deficits in a mouse model of Alzheimer disease. Hippocampus. 2012;22(5):1040-50.
102. Yang G, Pan F, Gan WB. Stably maintained dendritic spines are associated with lifelong memories. Nature. 2009;462(7275):920-4.

103. Xu T, Yu X, Perlik AJ, Tobin WF, Zweig JA, Tennant K, et al. Rapid formation and selective stabilization of synapses for enduring motor memories. Nature. 2009;462(7275):915-9.
104. Kim JW, Zhang YH, Zern MA, Rossi JJ, Wu J. Short hairpin RNA causes the methylation of transforming growth factor-beta receptor II promoter and silencing of the target gene in rat hepatic stellate cells. Biochemical and biophysical research communications. 2007;359(2):292-7.
105. Raoul C, Abbas-Terki T, Bensadoun JC, Guillot S, Haase G, Szulc J, et al. Lentiviral-mediated silencing of SOD1 through RNA interference retards disease onset and progression in a mouse model of ALS. Nature medicine. 2005;11(4):423-8.
106. Aigner A. Gene silencing through RNA interference (RNAi) in vivo: strategies based on the direct application of siRNAs. Journal of biotechnology. 2006;124(1):12-25.
107. Boudreau RL, Spengler RM, Davidson BL. Rational design of therapeutic siRNAs: minimizing off-targeting potential to improve the safety of RNAi therapy for Huntington's disease. Molecular therapy : the journal of the American Society of Gene Therapy. 2011;19(12):2169-77.
108. Vandenberghe LH, Xiao R, Lock M, Lin J, Korn M, Wilson JM. Efficient serotype-dependent release of functional vector into the culture medium during adeno-associated virus manufacturing. Human gene therapy. 2010;21(10):1251-7.
109. Anderson RD, Haskell RE, Xia H, Roessler BJ, Davidson BL. A simple method for the rapid generation of recombinant adenovirus vectors. Gene therapy. 2000;7(12):1034-8.
110. Miller VM, Gouvion CM, Davidson BL, Paulson HL. Targeting Alzheimer's disease genes with RNA interference: an efficient strategy for silencing mutant alleles. Nucleic acids research. 2004;32(2):661-8.
111. Grzelinski M, Urban-Klein B, Martens T, Lamszus K, Bakowsky U, Hobel S, et al. RNA interference-mediated gene silencing of pleiotrophin through polyethylenimine-complexed small interfering RNAs in vivo exerts antitumoral effects in glioblastoma xenografts. Human gene therapy. 2006;17(7):751-66.
112. Lim J, Simanek EE. Triazine dendrimers as drug delivery systems: from synthesis to therapy. Advanced drug delivery reviews. 2012;64(9):826-35.
113. Gomez D, Kessler K, Michel JB, Vranckx R. Modifications of chromatin dynamics control Smad2 pathway activation in aneurysmal smooth muscle cells. Circulation research. 2013;113(7):881-90.
114. Jiang S, Park DW, Stigler WS, Creighton J, Ravi S, Darley-Usmar V, et al. Mitochondria and AMP-activated protein kinase-dependent mechanism of efferocytosis. The Journal of biological chemistry. 2013;288(36):26013-26.
115. Nakajima H, Kubo T, Semi Y, Itakura M, Kuwamura M, Izawa T, et al. A rapid, targeted, neuron-selective, in vivo knockdown following a single intracerebroventricular injection of a novel chemically modified siRNA in the adult rat brain. Journal of biotechnology. 2012;157(2):326-33.
116. Bellucci A, Westwood AJ, Ingram E, Casamenti F, Goedert M, Spillantini MG. Induction of inflammatory mediators and microglial activation in mice transgenic for mutant human P301S tau protein. Am J Pathol. 2004;165(5):1643-52.

10 APPENDIX

10.1 Experimental Materials

10.1.1 Chemicals and Kits

Table 1.1. Chemicals, solutions and materials

Name	Catalog Number	Company
3-(4, 5-dimethylthiazol-2-yl)-2, 5-diphenyltetrazolium bromide	M2128	Sigma-Aldrich, St. Louis, MO
3, 3'-diaminobenzidine	18865	SERVA Electrophoresis, Heidelberg, Germany
4-(2-hydroxyethyl)-1-piperazineethanesulfonic acid	H3375	Sigma-Aldrich, St. Louis, MO
4',6-diamidino-2-phenylindole	62248	Thermo Fisher Scientific, Waltham, MA
5M NaCl solution	71386	Sigma-Aldrich, St. Louis, MO
Agarose	A9539	Sigma-Aldrich, St. Louis, MO
Ammonium persulfate	9592	Carl Roth, Karlsruhe, Germany
B-27	1.8E+07	Life technologies, Carlsbad, CA
Cytosine arabinoside	C3350000	Sigma-Aldrich, St. Louis, MO
Click-iT® TUNEL assay kit	C10246	Life technologies, Carlsbad, CA

DEPC-water	750023	Life technologies, Carlsbad, CA
Dimethyl sulfoxide	D8418	Sigma-Aldrich, St. Louis, MO
DL-Dithiotreitol	43819	Sigma-Aldrich, St. Louis, MO
D-Manitol	M1902	Sigma-Aldrich, St. Louis, MO
ECL western blotting substrate	32106	Thermo Fisher Scientific, Waltham, MA
Ethylene glycol tetraacetic acid	3777	Sigma-Aldrich, St. Louis, MO
Ethylene diamine tetraacetic acid	EDS	Sigma-Aldrich, St. Louis, MO
Eukitt® quick-hardening mounting medium	3989	Sigma-Aldrich, St. Louis, MO
Gentamycin	G1914	Sigma-Aldrich, St. Louis, MO
GolgiStain™ kit	PK401	FD NeuroTechnologies, Columbia, MD
Hank's balanced salt solution	14180046	Life technologies, Carlsbad, CA
Isoflurane	CDS019936	Sigma-Aldrich, St. Louis, MO
Ketamine	LO35/7	Pharmacia GmbH, Berlin, Germany
L-glutamine	49419	Sigma-Aldrich, St. Louis, MO
Methanol	34860	Sigma-Aldrich, St. Louis, MO

Micro BCA protein assay kit	23235	Thermo Fisher Scientific, Waltham, MA
Normal donkey serum	S30	Millipore, Billerica, MA
Normal goat serum	S-1000	Vector, Burlingame, CA
Nucleospin® RNA II kit	740955	Machery-Nagel, Dueren, Germany
Page ruler plus pre-stained protein ladder	26619	Thermo Fisher Scientific, Waltham, MA
Paraformaldehyde	158127	Sigma-Aldrich, St. Louis, MO
Pentobarbital	N.A.	Wirtschaftsgenossenschaft deutscher Tierärzte e. G.,Garbsen, Germany
Phenol red	P3532	Sigma-Aldrich, St. Louis, MO
Phosphatase inhibitor	78420	Thermo Fisher Scientific, Waltham, MA
Polyethyleneimine	764604	Sigma-Aldrich, St. Louis, MO
Polyvinylidene fluoride membranes	162-0177	Bio-Rad Laboratories, Hercules, CA
Protease inhibitor	78429	Thermo Fisher Scientific, Waltham, MA
Rotiphorese® Gel 30	3029	Carl Roth, Karlsruhe, Germany
Skim milk powder	70166	Sigma-Aldrich, St. Louis, MO

Sodium chloride	S7653	Sigma-Aldrich, St. Louis, MO
Sodium dodecyl sulfate	L3771	Sigma-Aldrich, St. Louis, MO
Sucrose	4621	Carl Roth, Karlsruhe, Germany
SuperScript® III One-Step RT-PCR System	12574-026	Life technologies, Carlsbad, CA
SYBR® Safe	S33102	Life technologies, Carlsbad, CA
Tagman® Universal Master Mix II with UNG	4440038	Life technologies, Carlsbad, CA
Tris-base	T1503	Sigma-Aldrich, St. Louis, MO
Tris-HCl	T5941	Sigma-Aldrich, St. Louis, MO
Triton X-100	T8787	Sigma-Aldrich, St. Louis, MO
Trypsin	T2600000	Sigma-Aldrich, St. Louis, MO
Tween-20	P9416	Sigma-Aldrich, St. Louis, MO
Xylazine hydrochloride	7916440	Bayer Healthcare, Leverkusen, Germany

10.1.2 **Buffers and Solutions**

Table 1.2. Buffers and solutions

0.1 M PB	
Na_2HPO4	20.68 g
NaH_2PO4	3.18 g
Adjust pH to 7.4	
1 x PBS, pH 7.4	
NaCl	9 g
Na_2HPO_4	0.527 g
KH_2PO_4	0.144 g
ddH_2O	1000 mL
Adjust pH to 7.4	
1 x TBS/Tween 20	
Tris-base	2.42 g
Sodium chloride	29.2 g
Tween 20	0.5 mL
ddH_2O	1000 mL
0.5 M Tris, pH 6.8	
Tris-HCl	Tris-HCl

ddH_2O	ddH2O
Adjust pH to 6.8	
1.5 M Tris pH 8.8	
Tris-HCl	23.6 g
ddH_2O	100 mL
Adjust pH to 8.8	
1x Electrophoresis Buffer	
Tris-base	3 g
Glycine	14.4 g
SDS	1 g
ddH_2O	1000 mL
5 x SDS Loading Buffer	
1 M Tris-HCl, pH 6.8	7 mL
Glyerol	3 mL
SDS	1 g
DL-dithiotreitol	0.93 g
β-Mercaptoethanol	0.1 mL

Bromophenol blue sodium salt	1.2 mg
Transfer Buffer	
Tris-base	3 g
Glycine	14.4 g
Methanol (100 %)	100 mL
ddH_2O	1000 mL
5 % Blocking Buffer	
Skim milk powder	5 g
1X TBS	100 mL
Stripping Buffer	
Glycine	15 g
SDS	1 g
Tween 20	10 mL
ddH_2O	1000mL
pH = 2.2	
Protein Extraction Buffer	
D-Manitol	0.25 M

Tris-HCl	0.05 M
Ethylene diamine tetraacetic acid	1 mM
Ethylene glycol tetraacetic acid	1 mM
DL-dithiotreitol	1 mM
Triton X-100	10 µL/mL
Protease inhibitor	1:100
Phosphatase inhibitor	1:100
pH = 7.8	
Neurobasal Medium	
4-(2-hydroxyethyl)-1-piperazineethanesulfonic acid	4.82 mM
L-glutamine	0.11 mM
Gentamycin	21 µM
B-27	1:1000
Phenol red	28 µM
pH = 7.2	
SDS-PAGE	

	10 % Separating Gel	4 % Stacking Gel
ddH2O	4	6.1
1.5 M Tris, pH 8.8	2.5	X
0.5 M Tris, pH 6.8	X	2.5
SDS 10 %	0.100	0.1
Rotiphorese® Gel 30	3.34	1.3
10 % APS	0.05	0.05
TEMED	0.01	0.02
Total (mL)	10	10

10.1.3 **Primer for RT-PCR**

Table 1.3. Primers and programs for RT-PCR

Gene Name	GenBank Accession	Sequence	Program	Product length (nt)
Human MAPT	NM_005910.4	Forward: TGACACGGACGCTGGCCTGAA Backward: CACTTGGAGGTCACCTTGCTC	60 °C/30 min; 94 °C/3 min; 30× (94 °C/1 min; 66 °C/1 min; 68 °C/2 min); 68 °C/10 min; 4 °C/∞	855
Mouse Gapd	M32599.1	Forward: AGGCCGGTGCTGAGTATGTC Backward: TGCCTGCTTCACCACCTTCT	60 °C/30 min; 95 °C/2 min; 30× (95 °C/30 sec; 57 °C/1 min; 70 °C/2 min); 70 °C/10 min; 4 °C/∞	530

10.1.4 **Primer for qPCR**

Table 1.4. Primers for qPCR

Gene Name	Assay ID	Company
MAPT	Hs00902194_m1	Life technologies, Carlsbad, CA

OAS1	Hs00973637_m1	Life technologies, Carlsbad, CA
PPiA	Hs04194521_s1	Life technologies, Carlsbad, CA
PPiB	Hs00168719_m1	Life technologies, Carlsbad, CA
GAPDH	Hs02758991_g1	Life technologies, Carlsbad, CA
PSMC1	Hs02386942_g1	Life technologies, Carlsbad, CA

Table 1.5. Accell siRNAs

Name	**Catalog Number**	**Company**
Accell™ SMART pool siRNAs (human MAPT)	E-012488-00-0005	Thermo Fisher Scientific, Waltham, MA
Accell™ Non-targeting Control Pool	D-001910-10	Thermo Fisher Scientific, Waltham, MA
Accell Green Non-targeting Control siRNA	D-001950-01	Thermo Fisher Scientific, Waltham, MA

10.1.5 **Antibodies**

Table 1.6. First antibodies

Name	Host/Class	Concen-tration	Catalog Number	Company
anti-MHC II	Rat/ Monoclonal	1:500	MABF33	Millipore, Billerica, MA
anti-GAPDH	Rabbit/Polyclonal	1:1000	ABS16	Millipore, Billerica, MA
anti-GFAP	Mouse/Monoclonal	1:1000	MA5-15086	Millipore, Billerica, MA
anti-Iba-1	Rabbit/Polyclonal	1:1000	019-19741	Wako Pure Chemical Industries, Chuo-ku, Japan
anti-NeuN	Rabbit/Polyclonal	1:1000	ABN78	Millipore, Billerica, MA
AT180	Mouse/Monoclonal	1:500	MN1040	Thermo scientific, Waltham, MA
CP13	Mouse/Monoclonal	1:500	N.A.	Albert Einstein College of Medicine, NY, NY
MC1	Mouse/Monoclonal	1:500	N.A.	Albert Einstein College of Medicine, NY, NY
HT7	Mouse/Monoclonal	1:1000	MN1000	Thermo Fisher Scientific, Waltham, MA

Table 1.7. Secondary antibodies

Name	Host/Conju-gation	Concen-tration	Catalog Number	Company
Anti-Mouse IgG	Goat/HRP	1:2000	sc-2005	Santa Cruz Biotechnology, Dallas, TX
Anti-Rabbit IgG	Goat/HRP	1:2000	sc-2004	Santa Cruz Biotechnology, Dallas, TX
Anti-Mouse IgG (H+L)	Donkey/ Biotin	1:1000	715-066-150	Jackson ImmunoResearch Europe, Suffolk, UK
Anti-Rabbit IgG (H+L)	Goat/ Biotin	1:1000	111-066-144	Jackson ImmunoResearch Europe, Suffolk, UK
Anti-mouse	Goat/Alexa 488	1:500	115-546-146	Jackson ImmunoResearch Europe, Suffolk, UK
Anti-rabbit Cy5	Donkey/ Cy5	1:500	111-175-144	Jackson ImmunoResearch Europe, Suffolk, UK

10.1.6 **Devices and Software**

Table 1.8. Software

Fiji Software	http://fiji.sc/Fiji
Imagelab™ Software	Bio-Rad Laboratories, Hercules, CA

Imaris Software	Bitplane, Zurich, Switzerland
Morris Water Maze System	Biobserve, St. Augustin, Germany
Novel Open Field System	Biobserve, St. Augustin, Germany
Sigmaplot Standard Statistical Software Package	Systat Software, Chicago, IL
Stereo-investigator Software	MicroBrightField, Inc., Williston, VT, USA
TSE Rotarod System	Sophisticated life Science Research Instrumentation, Bad Homburg, Germany
Viewer^2 Software	Biobserve, St. Augustin, Germany

Table 1.9. Devices

ChemiDOC XRS+	Bio-Rad Laboratories, Hercules, CA
Confocal Leica TCS SP5 II	Leica, Wetzlar, Germany
Cryomicrotome-CM3050 S	Leica, Wetzlar, Germany
E-330 Camera	Olympus, Orimpasu Kabushiki-Gaisha, Japan
Fully Automated Inverted Research Microscope DMI6000 B	Leica, Wetzlar, Germany

Heracell 150i CO2 Incubator	Thermo Fisher Scientific, Waltham, MA
HERAEUS Fresco 17 Centrifuge	Thermo Fisher Scientific, Waltham, MA
HERAEUS Megafuge 16 Centrifuge	Thermo Fisher Scientific, Waltham, MA
HERAfreeze® BASIC SI -86 ºC	Thermo Fisher Scientific, Waltham, MA
Labcycler Gradient	SENSOQuest, Germany
Microinjection Syringe	World Precision Instruments, Sarasota, FL
Microplate Reader	FLUOstar Omega, BMG LABTECH, Ortenberg, Germany
Mini Trans-Blot® Cell	Bio-Rad Laboratories, Hercules, CA
PowerPac™ HC Power Supply	Bio-Rad Laboratories, Hercules, CA
Stereotactic Frame	David Kopf Instruments, Tujunga, CA
Stereo-investigator	MicroBrightField, Inc., Williston, VT, USA
Thermomixer Comfort	Eppendorf, Germany
Trans-Blot Turbo	Bio-Rad Laboratories, Hercules, CA
UltraRocker Rocking Platform	Bio-Rad Laboratories, Hercules, CA
Vortex Genie 2	Scientific Industries, USA

10.2 Curriculum Vitea

Personal Information

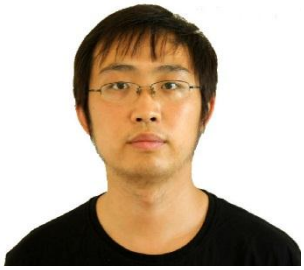

Name: Hong Xu
Sex: Male
Born: November 26th, 1983
Citizenship: PR. China
Email: hong.xu@dzne.de
Address:Max-Lebsche-Platz 30, 81377

Education

09/2006-03/2009:
School of Life Science and Technology, Tongji University, Shanghai, P.R.China.
Major: Biochemistry and Molecular Biology
Degree: Master of Science

09/2002-07/2006:
School of Resource, Southwestern Forestry College, Yunnan Province, P.R. China,
Major: Biotechnology
Degree: Bachelor of Science

Research Experiences

09/2011-Present:
German Center for Neurodegenerative Diseases e.V. (DZNE) Technical University Munich (TUM) Dept. for Translational Neurodegeneration, München, Germany.
Supervisor: Prof. Dr. Günter U. Höglinger
PhD Thesis: siRNA as therapeutic Strategy by neurodegenerative disease

04/2010-09/2011:
Marburg University, Marburg, Germany.
Supervisor: Prof. Dr. Günter U. Höglinger
PhD Thesis: siRNA as therapeutic Strategy by neurodegenerative disease

09/2006-03/2009:
Institute of Protein Research, Tongji University, Shanghai, China.
Supervisor: Prof. Shilong Wang
Master Thesis: HIV Polypeptide Inhibitor.

12/2005~06/2006:

School of Resource, Southwestern Forestry College, Yunnan Province, P.R. China

Supervisor: Dr. De He
Bachelor project: Distribution of Topo II in Three Life Domains.

Congress and training

11/2014: Annual conference of society for neuroscience, Washington DC, USA

06/2014: The Movement Disorder Society's (MDS) 18th International Congress of Parkinson's Disease and Movement Disorders, Stockholm, Sweden

06/2013: The Movement Disorder Society's (MDS) 17th International Congress of Parkinson's Disease and Movement Disorders, Sydney, Australia

03/2013: Deutscher Parkinson Kongress 2013, Würzburg, Germany

07/2012: "100 years of lewy bodies-where are we now?" Congress, Munich, Germany

11/2010: "Neurowind", Berlin, Germany

07/2008-09/2008: Training on the Technology of Biology Shanghai Centers for Disease Control and Prevention HIV pseudovirus fusion experiment, Shanghai, P.R.China

05/2007-06/2007: Training on the Technology of Biology Institute of Biochemistry and Cell Biology, Chinese Academy of Sciences, Protein separation and purification, Shanghai, P.R.China

Language
Chinese: Native
English: Fluent
German: Basic

10.3 List of publications

Articles:

1. Xu H, Roesler TW, Carlsson T, de Andrade A, Bruch J, Hoellerhage M, Oertel WH, Hoeglinger GU. Memory Deficits Correlate with Tau and Spine Pathology in P301S MAPT Transgenic Mice. Neuropathology and applied neurobiology. 2014 Dec; 40(7):833-43. doi: 10.1111/nan.12160.

2. Xu H, Roesler TW, Carlsson T, de Andrade A, Fiala O, Hoellerhage M, Oertel WH, Goedert M, Aigner A, Hoeglinger GU. Tau Silencing by siRNA in the P301S Mouse Model of Tauopathy. Current Gene Therapy. 2014: in press.

3. Bruch J*, Xu H*, de Andrade A, Höglinger GU, Mitochondrial Complex 1 Inhibition Increases 4-Repeat Isoform Tau by SRSF2 Upregulation. PLoS One. 2014 Nov 17;9(11):e113070. doi: 10.1371/journal.pone.0113070. * These authors contributed equally to the work

4. Hoellerhage M, Deck R, de Andrade A, Xu H, Roesler TW, Mohamed S, Carlsson T, Yamada ES, Seham A, Goedert M, Oertel WH, Hoeglinger GU. Piericidin A Aggravates Tau Pathology in P301S Transgenic Mice. PLoS ONE, 2014: in press.

Abstracts:

1. Xu H, Rösler TW, Carlsson T, Oertel WH, Höglinger GU. Memory Deficits correlate with tau and spine pathology. 44th Annual Conference of Society for Neuroscience, Washington DC, USA. 2014 December 15-19. Abstract no. 4080.

2. Xu H, de Andrade A, Carlsson T, Oertel WH, Rösler TW, Höglinger GU. Memory Deficits Correlate with Tau and Spine Pathology in P301S MAPT Transgenic Mice. The Movement Disorder Society's (MDS) 18th International Congress of Parkinson's Disease and Movement Disorders, Stockholm, Sweden. 2014 June 8-12. Abstract no. 550531.

3. Xu H, de Andrade A, Carlsson T, Oertel WH, Rösler TW, Höglinger GU. Intracerebral siRNA Injection in the P301S Transgenic Mouse Model. The Movement Disorder Society's (MDS) 17th International Congress of Parkinson's Disease and Movement Disorders, Sydney, Australia. 2013 June 16-20. Abstract no. 550927.

Neuropathology and Applied Neurobiology (2014), **40**, 833–843 doi: 10.1111/nan.12160

Memory deficits correlate with tau and spine pathology in P301S *MAPT* transgenic mice

H. Xu*†, T. W. Röslert, T. Carlsson‡§, A. de Andrade†§, J. Bruch*†, M. Höllerhage*, W. H. Oertel§ and G. U. Höglinger*†§

**Department of Neurology, Technical University Munich, †Department of Translational Neurodegeneration, German Center for Neurodegenerative Diseases (DZNE), Munich, §Department of Neurology, Philipps-University, Marburg, Germany, and ‡Department of Pharmacology, Institute of Neuroscience and Physiology, Sahlgrenska Academy, University of Gothenburg, Gothenburg, Sweden*

H. Xu, T. W. Rösler, T. Carlsson, A. de Andrade, J. Bruch, M. Höllerhage, W. H. Oertel and G. U. Höglinger (2014) *Neuropathology and Applied Neurobiology* **40**, 833–843
Memory deficits correlate with tau and spine pathology in P301S *MAPT* transgenic mice

Aim: P301S *MAPT* transgenic mice (P301S mice) are a widely used model of frontotemporal dementia and parkinsonism linked to chromosome 17 with tau pathology (FTDP-17-tau). However, a systematic correlation between cognitive deficits and cellular tau pathology at different ages is still missing. Therefore, our study investigated memory deficits of P301S mice in relation to pathological tau species and dendritic spine pathology throughout adulthood. **Methods:** We analysed P301S mice behaviourally with the novel open field, rotarod, and Morris water maze tests to measure deficits in locomotion, balance and cognition, respectively; immunohistochemically with different tau antibodies for specific tau species; and with Golgi staining for dendritic spine pathology. **Results:** We confirmed the occurrence of locomotor deficits at an age of 5 months and newly report memory deficits from 2.5 months of age onwards. At this early age, MC1 and CP13, but not AT180 immunoreactivity, was prominent in the hippocampus of P301S mice. Neuronal cell loss in the hippocampus of P301S mice was not observed to occur till 6 months of age. However, there was a significant reduction in the density of dendritic spines from young adulthood onwards in hippocampal pyramidal neurones. **Conclusion:** In P301S mice, memory deficits precede the onset of locomotor dysfunction and coincide with the appearance of conformationally changed, S202-phosphorylated tau and reduced spine density in the absence of neuronal cell loss in the hippocampus. Our finding provides insights into the toxic effects of different tau species *in vivo* and may facilitate the development of new therapies against neurodegenerative tauopathies.

Keywords: dendritic spine, FTDP-17-tau, memory deficit, P301S transgenic mouse, tau, tauopathy

Introduction

The microtubule-associated protein tau is abundantly expressed in the central nervous system and has been linked to the pathology of several neurodegenerative diseases, jointly termed tauopathies. Tau was found to participate in stabilizing and assembling microtubules [1], however, until today the full physiological function of tau remains unknown. In adult neuronal cells, mainly six isoforms of tau exist in a homeostatic balance [2]. Mutations of the tau encoding gene (*MAPT*), altered isoform expression, hyperphosphorylation or conformational changes of the tau protein can disturb the physiological balance, leading to tau pathologies [3]. Tauopathies can show diverse clinical phenotypes ranging from dementia

Correspondence: Günter U. Höglinger, Department of Translational Neurodegeneration, German Center for Neurodegenerative Diseases (DZNE), Max-Lebsche-Platz 30, 81377 Munich, Germany. Tel: +49 89 44007 8406; Fax: +49 89 44007 8420; E-mail: guenter.hoeglinger@dzne.de

to movement disorders [4]. Despite this variability, tau is the convergence point behind these multiple diseases which makes it an attractive target for therapy. The hereditary tauopathy FTDP-17-tau is caused by *MAPT* mutations and is clinically characterized by behavioural disturbance, cognitive impairment and parkinsonism. The P301S mutation was found in an early onset FTDP-17-tau patient [5]. To study the effect of this mutation, P301S mice were constructed to overexpress 0N4R human P301S mutant tau under the murine thy1 promoter. This model shows ultrastructural and biochemical similarities to human tauopathies in the brain and spinal cord, with an increase of insoluble tau from 5 months of age onwards [6,7]. The appearance of insoluble tau and neuronal cell loss in the anterior horn of the spinal cord were found to coincide with the onset of a hind limb motor phenotype at 5 months of age [8].

In some tauopathies, atrophy and structural changes have been reported in the hippocampus which is known to play a role in encoding information before memory formation [9,10]. Hippocampal neurones have protrusions from the surface of neuronal dendrites which are called dendritic spines. They receive excitatory inputs from afferent synapses. Abnormalities in the formation, plasticity and maintenance of dendritic spines have been described in human brain disorders including tauopathies with dementia and cognitive impairment [11,12]. Importantly, reduced spine density in the CA1 region of the hippocampus was found in mouse models of Alzheimer's disease, and a rescue of dendritic spine loss could reverse the cognitive impairment [13,14].

As memory deficits and hippocampal structural abnormalities have so far not been reported in P301S mice, we aimed to search for hippocampal structural deficits and to correlate these with the onset of behavioural deficits. We also aimed at relating the occurrence of different tau species (phosphorylated, conformationally changed) to the onset of structural alterations and behavioural deficits.

Material and methods

Mice

Homozygous transgenic mice overexpressing human tau with the P301S mutation on a C57BL/6 background, originally developed by Michel Goedert (University of Cambridge, UK) [6] and wild type C57BL/6 controls were used. Animals were kept at 23 ± 1°C under standard 12 h light-dark cycle with free access to food and water. They were handled according to the EU Council Directive 2010/63/EU, the Guide for the Care and Use of Laboratory Animals (National Research Council 2011) and the guidelines of the local institutional committee.

Behavioural experiments

A schematic time course of the behavioural tests is shown in Figure 1**A**. Nineteen P301S mice were investigated monthly with the rotarod test from 2 to 6 months of age. Fifteen P301S mice were subjected monthly to the novel open field from 2 to 6 months of age and to the Morris water maze test at 2.5 and 5.5 months. The same numbers of the wild type mice were taken as controls for all testing sessions and time points.

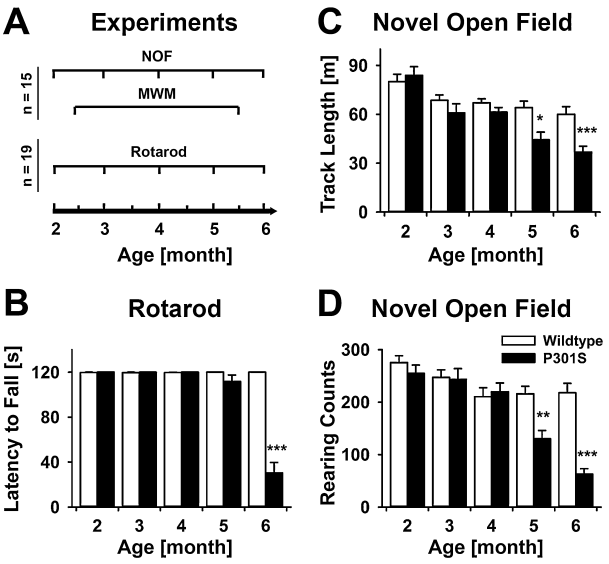

Figure 1. Behavioural deficits of the P301S mice between 2 and 6 months of age. (**A**) Schematic diagram of the experimental schedule. Nineteen P301S mice underwent the rotarod test every month from 2 to 6 months of age. Fifteen P301S mice underwent the novel open field test monthly from 2 to 6 months of age and the Morris water maze test at 2.5 and 5.5 months of age. Same numbers of wild type mice were taken as controls. (**B**) Compared with wild type mice, P301S mice showed a shorter latency to fall at 6 months of age in the rotarod test. (**C**,**D**) Reduced exploratory activity of the P301S mice was detected by shorter track length (**C**) and less rearing counts (**D**) compared to wild type mice at month 5 and 6. Data are presented as mean + SEM. P301S mice *vs.* wild type mice, paired *t*-test, $^{*}P < 0.05$, $^{**}P < 0.01$, $^{***}P < 0.001$.

Novel open field

For the investigation of locomotor activity and the willingness to explore, each mouse ($n = 15$ per group) was tested at 2, 3, 4, 5 and 6 months of age in a 32 cm × 32 cm box for 30 min under dim light (2.0 lux). A video tracking system (Biobserve, St. Augustin, Germany) was used to record track length. The rearing times were detected by sensors at a height of 8 cm from the bottom of the boxes and recorded by the Viewer2 software (Biobserve).

Rotarod

To monitor balancing ability, a rotarod system (TSE Systems, Bad Homburg, Germany) was used at 2, 3, 4, 5 and 6 months of age. Each mouse ($n = 19$ per group) was placed on a rod (diameter 30 mm), which rotated at a constant speed of 10 rpm for a maximum of 2 min. When a mouse fell down, it interrupted the light beams at the bottom of the chamber. The latency to fall was recorded. One day before testing, mice were given four trials of training to familiarize them with the test situation.

Morris water maze

To analyse spatial learning and memory, the Morris water maze test was performed at 2.5 and 5.5 months of age ($n = 15$ per group) in a cylindrical water basin (diameter 120 cm) filled with water to a depth of 31 cm. The water was dyed with tasteless and odourless non-dairy creamer. A platform (diameter 12 cm) was hidden 1 cm below the water surface. Four large signs were placed on one each wall of the room as visual cues. The whole test procedure consisted of 3-day pre-training, 4-day training and 1-day probe trial. During the pre-training period, mice had 6 test runs with visible platform on the first day, followed by 6 runs each on day 2 and 3 with a hidden platform. One run lasted a maximum of 2 min. Mice that did not find the platform were gently guided to the platform and allowed to stay on it for at least 15 s. During pre-training, the position of the platform varied from day to day. During the training period, mice had one trial per day to find the hidden platform in a fixed position within 1 min on four consecutive days. In the probe trial 1 day thereafter, each mouse was placed in the tank without the platform for 1 min to swim freely. The positions of the platform during the training period were changed randomly for the two testing session at 2.5 and 5.5 months. Tracks of training and probe trial were recorded with the Viewer2 software (Biobserve).

Tissue extraction and immunoblot

2- and 6-month-old P301S mice ($n = 3$ per group) were sacrificed by cervical dislocation. The brains were quickly removed and transferred to a Petri-dish containing ice-cold phosphate buffered saline. The hippocampi were dissected under a stereomicroscope (Leica, Wetzlar, Germany), homogenized in T-PER tissue protein extraction reagent (Thermo Fisher Scientific, Waltham, MA, USA) containing proteinase and phosphatase inhibitor cocktails (both 1:100, v/v, Thermo Fisher Scientific) and subsequently centrifuged for 30 min at 80 000 *g*. Supernatants were separated and taken as the soluble fraction. The pellets were extracted following the protocol described previously [7] with minor modifications. Briefly, the pellets were resuspended in extraction buffer (10 mM Tris-HCl, pH = 7.4, 0.8 M NaCl, 10% sucrose, 1:100, v/v, proteinase inhibitor cocktail, 1:100, v/v, phosphatase inhibitor cocktail) and centrifuged for 20 min at 4000 *g* to remove cell fragments. Sarkosyl (Sigma-Aldrich, St. Louis, MO, USA) was added to supernatants to 1% final concentration and incubated for 1.5 h at room temperature. Subsequently, the samples were centrifuged at 80 000 *g* for 30 min. The pellets were resuspended using the Tris-HCl solution (50 mM, pH = 7.4) to give the sarkosyl-insoluble fraction. Soluble and sarkoysl-insoluble fractions were separated by SDS-PAGE gel (Any kD Mini-PROTEAN TGX, Bio-Rad Laboratories, Hercules, CA, USA). Tau species were detected by AT180 (made in mouse, 1:1000, Thermo Fisher Scientific), CP13 and MC1 (both made in mouse, 1:1000, kindly provided by the Department of Pathology, Albert Einstein College of Medicine, New York, NY, USA) as primary antibodies and actin (made in goat, 1:1000, Santa Cruz Biotechnology, Santa Cruz, CA, USA) was used as control. Primary antibodies were revealed by peroxidase conjugated anti-mouse IgG secondary antibody (Vector Labs, Burlingame, CA, USA) and ECL prime solution (GE Healthcare, Cleveland, OH, USA). Images were taken by a gel-imager (Chemidoc™, Bio-Rad Laboratories) and analysed by the Imagelab™ software (Bio-Rad Laboratories). For relative signal quantification, the optical densities were normalized to actin and 6-month values were related to 2 months (set as 1).

Immunohistochemistry

P301S and wild type mice ($n \geq 3$ per group and time-point) were sacrificed at 2, 3, 4, 5 or 6 months of age by an intraperitoneal (i.p.) injection of pentobarbital (600 mg/kg). They were perfused transcardially with 0.1 M phosphate buffer for 2 min, then fixed for 10 min with 4% paraformaldehyde. Brains were removed from the skull and post-fixed in 4% paraformaldehyde at 4°C for 48 h and cryo-protected in 30% sucrose solution at 4°C. Brains were cut into 30-µm-thick coronal sections with a cryomicrotome (CM3050 S, Leica).

Free floating sections were immunostained with the following tau antibodies: AT180 (1:500); CP13 and MC1 (1:500). Neurons were immunostained with the anti-NeuN antibody (made in rabbit, 1:1000, Millipore, Darmstadt, Germany). Antibodies were diluted in normal donkey serum (Millipore) and incubated with the sections for 10 h at 4°C. The staining was revealed using biotinylated secondary antibodies (donkey anti-mouse, IgG (H+L), 1:1000, Jackson ImmunoResearch Europe, Suffolk, UK) and 3,3′-diaminobenzidine (SERVA Electrophoresis, Heidelberg, Germany) as substrate.

Microscopy

For optical density measurements, images of mouse brains were captured with a microscope (DM6000B, Leica) under controlled temperature and illumination. The grey value of the area of interest was measured with the Fiji software (http://fiji.sc/Fiji). The grey value measured in the corpus callosum, where no specific staining was observed, was taken as blank control in each individual animal.

Golgi staining and dendritic spine quantification

P301S and wild type mice ($n = 4$ per group) were sacrificed at 2.5 and 5.5 months of age by cervical dislocation. Brains were quickly removed and briefly cleaned with Millipore water. The GolgiStain™ kit (FD NeuroTechnologies, Columbia, MD, USA) was used following the manufacturer's guidelines. Briefly, the dissected brains were immediately impregnated in the solution for 14 days, cut on a cryomicrotome into 200-µm-thick coronal sections and later covered with Corbit-Balsam (Merck, Darmstadt, Germany). Dendritic spines were chosen from 2–3 basal and 2–3 apical dendrites of 10 Golgi-impregnated pyramidal neurons in the CA1 area of the hippocampus of each brain. Only secondary to quaternary branches of dendrites within a distance range of 30–120 µm from the cell body were analysed. Images were taken with a 63× immersion objective on a confocal microscope (DMi6000B + TCS SP5II, Leica) with an unbiased method by blinding the names of slices with random labels and removing labels after the quantification. Dendrites with more than 10 µm length were first reconstructed into 3D images and then quantified to calculate spine density, length, cross-sectional area and volume using Imaris software (Bitplane, Zurich, Switzerland).

Statistical analysis

All data are presented as means + standard error (SEM). Comparisons between groups were done by *t*-tests. Multiple comparisons were performed either by one-way ANOVA or repeated measures ANOVA, followed by Student–Newman–Keuls's *post hoc* test. Calculations were made with the Sigmaplot Standard Statistical Software Package (Systat Software, Chicago, IL, USA). A statistically significant difference was assumed at $P < 0.05$.

Results

Decline in balancing ability

The rotarod test (Figure 1**B**) demonstrated an abrupt decline of balancing ability in the P301S mice [RMANOVA, $F(4,72) = 69.566$, $P < 0.001$], when compared to wild type mice, at 6 months of age [paired $t(18) = 9.735$, $P < 0.001$].

Age-dependent decline in exploratory activity

The novel open field (Figure 1**C**) demonstrated a age-dependent decrease in exploratory activity (track length within 30 min) for both P301S mice [RMANOVA, $F(4,56) = 16.137$, $P < 0.001$] and wild type mice [RMANOVA, $F(4,56) = 4.512$, $P = 0.003$]. A reduction occurred in the P301S mice compared to the wild type mice at 5 and 6 months of age [P301S *vs*. wild type at: 5 months: paired $t(14) = 2.806$, $P = 0.014$; at 6 months: paired $t(14) = 4.643$, $P < 0.001$].

Also rearing counts (Figure 1**D**) showed an age-dependent decrease in both P301S mice [RMANOVA, $F(4,56) = 26.297$, $P < 0.001$] and wild type mice

[RMANOVA, $F(4,56) = 3.165$, $P = 0.020$]. The difference between P301S mice and wild type mice was significant at 5 and 6 months of age [P301S *vs.* wild type at: 5 months: paired $t(14) = 4.388$, $P = 0.001$; 6 months: paired $t(14) = 6.710$, $P < 0.001$].

Early onset of memory deficits

In the Morris water maze, P301S mice showed a worse learning curve than wild type mice at 2.5 months of age (Figure 2**A**). Over the 4-day training period, there was a training-day-dependent reduction of the latency to find the hidden platform for wild type mice [RMANOVA, $F(3,42) = 9.458$, $P < 0.001$], but not for the P301S mice [RMANOVA, $F(3,42) = 0.440$, $P = 0.726$], with differences between wild type mice and P301S mice being significant at day 4 [paired $t(14) = 2.280$, $P = 0.039$]. In the probe trial (Figure 2**B**), the target quadrant occupancy of the wild type mice was higher than that of the P301S mice [paired $t(15) = 3.286$, $P = 0.005$].

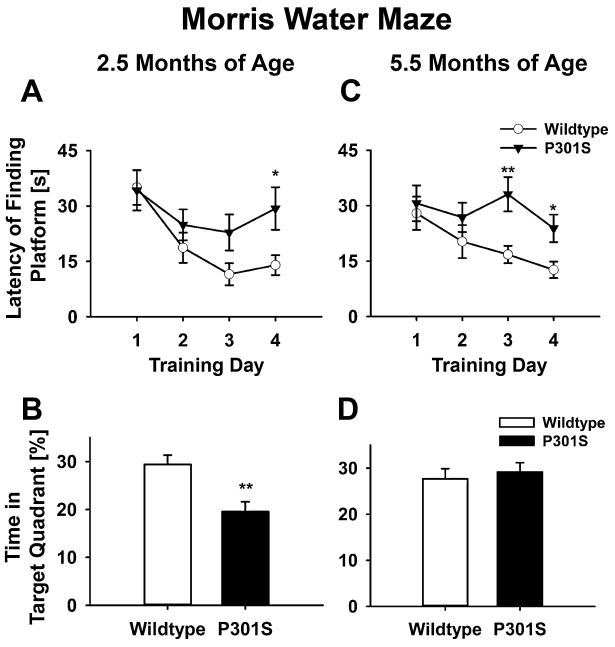

Figure 2. Memory deficits in P301S mice compared with the wild type mice in the Morris water maze. (**A**) At 2.5 months of age, P301S mice spent more time to find the platform after 4 days training compared to wild type mice. (**B**) At 2.5 months of age the P301S mice spent a shorter period of time in the target quadrant in the probe trial. (**C**) Again, at 5.5 months of age, P301S mice had a longer latency to find the platform than wild type mice. (**D**) However, no difference was found for the preference of the target quadrant between the two groups. Data are presented as mean + SEM. P301S mice *vs.* wild type mice, paired *t*-test, $^{*}P < 0.05$, $^{**}P < 0.01$.

Also at the age of 5.5 months, the learning curve for P301S mice was worse than that of wild type mice (Figure 2**C**). Again, a training-day-dependent improvement in the latency to find the platform was found in control mice [RMANOVA, $F(3,39) = 3.254$, $P = 0.032$], but not in P301S mice [RMANOVA, $F(3,39) = 0.608$, $P = 0.614$], with differences between P301S and wild type being significant at days 3 and 4 [day 3: paired $t(14) = 3.915$, $P = 0.002$; day 4: paired $t(14) = 2.855$, $P = 0.013$]. In the probe trial (Figure 2**D**), the target quadrant occupancies of both cohorts did not differ from each other [paired $t(14) = 0.499$, $P = 0.625$].

The swimming speed during the training days did not vary either within or between both investigated groups at both time points examined.

Age-dependent tauopathy in the hippocampus

Immunoreactivity with the AT180 antibody, raised against paired helical filament (PHF)-tau, phosphorylated at threonine 231, was not only observed in the hippocampus of P301S mice in the pyramidal cell layer (Py) of cornu ammonis (CA) 1, CA2 and CA3 region, but also in the oriens radiatum (Or), stratum lacunosum moleculare (LMol) and stratum radiatum (Sr) of the CA1/CA2 and stratum lucidum (SLu) of the CA3 region (Figure 3**A**). The dentate gyrus molecular layer (Mol) and granular layer of the dentate gyrus (GrDG) remained free of staining. Optical density measurements showed an age-dependent increase of AT180 immunoreactivity in the hippocampus [ANOVA, $F(4,85) = 41.265$, $P < 0.001$] at 5 and 6 months of age (Student–Newman–Keuls method *post hoc* test; 5 *vs.* 2, $P < 0.001$; 6 *vs.* 2, $P < 0.001$).

We also detected human tau with pathological conformation in the hippocampus of 2-month-old P301S mice with the MC1 antibody (Figure 3**B**). The SLu of the CA3 region was the most immunoreactive region. Or, LMol and Sr of the CA1/CA2 region were stained as well. In these regions in the hippocampi of P301S mice, missorting of tau was detected with a somato-dendritic pattern. In contrast, the Py, Mol and GrDG remained unstained. Optical density of the MC1-immunoreactivity in the hippocampal region showed an age-dependent increase in P301S mice [ANOVA, $F(4,85) = 3.851$, $P = 0.006$] at month 6 (Student–Newman–Keuls method *post hoc* test; 6 *vs.* 2, $P = 0.016$).

The CP13 antibody was used to visualize tau phosphorylated at serine S202 (Figure 3**C**). CP13

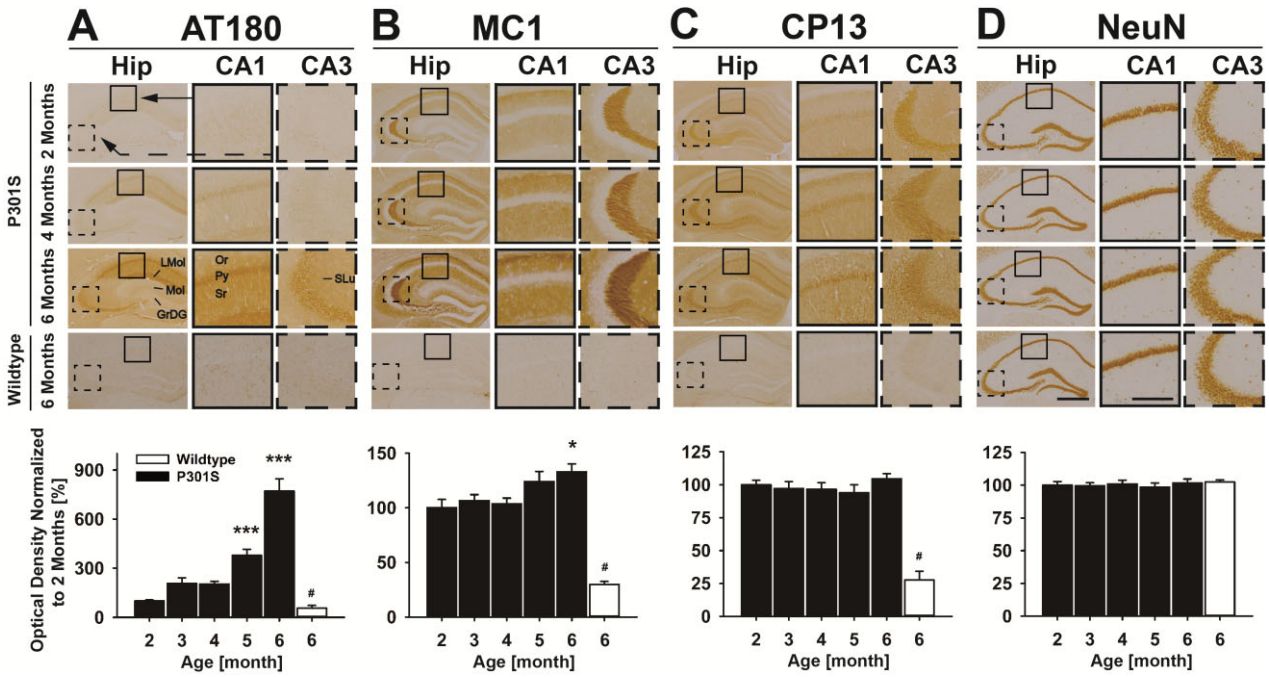

Figure 3. Immunohistochemistry of the hippocampus (Hip) of the P301S mice at 2, 3, 4, 5 and 6 months of age and wild type mice (6 months of age). (**A**) Immunoreactivity for the AT180 antibody, recognizing PHF-tau, increased dramatically with aging in the brains of P301S mice. At 6 months of age, the optical density of the AT180 staining increased up to sevenfold higher than that at 2 months of age. AT180 immunoreactivity was localized both in fibres and cell bodies. (**B**) Staining with the MC1 antibody showed an age-dependent increase in conformationally changed tau. Optical density measurement showed an increased density in the hippocampi of P301S mice at 6 months of age compared to that in 2-month-old P301S mice and wild type mice. From 2 months of age onwards, pathological tau was prominently revealed in the stratum lucidum and mossy fibres of the hippocampus but not in the pyramidal cell bodies (Py). (**C**) The immunoreactivity with the CP13 antibody recognizing tau phosphorylated at the S202 in P301S mice was also localized both in fibres and cell bodies. No age-dependent increase in CP13 immunoreactivity was found in P301S mice. (**D**) NeuN staining was used to visualize neuronal nuclei. There was no difference in NeuN immunoreactivity between the groups suggesting an absence of neuronal cell loss in the hippocampus of P301S mouse. Scale bar = 500 μm in the Hip images; Scale bar = 200 μm in the CA1/CA3 images. Optical density is presented as mean + SEM. P301S 3, 4, 5, 6 *vs.* 2 months of age, ANOVA, *post hoc* Student–Newman–Keuls $^{*}P < 0.05$, $^{***}P < 0.001$. P301S *vs.* wild type 6 months of age, *t*-test, $\#P < 0.05$.

immunoreactivity was already prominent in brains of 2-month-old P301S mice, particularly in the Py of CA1, CA2 and CA3, in the Or, LMol and Sr of CA1/CA2, and in the SLu of CA3. However, CP13 immunoreactivity in the hippocampus did not show any increase with aging [ANOVA, $F(4,85) = 0.717$, $P = 0.582$].

The NeuN antibody was used to label nuclei of neurons (Figure 3**D**). We did not find any age-dependent difference within the hippocampal region [ANOVA, $F(4,85) = 0.196$, $P = 0.940$] by optical density measurements, indicating that there was no neuronal cell loss in the CA1/CA2 and the CA3 regions in P301S mice.

To further investigate the change of different tau species in younger and older P301S mice, Western blot analyses of P301S mouse brain samples (2 months *vs.* 6 months of age) were carried out. In the soluble fraction, the MC1^{+} tau with pathological conformation increased significantly, while the levels of AT180^{+} PHF-tau and CP13^{+} S202-phosphorylated tau did not change (Figure 4**A**). In the sarkosyl-insoluble fraction, MC1^{+} tau was neither observed in young nor in old P301S mice; in contrast, both AT180^{+} and CP13^{+} tau were undetectable in young mice, but observed in 6-month-old mice (Figure 4**B**).

Low dendritic spine density and abnormal spine size

P301S mice showed a lower average spine density compared with wild type mice at both, 2.5 [paired

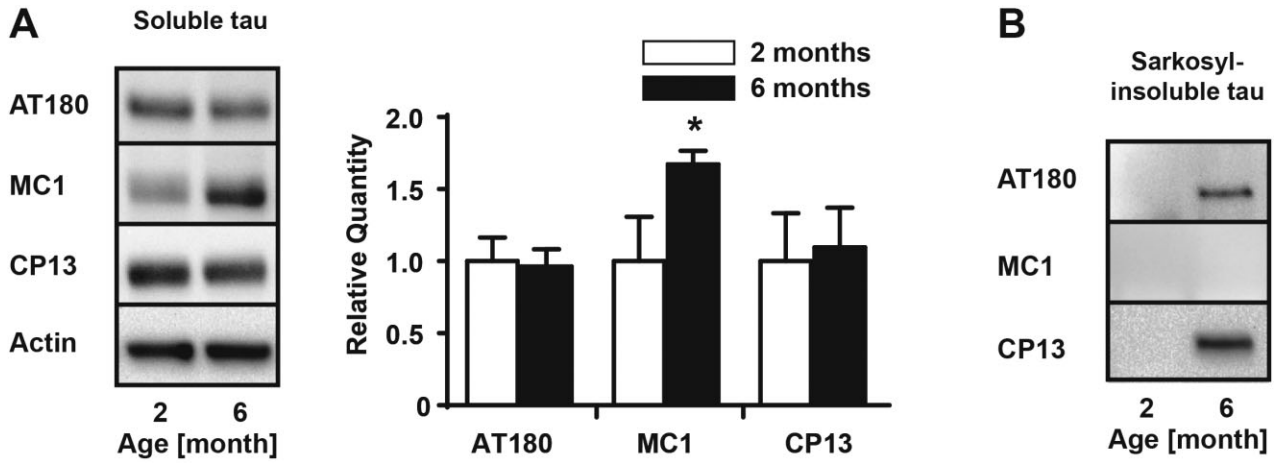

Figure 4. Age-dependent change of tau species in the soluble and sarkosyl-insoluble fraction of P301S mouse brain homogenates at 2 and 6 months of age. (**A**) In the soluble fraction, PHF-tau (AT180), tau with pathological conformation (MC1) and S202-phosphorylated tau (CP13) were detected at both ages. Only MC1$^+$ tau increased in older mice whereas the levels of AT180$^+$ tau and CP13$^+$ tau did not change. (**B**) In the sarkosyl-insoluble fraction of 2-month-old mice, none of these antibodies detected tau; however, at 6 months of age, AT180$^+$ and CP13$^+$ tau was detected, whereas MC1$^+$ tau remained undetectable. Data are presented as mean + SEM. P301S mice 2 *vs.* 6 months of age, paired *t*-test, $^*P < 0.05$.

$t(191) = 5.656$, $P < 0.001$] and 5.5 months of age [paired $t(191) = 7.494$, $P < 0.001$] (Figure 5**A**,**E**,**F**). In the wild type mice, we found an increase in the average spine density between 2.5 and 5.5 months [paired $t(191) = 3.189$, $P = 0.002$], which was not seen in P301S mice [paired $t(191) = 1.313$, $P = 0.191$] (Figure 5**A**,**E**,**F**).

The average spine length in the P301S mice was shorter than in wild type mice at 2.5 months of age [paired $t(191) = 9.140$, $P < 0.001$] (Figure 5**B**,**E**). With increasing age, the wild type mice showed a decrease of the average spine length [paired $t(191) = 6.398$, $P < 0.001$], but there was no change in P301S mice [paired $t(191) = 1.053$, $P = 0.293$].

Concerning the average spine cross-sectional area and volume (Figure 5**C**,**D**), the P301S mice showed smaller spines compared to wild type mice at 2.5 months of age [area: paired $t(191) = 9.180$, $P < 0.001$; volume: paired $t(191) = 8.190$, $P < 0.001$], but not at 5.5 months of age. When comparing the average spine area and volume from 2.5 to 5.5 months of age, the P301S mice revealed an increase of average spine area [paired $t(191) = 2.785$, $P = 0.006$] and volume [paired $t(191) = 3.650$, $P < 0.001$]. In contrast, the wild type mice showed a decrease of average spine area [paired $t(191) = 6.009$, $P < 0.001$] and volume [paired $t(191) = 5.702$, $P < 0.001$] (Figure 5**C**,**D**).

Discussion

In the present study, we report for the first time deficits of hippocampus-dependent visuospatial memory in the Morris water maze in P301S mice with onset at an early age of 2.5 months, thus preceding the locomotor dysfunction found in the open field and the balancing dysfunction in the rotarod test. At this young age, we histologically observed predominate tau immunoreactivity with pathological conformation (MC1 antibody) and S202-phosphorylation (CP13 antibody), but no PHF-tau (AT180 antibody) in the hippocampus. Biochemically, all three tau species were evident in the soluble but not in the insoluble fraction of brain homogenates at this age. Although this did not lead to neuronal cell loss in the hippocampus, there was a significant reduction in the density of dendritic spines.

The balancing ability of the P301S mice started to decrease at 5 months in the rotarod test and deteriorated sharply at 6 months. Similarly, the exploring activity of P301S mice in the novel open field showed no statistical difference as compared to the wild type mice at 2, 3 and 4 months of age but decreased abruptly at month 5 and deteriorated further at month 6, suggesting that the lack of exploring activity briefly precedes the loss of balancing ability. Similar results have been reported previously in the

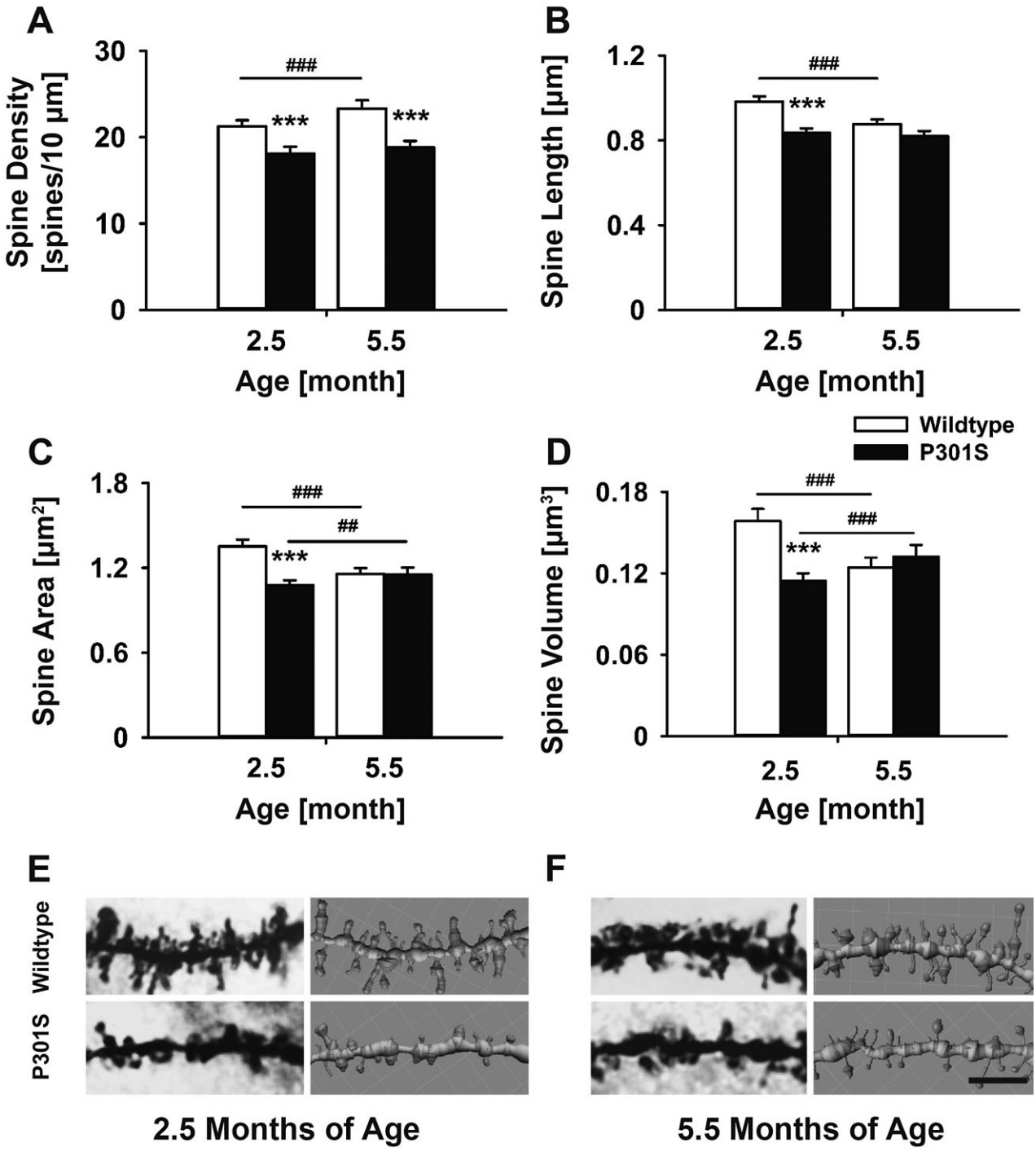

Figure 5. Dendritic spines of the P301S mice and the wild type mice at 2.5 and 5.5 months of age. (**A**) The P301S mice revealed a lower average spine density at both 2.5 and 5.5 months of age. (**B**) The average spine length of the P301S mice was shorter than that of wild type mice at 2.5 months of age and did not differ from each other at 5.5 months. (**C**) The average spine area of the P301S mice was smaller than that of wild type mice at 2.5 months of age and the difference was not found any more at 5.5 months. An increase of average spine area was observed at 5.5 months of age in P301S mice. (**D**) The average spine volume showed similar patterns to the spine area. (**E**,**F**) Representative image of dendritic spines form 2.5- and 5.5-month-old mouse brains (left side) with relative reconstructed 3D images (right side). Scale bar = 3 µm. Data are presented as mean + SEM. P301S mice *vs.* wild type mice, paired *t*-test, $^{***}P < 0.001$. 2.5 *vs.* 5.5 months of age within each group, paired *t*-test, $^{\#\#}P < 0.01$, $^{\#\#\#}P < 0.001$.

same mouse model, as well as other mouse models of FTDP-17-tau [8,15,16].

We also investigated the memory-related behaviour [17,18] of P301S mice with the Morris water maze. In our study, the P301S mice displayed a worse learning curve than wild type mice at 2.5 months of age. They spent more time to find the hidden platform by the end of training day 4. In the probe trial, the P301S mice also exhibited a lack of preference to the target quadrant. These results indicate an early onset memory deficit in P301S mice. At 5.5 months of age, mice were tested again and the learning ability of the P301S mice was still inferior compared to wild type mice. Nevertheless, in the probe trial, the performance of both groups showed similar preferences to the target quadrant. Such memory deficit was not found in a former study using the same mouse model at 2 months of age, in which the authors concluded that they cannot rule out occurrence of such deficits at older ages [8]. Only a trend of an increased latency to find the hidden platform in Morris water maze was described in a different heterozygous P301S transgenic mouse line at 10 months of age [19]. Thus, our study is the first to provide clear evidence of visuospatial memory dysfunction in a P301S mouse model.

The histological correlations of our study focused also on the hippocampal region, which is considered to be the anatomical substrate of visuospatial memorization. The toxicity of tau is still controversial due to the existence of various tau species. Many studies have focused on S202-phosphorylated tau and PHF-tau as putatively toxic species. Immunohistochemically, we found an age-dependent increase of AT180$^+$ PHF-tau and MC1$^+$ conformationally altered tau in the hippocampus of P301S mice. The immunoreactivities of these three antibodies showed a diffuse distribution rather than a condensed pattern and the hippocampal region was free of Thioflavin-S staining from 2 to 6 months of age, suggesting the absence of tau inclusions. Biochemical analysis showed that the increase in AT180$^+$ PHF-tau was due to an increase in sarkosyl-insoluble, but not in the soluble protein fraction, which partly confirmed the results of a previous study [7]. This was accompanied by an increase in CP13$^+$ S202-phosphorylated tau in the sarkosyl-insoluble fraction. Interestingly, the increase of MC1$^+$ tau was limited to the soluble fraction and was not at all observed in the insoluble fraction. The increased AT180 and CP13 immunoreactivities in the sarkosyl-insoluble fraction can be a sign for an early state of tau inclusion formation in the mouse brains. In sum, an increase in soluble MC1$^+$ tau and in insoluble AT180$^+$ and CP13$^+$ tau correlated with the onset of motor deficits at older age rather and might be implicated in this dysfunction. On the other hand, in the soluble fraction, all three pathological tau species were present in the brains of the P301S mice as early as 2 months of age, which coincides with the onset of memory deficits in the Morris water maze. In addition, we also found a missorting of tau in the hippocampus revealing a somato-dendritic distribution at this early age, whereas tau normally shows an axonal distribution [20]. Such missorting has been previously reported in another transgenic mouse model of FTDP-17-tau with the deletion of lysine 280 on human tau [21,22], and it was believed to be disruptive to postsynaptic function of Fyn (proto-oncogene tyrosine-protein kinase Fyn) and further to hinder postsynaptic activities [23]. Moreover, it seems to be strongly associated with the development of memory deficits [24].

As the hippocampus-dependent memory deficits of P301S mice were found without obvious neuronal cell loss in this region, we further investigated the dendritic spines of pyramidal neurones. Dendritic spines receive inputs from axons via synapses [25] and regulate the acquisition of new memory and maintenance of old memory by their dynamic alternations [12]. Theoretically, newly generated smaller spines are believed to seed new memories, while larger spines seem to maintain old memories that could last lifelong [26,27]. Changed quantity and quality of dendritic spines have been already associated with memory deficit and memory dysfunction of several mouse models of tauopathies [13,14,28,29]. We found that in the brains of P301S mice, the average spine density, length, area and volume were lower than those of wild type mice at 2.5 months of age. These results co-occurred with the worse learning curve in the Morris water maze. A lower spine density and smaller size make it harder for P301S mice to seed new memories about the task. At 5.5 months of age, the average density of spines in P301S mice did not statistically differ from those at 2.5 months of age, but we observed a relatively larger average spine area and volume. On the contrary, the spine density in wild type mouse brains increased with age with smaller spines on average. A lower spine density and larger spine size at the older age suggest that P301S mice have a deficit of synaptogenesis or synapse elimination. In this situation, they may maintain and reinforce old

memories but have problems in acquiring new memories [12]. We assume that the repeated task of Morris water maze at 5.5 months of age is a mixture of forming new memories and revising old memories. Thus, the reduced spine density which disrupts the acquisition of new memories due to less seeding points for memory could still be the reason for the worse learning curves of the P301S mice at the 5.5-month test. But once the memory has been formed, even though at a slower pace, the adaptation of old memory may have taken place in the task which enabled the mice to show almost the same performance in the probe trial later.

In summary, we found that the memory deficit and low spine density of the P301S mice appeared at a relatively early stage of tauopathy when predominately $AT180^+$ PHF-tau, $CP13^+$ S202-phosphorylated tau and $MC1^+$ tau of pathological conformation were detectable in the soluble fraction of brain homogenates. The memory deficit occurred in absence of detectable neuronal cell loss, but in presence of reduced spine density in the hippocampal region. The appearance of motor deficits was found after the onset of memory deficits, at a time when the PHF-tau and S202-phosphorylated tau increased dramatically in the sarkosyl-insoluble fraction. Our data suggest that tauopathy-induced impaired synaptic connectivity in the hippocampus leads to memory deficits in P301S mice at an early age. This newly recognized behavioural deficit and suggested patho-anatomical substrate may be helpful as a read-out for the development of new therapeutic tau-targeting interventions.

Acknowledgements

This work was supported by the Deutsche Forschungsgemeinschaft (HO2402/6-1, HO2402/8-1), the German Ministry of Education and Research (BMBF GEF 10-54), the German Academic Exchange Service (DAAD to H.X. and A.C.F.d.A.), the seventh Framework Programme (FP7/2007-2013) under grant agreement no. 220656 (to T.C.). Dr Wolfgang H. Oertel is Senior research Professor of the Charitable Hertie Foundation, Frankfurt/Main, Germany. We are very grateful to Dr M. Goedert for kindly providing the pair breeders of P301S transgenic mice and Mr Robin Konhaeuser for technical assistance. The authors declare no competing financial interests.

References

1 Gotz J, Xia D, Leinenga G, Chew YL, Nicholas H. What renders tau toxic. *Front Neurol* 2013; **4**: 72
2 Buee L, Bussiere T, Buee-Scherrer V, Delacourte A, Hof PR. Tau protein isoforms, phosphorylation and role in neurodegenerative disorders. *Brain Res Brain Res Rev* 2000; **33**: 95–130
3 Spillantini MG, Goedert M. Tau pathology and neurodegeneration. *Lancet Neurol* 2013; **12**: 609–22
4 Lee VM, Goedert M, Trojanowski JQ. Neurodegenerative tauopathies. *Annu Rev Neurosci* 2001; **24**: 1121–59
5 Bugiani O, Murrell JR, Giaccone G, Hasegawa M, Ghigo G, Tabaton M, Morbin M, Primavera A, Carella F, Solaro C, Grisoli M, Savoiardo M, Spillantini MG, Tagliavini F, Goedert M, Ghetti B. Frontotemporal dementia and corticobasal degeneration in a family with a P301S mutation in tau. *J Neuropathol Exp Neurol* 1999; **58**: 667–77
6 Allen B, Ingram E, Takao M, Smith MJ, Jakes R, Virdee K, Yoshida H, Holzer M, Craxton M, Emson PC, Atzori C, Migheli A, Crowther RA, Ghetti B, Spillantini MG, Goedert M. Abundant tau filaments and nonapoptotic neurodegeneration in transgenic mice expressing human P301S tau protein. *J Neurosci* 2002; **22**: 9340–51
7 Delobel P, Lavenir I, Fraser G, Ingram E, Holzer M, Ghetti B, Spillantini MG, Crowther RA, Goedert M. Analysis of tau phosphorylation and truncation in a mouse model of human tauopathy. *Am J Pathol* 2008; **172**: 123–31
8 Scattoni ML, Gasparini L, Alleva E, Goedert M, Calamandrei G, Spillantini MG. Early behavioural markers of disease in P301S tau transgenic mice. *Behav Brain Res* 2010; **208**: 250–7
9 Lepage M, Habib R, Tulving E. Hippocampal PET activations of memory encoding and retrieval: the HIPER model. *Hippocampus* 1998; **8**: 313–22
10 Joëls M. Functional actions of corticosteroids in the hippocampus. *Eur J Pharmacol* 2008; **583**: 312–21
11 Belly A, Bodon G, Blot B, Bouron A, Sadoul R, Goldberg Y. CHMP2B mutants linked to frontotemporal dementia impair maturation of dendritic spines. *J Cell Sci* 2010; **123**: 2943–54
12 Kasai H, Fukuda M, Watanabe S, Hayashi-Takagi A, Noguchi J. Structural dynamics of dendritic spines in memory and cognition. *Trends Neurosci* 2010; **33**: 121–9
13 Perez-Cruz C, Nolte MW, van Gaalen MM, Rustay NR, Termont A, Tanghe A, Kirchhoff F, Ebert U. Reduced spine density in specific regions of CA1 pyramidal neurons in two transgenic mouse models of Alzheimer's disease. *J Neurosci* 2011; **31**: 3926–34
14 Ricobaraza A, Cuadrado-Tejedor M, Marco S, Pérez-Otaño I, García-Osta A. Phenylbutyrate rescues dendritic spine loss associated with memory deficits in a mouse model of Alzheimer disease. *Hippocampus* 2012; **22**: 1040–50

15 Boekhoorn K, Terwel D, Biemans B, Borghgraef P, Wiegert O, Ramakers GJ, de Vos K, Krugers H, Tomiyama T, Mori H, Joels M, van Leuven F, Lucassen PJ. Improved long-term potentiation and memory in young tau-P301L transgenic mice before onset of hyperphosphorylation and tauopathy. *J Neurosci* 2006; **26**: 3514–23
16 Ikeda M, Shoji M, Kawarai T, Kawarabayashi T, Matsubara E, Murakami T, Sasaki A, Tomidokoro Y, Ikarashi Y, Kuribara H, Ishiguro K, Hasegawa M, Yen SH, Chishti MA, Harigaya Y, Abe K, Okamoto K, St George-Hyslop P, Westaway D. Accumulation of filamentous tau in the cerebral cortex of human tau R406W transgenic mice. *Am J Pathol* 2005; **166**: 521–31
17 D'Hooge R, De Deyn PP. Applications of the Morris water maze in the study of learning and memory. *Brain Res Brain Res Rev* 2001; **36**: 60–90
18 Dudchenko PA. An overview of the tasks used to test working memory in rodents. *Neurosci Biobehav Rev* 2004; **28**: 699–709
19 Dumont M, Stack C, Elipenahli C, Jainuddin S, Gerges M, Starkova NN, Yang L, Starkov AA, Beal F. Behavioral deficit, oxidative stress, and mitochondrial dysfunction precede tau pathology in P301S transgenic mice. *FASEB J* 2011; **25**: 4063–72
20 Li X, Kumar Y, Zempel H, Mandelkow EM, Biernat J, Mandelkow E. Novel diffusion barrier for axonal retention of Tau in neurons and its failure in neurodegeneration. *EMBO J* 2011; **30**: 4825–37
21 Eckermann K, Mocanu MM, Khlistunova I, Biernat J, Nissen A, Hofmann A, Schonig K, Bujard H, Haemisch A, Mandelkow E, Zhou L, Rune G, Mandelkow EM. The beta-propensity of Tau determines aggregation and synaptic loss in inducible mouse models of tauopathy. *J Biol Chem* 2007; **282**: 31755–65
22 Mocanu MM, Nissen A, Eckermann K, Khlistunova I, Biernat J, Drexler D, Petrova O, Schonig K, Bujard H, Mandelkow E, Zhou L, Rune G, Mandelkow EM. The potential for beta-structure in the repeat domain of tau protein determines aggregation, synaptic decay, neuronal loss, and coassembly with endogenous Tau in inducible mouse models of tauopathy. *J Neurosci* 2008; **28**: 737–48
23 Ittner LM, Ke YD, Delerue F, Bi M, Gladbach A, van Eersel J, Wolfing H, Chieng BC, Christie MJ, Napier IA, Eckert A, Staufenbiel M, Hardeman E, Gotz J. Dendritic function of tau mediates amyloid-beta toxicity in Alzheimer's disease mouse models. *Cell* 2010; **142**: 387–97
24 Hochgrafe K, Sydow A, Mandelkow EM. Regulatable transgenic mouse models of Alzheimer disease: onset, reversibility and spreading of Tau pathology. *FEBS J* 2013; **280**: 4371–81
25 Zito K, Scheuss V, Knott G, Hill T, Svoboda K. Rapid functional maturation of nascent dendritic spines. *Neuron* 2009; **61**: 247–58
26 Yang G, Pan F, Gan WB. Stably maintained dendritic spines are associated with lifelong memories. *Nature* 2009; **462**: 920–4
27 Xu T, Yu X, Perlik AJ, Tobin WF, Zweig JA, Tennant K, Jones T, Zuo Y. Rapid formation and selective stabilization of synapses for enduring motor memories. *Nature* 2009; **462**: 915–19
28 Zempel H, Thies E, Mandelkow E, Mandelkow EM. Abeta oligomers cause localized Ca(2+) elevation, missorting of endogenous Tau into dendrites, Tau phosphorylation, and destruction of microtubules and spines. *J Neurosci* 2010; **30**: 11938–50
29 Kremer A, Maurin H, Demedts D, Devijver H, Borghgraef P, Van Leuven F. Early improved and late defective cognition is reflected by dendritic spines in Tau.P301L mice. *J Neurosci* 2011; **31**: 18036–47

Received 11 December 2013
Accepted after revision 21 May 2014
Published online Article Accepted on 28 May 2014

Send Orders for Reprints to reprints@benthamscience.net

Current Gene Therapy, **2014**, *14*, 000-000

Tau Silencing by siRNA in the P301S Mouse Model of Tauopathy

Hong Xu[1,2], Thomas W. Rösler[2], Thomas Carlsson[3,4], Anderson de Andrade[2,4], Ondrej Fiala[4,5], Matthias Höllerhage[1,2,4], Wolfgang H. Oertel[4], Michel Goedert[6], Achim Aigner[7] and Günter U. Höglinger[1,2,4,*]

[1]*Department of Neurology, Technical University Munich (TUM), Germany;* [2]*Department of Translational Neurodegeneration, German Center for Neurodegenerative Diseases (DZNE), Munich, Germany;* [3]*Department of Pharmacology, Institute of Neuroscience and Physiology, Sahlgrenska Academy, University of Gothenburg, Gothenburg, Sweden;* [4]*Department of Neurology, Philipps-University, Marburg, Germany;* [5]*Department of Neurology and Center of Clinical Neuroscience, Charles University, Prague, Czech Republic;* [6]*MRC Center for Brain Repair, University of Cambridge, UK;* [7]*Rudolf-Boehm-Institute for Pharmacology and Toxicology, Clinical Pharmacology, University of Leipzig, Germany*

Abstract: Suppression of tau protein expression has been shown to improve behavioral deficits in mouse models of tauopathies, offering an attractive therapeutic approach. Experimentally this had been achieved by switching off the promoters controlling the transgenic human tau gene (*MAPT*), which is not possible in human patients. The aim of the present study was therefore to evaluate the effectiveness of small interfering RNAs (siRNAs) and their cerebral delivery to suppress human tau expression *in vivo,* which might be a therapeutic option for human tauopathies. We used primary cortical neurons of transgenic mice expressing P301S-mutated human tau and Lund human mesencephalic (LUHMES) cells to validate the suppressive effect of siRNA *in vitro*. For measuring the effect *in vivo,* we stereotactically injected siRNA into the brains of P301S mice to reveal the suppression of tau by immunochemistry (AT180, MC1, and CP13 antibodies). We found that the Accell™ SMART pool siRNA against *MAPT* can effectively suppress tau expression *in vitro* and *in vivo* without a specific delivery agent. The siRNA showed a moderate distribution in the hippocampus of mice after single injection. NeuN, GFAP, Iba-1, MHC II immunoreactivities and the terminal deoxynucleotidyl transferase dUTP nick end labeling (TUNEL) assay showed neither signs of neurotoxicity or neuroinflammation nor apoptosis when *MAPT* siRNA is present in the hippocampus. Our data suggest that siRNA against *MAPT* can serve as a potential tool for gene therapy in tauopathies.

Keywords: FTDP-17-tau, *in vitro*, *in vivo*, P301S *MAPT* transgenic mouse, RNAi, siRNA tauopathy.

INTRODUCTION

The term tauopathy refers to a group of neurodegenerative diseases, including Alzheimer's disease (AD), Pick's disease (PiD), progressive supranuclear palsy (PSP) and frontotemporal dementia with parkinsonism linked to chromosome 17 with tau pathology (FTDP-17-tau) [1]. Although tauopathies exhibit quite distinct clinical features, they share similar pathological abnormalities of the microtubule-associated protein tau, which is encoded by the *MAPT* gene. Tau forms the filamentous core of the neurofibrillary tangles (NFTs) in AD, PSP and FTDP-17-tau, and the Pick bodies in PiD [1]. Mutations in the *MAPT* gene encoding tau, conformational changes and hyperphosphorylation of tau are associated with tauopathies. Recent *in vitro* and *in vivo* studies indicated that various species of tau can spread and seed tauopathies in a prion-like manner [2, 3]. Although the spreading hypothesis is still controversial, it was found that a suppression of transgenic tau by switching off its expression can stop the progression of tau pathology and reverses behavioral deficits in several mouse models [4-6]. Physiologically and behaviorally, tau knockout mice did not show crucial changes compared to wild-type mice [7] indicating a high tolerance towards tau reduction. These observations suggest that the suppression of tau expression might be a therapeutic approach in tauopathies.

For the development of therapeutic strategies to suppress endogenous human tau in the central nervous system, high efficacy and safety are strictly needed. In view of this, RNA interference (RNAi) shows promising potential. RNAi was first described as an innate cellular gene regulation system that adjusts for redundant transcription events and protects against the invasion of viruses [8, 9]. During RNAi, different sources of endogenous or exogenous RNAs are processed into small RNAs and then further cleaved by an endoribonuclease (Dice complex) into 21-nucleotide small interfering RNAs (siRNAs), which bind to the RNA-induced silencing complex (RISC). The activated complex recognizes the target mRNA according to sequence homology of the bound siRNA and specifically silences gene expression by digesting

*Address correspondence to this author at the Dept. of Translational Neurodegeneration, German Center for Neurodegenerative Diseases (DZNE), Max-Lebsche-Platz 30, 81377 Munich, Germany;
Tel: +49-89-44007-8406; Fax: +49-89-44007-8420;
E-mail: guenter.hoeglinger@dzne.de

1566-5232/14 $58.00+.00

the target mRNA [10]. siRNAs are highly specific with limited off-target effects and have a relatively short half-life *in vivo*. Previous studies showed promising effects of therapeutic RNAi administration in mouse models of neuronal diseases [11, 12], but were limited by the usage of viral vectors for siRNA delivery, low delivery efficiency, high neuronal toxicity or inflammatory responses. One siRNA study targeted the cyclin-dependent kinase 5 (CDK5) to suppress tau phosphorylation [13], but so far no study aimed at directly silencing tau by RNAi as a therapeutic strategy. Therefore, our study aimed at identifying an appropriate siRNA to target tau *in vivo* in a transgenic mouse overexpressing human tau with the FTDP-17-associated P301S mutation.

MATERIAL AND METHODS

Animals

P301S mice on a C57BL/6 background were used, developed by Michel Goedert [14]. Animals were treated according to the EU Council Directive 2010/63/EU, the Guide for the Care and Use of Laboratory Animals (National Research Council 2011) and the guidelines of the local institutional committee.

Primary Cells from P301S Mice

The preparation of primary cortical neurons was conducted by a revised protocol of a previous study [15]. Generally, pregnant P301S mice under deep isoflurane-anaesthesia (4%, inhaled) were decapitated and the embryos were removed at embryonic day 15. The cortex was dissected under a binocular and cell suspensions were prepared by mechanical trituration with trypsin (0.25%) in Hank's Balanced Salt Solution (HBSS, Life Technologies, Carlsbad, CA). 24-well plates were pre-coated overnight with 1 mg/mL polyethyleneimine (Sigma-Aldrich, St. Louis, MO). Homogenized cortical neural cells were plated at a density of 130,000 cells/cm^2 in 500 µL neurobasal medium: pH = 7.2; 4.82 mM 4-(2-hydroxyethyl)-1-piperazineethanesulfonic acid (HEPES, Sigma-Aldrich); 0.11 mM L-glutamine (Sigma-Aldrich); 21 µM gentamycin (Sigma-Aldrich); 1:1000 B-27 (Life Technologies), 28 µM phenol red (Sigma-Aldrich). The cells were maintained at 37 °C in a humidified incubator with an atmosphere of 5% CO_2. Cytosine arabinoside (10 µM, Sigma-Aldrich) was added 48 h after plating to prevent proliferation of astrocytes cells. The astrocytes on day 7-8 were less than 5% [15].

LUHMES Cell Cultures

The culturing of LUHMES cells was slightly modified from a previous study [16]. Briefly, the cells were proliferated in the growth medium and seeded out directly in differentiation medium at a density of 110,000/cm^2.

In vitro siRNA Delivery

Accell™ SMART pool siRNAs targeting human *MAPT* (*MAPT* siRNA), Accell™ non-targeting pool, and Accell™ green non-targeting siRNA (Thermo Fisher Scientific, Waltham, MA) were used to suppress tau expression or as controls, respectively. For primary neurons, siRNAs were diluted with neurobasal medium into 3 final concentrations of 50, 125 and 250 nM. 48 h after plating, the medium was replaced by fresh medium containing siRNAs followed by 96 h of incubation. For LUHMES cells, the same concentrations of siRNA and incubation time were used and the old medium was replaced by new differentiation medium containing siRNAs 48 h after differentiation. Subsequently, cells were harvested for mRNA extraction with lysis buffer RA1 (Macherey-Nagel, Düren, Germany), or for protein extraction with lysis buffer: pH = 7.8; 0.25 M D-mannitol (Sigma-Aldrich); 0.05 M Tris-HCl (Sigma-Aldrich); 1 mM ethylenediaminetetraacetic acid (EDTA, Sigma-Aldrich); 1 mM ethylene glycol tetraacetic acid (EGTA, Sigma-Aldrich); 1 mM dithiothreitol (DTT, Sigma-Aldrich); 10 µL/mL Triton X-100 (Sigma-Aldrich); 1:100 protease inhibitor (Thermo Fisher Scientific); and 1:100 phosphatase inhibitor (Thermo Fisher Scientific).

In vitro Cell Toxicity

Cortical primary neurons were treated with siRNA targeting *MAPT* (125, 250 and 500 nM) and non-targeting siRNA (500 nM). After 96 h of incubation, the medium was removed and a phosphate buffered saline solution with 0.5 mg/mL 3-(4, 5-dimethylthiazol-2-yl)-2, 5-diphenyltetrazolium bromide (MTT, Sigma-Aldrich) was added. After incubation in a humidified incubator for 1 h at 37 °C, the solution was removed and the plates were placed in a freezer at -80 ºC for at least 1 h. Then, dimethyl sulfoxide (DMSO, Sigma-Aldrich) was added and the plates were analyzed on a microplate reader (FLUOstar Omega, BMG LABTECH, Ortenberg, Germany).

Semi-Quantitative Reverse Transcription-PCR (RT-PCR)

The total mRNA of the cultured neurons was extracted by the Nucleospin® RNA II kit (Machery-Nagel, Düren, Germany). RT-PCR of *MAPT* (forward: TGACACGGACGCTGGCCTGAA; backward: CACTTGGAGGTCAC CTTGCTC) was done with the following program: 60 °C/30 min; 94 °C/3 min; 30× (94 °C/1 min; 66 °C/1 min; 68 °C/2 min); 68 °C/10 min; and 4 °C/∞. Mouse *Gapdh* was taken as internal control (forward: AGGCCGGTGCTGAGTATGTC; backward: TGCCTGCTTCACCACCTTCT) with the program: 60 °C/30 min; 95 °C/2 min; 30× (95 °C/30 sec; 57 °C/1min; 70 °C/2 min); 70 °C/10 min; and 4 °C/∞. The products of RT-PCR were separated by electrophoresis in 1.5% agarose (Sigma-Aldrich) gels containing SYBR® Safe (Life Technologies). Visualization was done by an imaging device (Chemidoc™, Bio-Rad Laboratories, Hercules, CA). The optical density was quantified with Imagelab™ software (Bio-Rad Laboratories) and normalized to the housekeeping gene *Gapdh*. All data were collected from at least 3 independent experimental repeats.

Quantitative PCR (qPCR)

The qRCR was performed on Stepone Plus real-time PCR system (Life Technologies) using the comparative threshold cycle (Ct) method. After extraction, concentrations of total mRNAs were determined by the Nanodrop 2000 (Thermo Fisher Scientific) and 1 µg of total mRNA from each sample was reversely transcripted into total cDNA by the iScript cDNA synthesis kit (Bio-Rad Laboratories).

qPCRs were done with Tagman® Universal Master Mix II with UNG (Life Technologies) and Tagman® gene expression assay kit. 25 ng of total cDNA as template and 4 reference genes were used for quantification. Following primers were used: *MAPT*, assay ID Hs00902194_m1; *OAS1*, assay ID Hs00973637_m1; *PPiA*, assay ID Hs04194521_s1; *PPiB*, assay ID Hs00168719_m1; *GAPDH*, assay ID Hs02758991_g1; *PSMC1*, assay ID Hs02386942_g1 (Life Technologies). The relative quantities of target mRNAs were normalized to non-treated control (set as 1). All data were collected from 3 independent experimental repeats.

Western Blot

Cell lysates were extracted by centrifugation with 13,000 g at 4 °C for 15 min. 10% Tris-HCl SDS-PAGE gel (Bio-Rad Laboratories) was used to separate the lysates in an electrophoresis system (Bio-Rad Laboratories). Separated proteins were transferred to polyvinylidene fluoride (PVDF) membranes (Bio-Rad Laboratories) for Western blotting. After 3 washes with Tris-buffered saline (TBS), membranes were blocked by a solution of 5% skim milk powder (wt/v) (Sigma-Aldrich) with 0.1% (v/v) tween-20 in TBS and incubated over night with the HT7 antibody (MN1000, made in mouse, 1:1000, Thermo Fisher Scientific) for human tau and anti-GAPDH (ABS16, made in rabbit, 1:1000, Millipore, Darmstadt, Germany) as control. Blots were incubated with peroxidase conjugated secondary antibodies (sc-2005, anti-mouse IgG; sc-2004, anti-rabbit IgG; 1:2000, Santa Cruz Biotechnology, Dallas, TX) against respective species for 1 h and visualized by an enhanced chemi-luminescence solution (Thermo Fisher Scientific). Images were taken on the Chemidoc imaging device (Bio-Rad Laboratories). Optical density measurements were done by Imagelab™ software (Bio-Rad Laboratories) and normalized to the housekeeping gene *Gapdh*. All data were collected from at least 3 independent experimental repeats.

Stereotactic Injection

siRNAs were prepared in sterile 0.9% NaCl solution. Mice at 5 months of age were anaesthetized by intraperitoneal (i.p.) injection of a 0.9% NaCl solution containing 0.2% ketamine (Pharmacia GmbH, Berlin, Germany) and 0.2% xylazine (Bayer Healthcare, Leverkusen, Germany) and placed into a stereotactic frame (David Kopf Instruments, Tujunga, CA). The intracerebral injections were performed with a microinjection syringe (World Precision Instruments, Sarasota, FL) placed at the following coordinates relative to bregma and the dura surface: AP: -0.18 cm, ML: ±0.15 cm, DV: -0.18 cm [17]. Two µL of siRNAs solutions containing different siRNA concentrations were injected at a rate of 0.2 µL/min. In *MAPT* siRNA-treated mice, the right hippocampi were injected with siRNA targeting *MAPT* and the left hippocampi with the same volume of non-targeting siRNA. In control mice (n = 4), only the left hippocampi were injected with 0.4 nmol non-targeting siRNA for 14 days. For testing the time-dependency of the siRNA effect, four groups of mice ($n \geq 4$ per group) were bilaterally injected, with 0.4 nmol of the *MAPT* and non-targeting siRNA on alternate sides, and sacrificed after 7, 14, 21 and 28 days, respectively. For testing the dose-dependency of the siRNA effect, three groups of mice ($n \geq 5$ per group) were injected bilaterally with 0.1 nmol, 0.2 nmol, and 0.4 nmol of both the siRNAs, and sacrificed 14 days later. For sacrifice, mice were anaesthetized with pentobarbital (100 mg/kg i.p.) and perfused transcardially with 0.1 M PBS for 2 min, followed by 10 min of 4% paraformaldehyde (PFA, Sigma-Aldrich). Brains were removed and post-fixed in 4% PFA at 4 °C for 48 h and cryoprotected at the same temperature in 30% sucrose solution.

Immunohistochemistry

30 µm coronal sections were made on a CM3050 cryostat (Leica, Wetzlar, Germany) and collected in 10 equally spaced series per brain. Brain sections were given random numbers, which were only disclosed after the analysis by a blinded investigator. Free floating sections were immunostained with the following antibodies: AT180 for paired helical filament (PHF)-tau (MN1040, made in mouse, 1:500, Thermo Fisher Scientific); anti-GFAP for astrocytes (MA5-15086, made in mouse, 1:1000, Millipore); anti-Iba-1 for microglia and macrophages (019-19741, made in rabbit, 1:1000, Wako Pure Chemical Industries, Chuo-ku, Japan); NeuN for neurons (ABN78, made in rabbit, 1:1000, Millipore); MC1 for conformationally changed tau and CP13 for S202-phosphorylated tau (both made in mouse, 1:500, kindly provided by the Department of Pathology, Albert Einstein College of Medicine, NY), anti-MHC II for major histocompatibility complex class II molecules positive cells (MABF33, made in rat, 1:250, Millipore). Sections were incubated overnight at 4 °C with the respective antibodies diluted with normal donkey serum. Bound antibodies were visualized with biotinylated secondary antibody (715-066-150, anti-mouse IgG (H+L); 111-066-144, anti-rabbit IgG (H+L); 1:1000, Jackson ImmunoResearch Laboratories, West Grove, PA) and 3,3'-diaminobenzidine (SERVA Electrophoresis, Heidelberg, Germany) as the substrate.

Immunofluorescent staining was done with the following antibodies: anti-PHF-tau AT180 (Thermo Fischer Scientific); anti-NeuN (Millipore). Secondary antibodies were goat anti-mouse Alexa 488 (1:500, Jackson ImmunoResearch Laboratories) and donkey anti-rabbit Cy5 (1:500, Jackson ImmunoResearch Laboratories). Nuclei were stained with 4',6-diamidino-2-phenylindole (DAPI) (1:1000, Thermo Fischer Scientific).

Optical Density Measurement

Images of histologically stained brain sections ($n \geq 4$ mice per group) were captured by an E-330 camera (Olympus, Orimpasu Kabushiki-Gaisha, Japan) with controlled exposure conditions. The grey values of the hippocampal regions, part of cortex (from retrosplenial granular to S1 cortex barrel field) and thalamus were measured by Fiji software (http://fiji.sc/Fiji). The medial globus pallidus, which showed no immunoreactivity with the used antibodies, was imaged to control for background grey values. The absolute values measured in the hippocampi were first corrected by the background grey values of the same section, and then normalized to the values of contralateral sides (non-targeting siRNA injected side).

Stereology

The hippocampi of the control and *MAPT* siRNA treated animals (n = 3 per group) were analyzed by stereol-

ogy. Five sections of each hippocampus ranging from-1.34 to -2.3 mm posterior to the bregma was analyzed by a stereo-investigator system (MicroBrightField, Inc., Williston, VT, USA) using optical fractionator method. NeuN-labelled neurons were counted with a counting frame of 20 X 20 µm under a 63x oil objective (Leica). Cells were counted only with the presence of its nucleus in the counting frame and total cell numbers were estimated by integration along the rostrocaudal extent of the structures. The sampling strategy gave a coefficient of error less than 0.09 with Gundersen method (m=1). The estimated cell numbers at non-treated and *MAPT* siRNA treated sides were normalized to the contralateral non-targeting siRNA treated side for comparisons. The whole stereological analysis was carried out with an unbiased method by blinding the labels of the slices.

Calculation of the Tau Suppression Area in µm^3 *In vivo*

All adjacent sections with visible suppressive effect on AT180 immunoreactivity were chosen from each mouse, which had been treated with 0.4 nmol *MAPT* siRNA and sacrificed 14 days later. The areas S of the affected regions were delineated on the sections i and measured by the Fiji software. The total effected volume was calculated as section Thickness 30 µm*sectioning Interval(10)* *inSi*.

Statistical Analysis

All data in the figures are presented as mean + standard error of the mean (SEM). Groups were compared by one-way ANOVA followed by Student-Newman-Keuls's *post hoc* test. Calculations were made with the Sigmaplot Standard Statistical Software Package (Systat Software, Chicago, IL). A P-value < 0.05 was considered to be statistically significant.

RESULTS

Cell Toxicity *In vitro*

The cytotoxicity of siRNAs after 96 h incubation was examined using the MTT assay on primary cortical neurons. No difference in cell viability was revealed between non-treated and siRNA-treated cells in the examined concentration range, i.e. up to 500 nM [ANOVA, F(4,10) = 0.219, P = 0.922] (Fig. **1A**).

Suppression of Tau Expression *In vitro*

Then, we verified the effective suppression of tau mRNA in primary cortical neurons of P301S mice by RT-PCR. At 3 different concentrations of *MAPT* siRNA, we detected a decrease of *MAPT* mRNA in a concentration-dependent manner after 96 h incubation (Fig. **1B**) [ANOVA, F(4,10) = 27.012, P < 0.001]. At 250 nM, the mRNA level of human *MAPT* decreased by about 60%, compared with non-treated cells (Student-Newman-Keuls method *post hoc* test; P < 0.001). Non-targeting siRNA (250 nM) did not induce a difference compared to non-treated cells.

Western blotting showed a concentration-dependent decrease of human transgenic tau protein levels in siRNA-treated cells compared to non-treated cells after 96 h incubation [ANOVA, F(4,10) = 16.542, P < 0.001]. At a *MAPT* siRNA concentration of 250 nM, human tau was suppressed about 40% (Student-Newman-Keuls method *post hoc* test; P < 0.001). Again, non-targeting siRNA (250 nM) did not induce a difference compared to non-treated cells (Fig. **1C**).

To further test the suppression effect in human cells, we used LUHMES cells. The morphology of *MAPT* siRNA treated cells showed no difference in comparison to non-targeting siRNA treated and non-treated cells (Fig. **1D**). The suppression was confirmed by qPCR in the 250 nM *MAPT* siRNA treated group (Fig. **1E**) [ANOVA, F(2,6) = 22.921, P = 0.002] in absence of the off-target effect identified by OAS1 2'-5'-oligoadenylate synthetase 1 gene [ANOVA, F(2,6) = 3.585, P = 0.095] [18] (Fig. **1F**).

Time-dependent Suppression of Tau *In vivo*

Based on the results of the *in vitro* findings and previous *in vivo* studies [11, 12], we chose to inject 0.4 nmol siRNA into each hippocampus. We examined the effect at 7, 14, 21 and 28 days after injection by optical density measurement of brain sections immunostained with the AT180 tau antibody. No significant difference between the siRNA-injected and the contralateral non-targeting siRNA-injected control side was found after 7 days (Fig. **2A**). 14 days after injection, the optical density on the *MAPT* siRNA-injected side was decreased to 54.7% (ANOVA, Student-Newman-Keuls method *post hoc* test; 14 days vs. control, P < 0.001). By analysis of adjacent sections, the volume with the suppressive effect was calculated to be 397 µm^3 (SD = 120.355). This effect disappeared after 21 and 28 days (Fig. **2A**, **B**).

To investigate possible neurotoxicity of the *MAPT* siRNA, we measured the optical density on sections stained with the NeuN antibody. No treatment-dependent difference was found [ANOVA, F(4, 64) = 0.529, P = 0.715] (Fig. **2C**, **D**). The optical densities of cortex and thalamus at the *MAPT* siRNA treated side did not differ to the non-targeting siRNA treated side.

Dose-dependent Suppression of Tau *In vivo*

To find out if the *MAPT*-targeting siRNA also exerts an effect at lower doses, we injected 0.1 and 0.2 nmol of siRNAs and compared these to 0.4 nmol. Based on the results of the time course experiments, we analyzed the effect after 14 days. The optical density of AT180-immunoreactivity differed between the groups [ANOVA, F(3,59) = 31.893, P < 0.001]. However, *post hoc* analysis demonstrated only a significant effect in the 0.4 nmol, but not in the 0.1 and 0.2 nmol *MAPT* siRNA groups (Fig. **3A, B**).

Again, no neurotoxicity was detectable by NeuN-immunoreactivity in the 0.1 and 0.2 nmol *MAPT* siRNA groups [ANOVA, F(3,59) = 0.101, P = 0.959] (Fig. **3C**, **D**).

Other Tau Species

Besides AT180-immunoreactive PHF-tau, we also wanted to find out if S202-phosphorylated tau (CP13 antibody) and conformationally changed tau (MC1 antibody) are reduced through *MAPT* siRNA application. With a single intracerebral injection of 0.4 nmol *MAPT* siRNA and

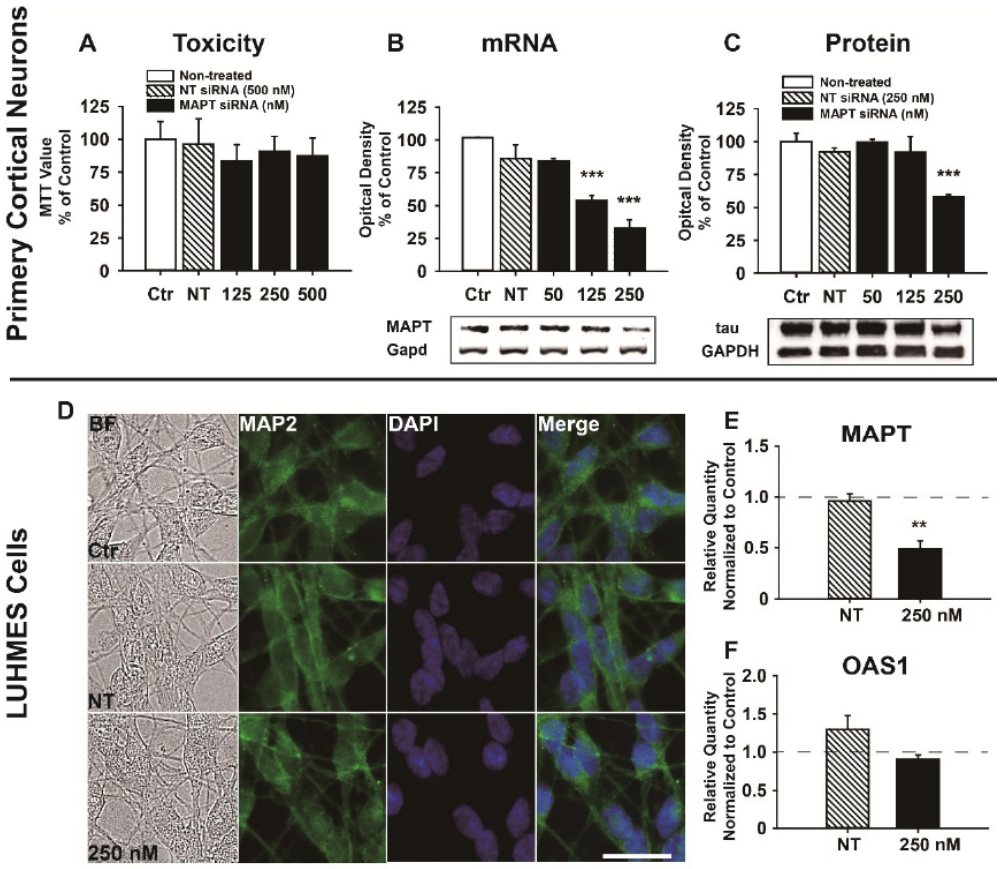

Fig. (1). Suppression of *MAPT* mRNA and tau protein levels by siRNA in primary cortical neurons of P301S mice. After 4 days incubation with 125, 250 or 500 nM *MAPT* siRNA, no cell toxicity was detected with the MTT test when compared to untreated cells (**A**). In a concentration- dependent manner (50, 125, 250 mM), *MAPT* siRNA reduced the tau mRNA level by up to 60% compared to non-treated cells (Ctr), while non-targeting (NT) control siRNA showed no effect (**B**). The panel below the graph shows a representative image of *MAPT* mRNA in comparison to mouse *Gapdh* mRNA. In a concentration-dependent manner, *MAPT* siRNA reduced the tau protein level by about 40% compared to non-treated controls (Ctr; **C**). The panel below the graph shows a western blot with human tau in treated cells in comparison to the mouse housekeeping protein *GAPDH*. The siRNAs treatment had no influence on the morphology of LUHMES cells (D). 250 nM of *MAPT* siRNA suppressed *MAPT* mRNA in the LUHMES cells (E). No off-target effect was detected in the *MAPT* siRNA treated cells (250 nM), indicated by the expression level of the OAS 1 gene (F). Dashed lines stand for non-treated controls (E, F). ** $P < 0.01$, *** $P < 0.001$, vs. Ctr, ANVOA, *post hoc* Student-Newman-Keuls. Scale bar = 200 μm.

14 days of exposure, we saw a clear decrease of both pathological tau species compared to the contralateral side injected with non-targeting siRNA (Fig. **4**).

Tau Suppression in Absence of Neuronal Loss

To ascertain that the tau suppressive effect occurred in absence of neurotoxicity, mouse brains with 0.4 nmol *MAPT* siRNA and 14 days exposure time were triple stained with the AT180 antibody, NeuN antibody and DAPI. Compared with the non-targeting siRNA treated side, AT180 immunoreactivity was strongly suppressed on the *MAPT* siRNA-treated side, whereas no neuronal cell loss or chromatin condensation were found by NeuN and DAPI staining in the very same area affected by tau silencing (Fig. **5**).

To confirm the absence of neuronal cell toxicity *in vivo*, stereology counting of the NeuN positive cells in the hippocampus was carried out. There was no difference observed between the *MAPT* siRNA treated side and the non-treated side after normalization to the non-targeting treated side (t-test, *MAPT* siRNA vs. non-treated, $P = 0.223$).

Cellular siRNA Distribution and Silencing Specificity

In order to visualize the cellular distribution of the siRNA in relation to the silencing effect, we mixed the *MAPT* siRNA (0.4 nmol) with green fluorescent non-targeting siRNA (0.04 nmol) and injected the mixture intracerebrally into mouse brains. After 14 days of exposure, brain sections were double stained with the AT180 antibody and DAPI. Confocal imaging showed that the siRNA had entered some, but not all neurons of the hippocampus (Fig. **6**). Where there was a green siRNA signal in the neurons indicating penetration of the siRNAs, no signal of the AT180 antibody was found. Inversely, cells without green siRNA signal still displayed AT180 immunoreactivity. This suggests a cell specific suppression of tau by the siRNA and further argues against a non-specific loss of AT180 immunoreactivity. The entrance of siRNA into the neuronal cells was further confirmed by immunofluorescent staining showing co-localization of green fluorescent siRNA and NeuN staining (S. Fig. **1**).

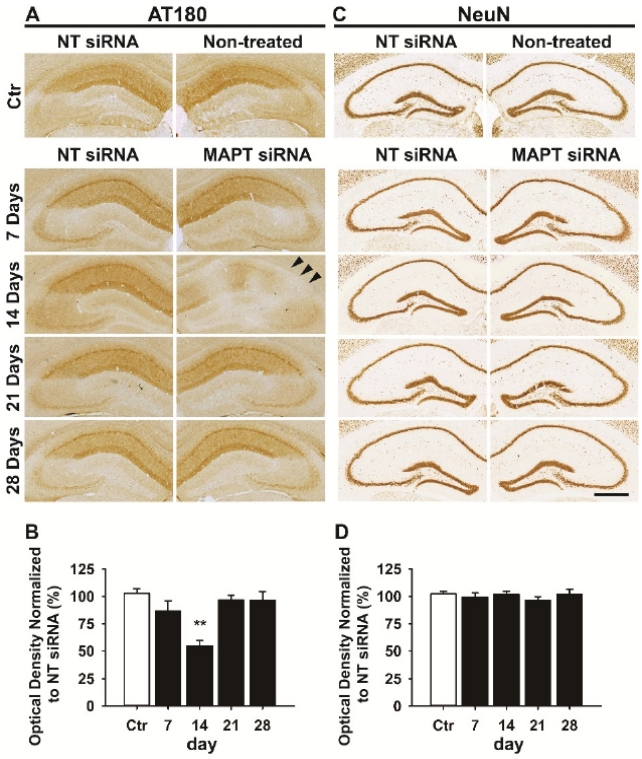

Fig. (2). Time-dependent effect of *MAPT* siRNA injected in the hippocampus of P301S mice. Mice received a single injection of 0.4 nmol *MAPT* siRNA in the right hippocampus and the same dose of non-targeting (NT) siRNA in the left hippocampus; the mice were sacrificed after 7, 14, 21 or 28 days. Control mice (Ctr) were injected with 0.4 nmol of NT siRNA in left hippocampus and sacrificed 14 days after injection. At 14, but not 7, 21, or 28 days after injection, AT180-immunoreactive tau was prominently suppressed (black arrowheads) compared to non-treated hippocampus (non-treated) (**A**). Optical density measurement confirmed a significant reduction of AT180-immunoreactivity in the hippocampus injected with *MAPT* siRNA in 14 days group compared to Ctr (**B**). No significant neuronal cell loss was observed in the hippocampus after injection of *MAPT* siRNA by microscopical inspection (**C**) or optical density measurement (**D**) after immunostaining with the NeuN antibody on adjacent sections. Scale bar = 500 µm. ** $P < 0.01$, vs. Ctr, ANOVA, *post hoc* Student-Newman-Keuls.

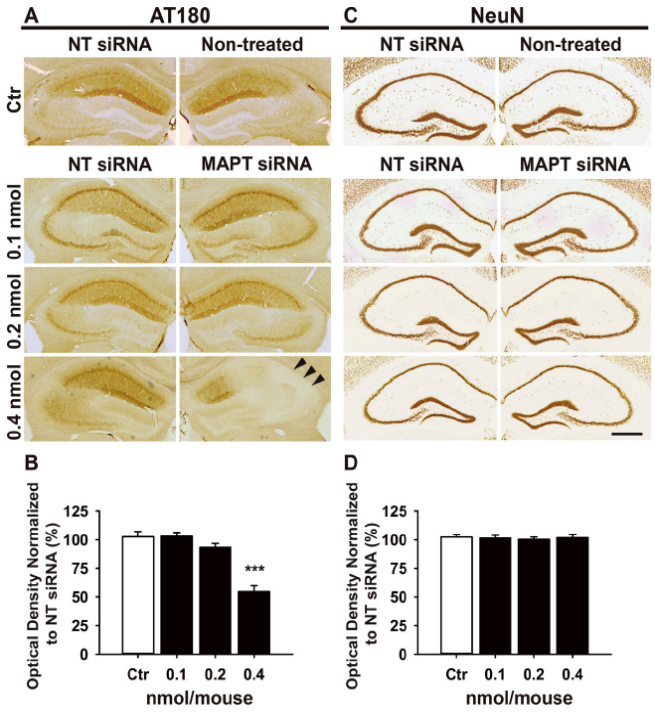

Fig. (3). Dose-dependent effect of *MAPT* siRNA injected in the hippocampus of P301S mice. Mice were injected with 0.1, 0.2 or 0.4 nmol of *MAPT* siRNA in the right hippocampus and the same doses of non-targeting (NT) siRNA in contralateral hippocampus. Control mice (Ctr) were injected with 0.4 nmol of NT siRNA in the left hippocampus. The mice were sacrificed after 14 days. Microscopic pictures show the AT180-immunoreactivity in the hippocampi (**A**). The black arrowheads highlight the area of reduced immunoreactivity in the 0.4 nmol *MAPT* siRNA group. Optical density measurement showed a significant reduction of AT180-immunoreactivity in 0.4 nmol *MAPT* siRNA treated hippocampi (**B**). Microscopic pictures show no difference for the NeuN immunoreactivity (**C**). Optical density measurement of the NeuN-immunoreactivity shows no difference between Ctr and other groups by staining with NeuN antibodies on adjacent sections (**D**). Scale bar = 500 µm. *** $P < 0.001$ vs. Ctr, ANOVA, *post hoc* Student-Newman-Keuls.

Absence of Inflammation and Apoptosis

Inflammation is a problem which might arise from siRNA injection. To test inflammation induced by injection of the *MAPT* siRNA, we used GFAP and Iba-1 antibodies to reveal astrocytes and activated microglia, respectively. Within the same anatomical area, where we saw a suppressive effect on tau after the *MAPT* siRNA injection (Fig. **7. A, B**), both GFAP and Iba-1 revealed no activation of astrocytes (Fig. **7. C, D**) or microgial cells (Fig. **7. E, F**) compared to the non-targeting siRNA-treated side. In addition, no induction of MHC II positive cell was found in the region (Fig. **7. G, H**). Apoptosis was identified by TUNEL staining; no TUNEL-positive neuron was detected in the hippocampal region with the presence of green siRNA signal (S. Fig. **1**).

DISCUSSION

In the present study we report for the first time that a commercially available siRNA can be applied *in vivo* by intracerebral injection without the use of a delivery reagent to suppress tau expression. We show a significant knock-down without any detectable neurotoxicity, inflammation or apoptosis in the hippocampus, where tau pathology is prominent and which correlates with behavioral read-outs of the P301S tauopathy mouse model [14, 19, 20]. A single injection resulted in moderate distribution, spatially confined to the area surrounding the injection site and transiently in a well-defined period of time; suppression of intracellular tau occurred very specifically in these neurons, where the siRNA molecules had entered.

Santa Cruz and colleagues [4] described that established neuronal tau-aggregates and corresponding behavioral impairments in mice over-expressing a mutated human FTDP-17 tau variant can be reversed by the shut-down of an inducible tau expression system. The study evoked the question, how such a gene knock-down could be achieved safely and efficiently with regard to human therapeutics. Since their

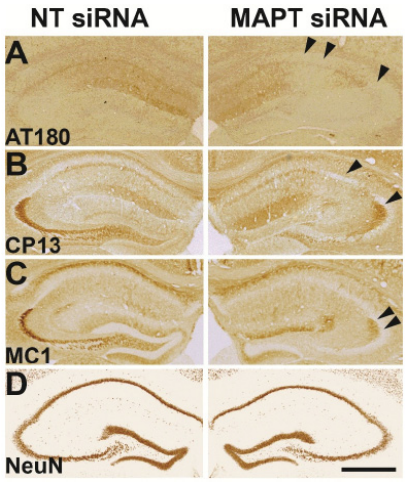

Fig. (4). Suppressive effect of *MAPT* siRNA on other tau species. P301S tau transgenic mice were treated with 0.4 nmol non-targeting (NT) and 0.4 nmol *MAPT* siRNA, and sacrifice 14 days later. Microscopic pictures showing the immunoreactivity for AT180-tau (**A**), CP13-tau (**B**), MC1-tau (**C**) and NeuN (**D**) on the adjacent sections of the hippocampi treated with NT and *MAPT* siRNA. The black arrowheads highlight the area with reduced immunoreactivity at the *MAPT* siRNA treated side compared to the non-targeting siRNA treated side. Scale bar = 500 µm.

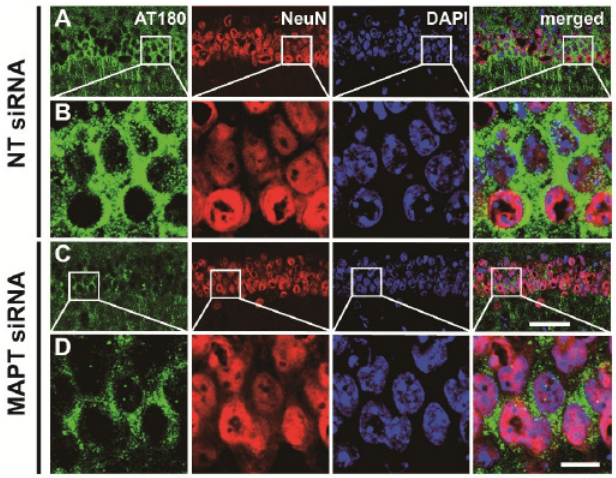

Fig. (5). Tau silencing in absence of neurotoxicity. P301S tau transgenic mice were treated with 0.4 nmol non-targeting (NT) and 0.4 nmol *MAPT* siRNA, and sacrifice 14 days later. Hippocampi were double immunostained for AT180 (green) and NeuN (red); nuclei were stained with DAPI (blue). The figures show confocal microscopic images as low magnification overviews (**A, C**) and high magnification details (**B, D**) of the Cornu Ammonis (CA) 1/CA2 region in representative hippocampi injected with NT siRNA (**A, B**) and *MAPT* siRNA (**C, D**). Note the specific reduction in AT180-immunoreactivity in absence of altered NeuN and DAPI signals following *MAPT* siRNA injection. Scale bar for **A**, **C** = 50 µm, Scale bar for **B**, **D** = 10 µm.

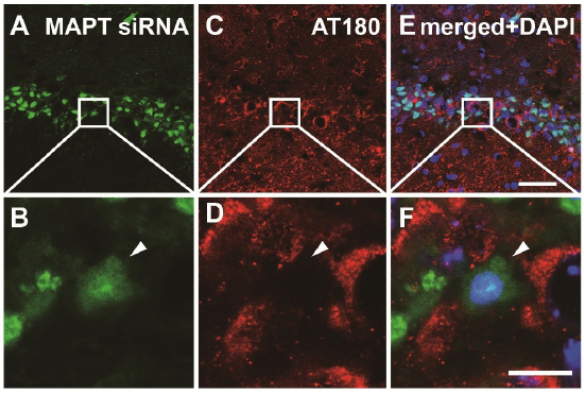

Fig. (6). Cell specific silencing. P301S tau transgenic mice were injected in the hippocampus with a mix of 0.4 nmol of *MAPT* and 0.04 nmol of green non-targeting siRNAs and sacrificed after 14 days. Confocal microscopic images in the CA1/CA2 region show the cellular distribution of siRNA (green, **A, B**), of AT180-immunoreactivity (red, **C**, **D**) and of DAPI-positive nuclei (blue, **E**, **F**) at low (**A**, **C, E**) and high magnification (**B**, **D, F**). The green and the red signal were mutually exclusive: the white arrowhead shows an example of a neuron with siRNA (green) distributed in the soma and nucleus, devoid of AT180 tau immunoreactivity. Note surrounding neurons without siRNA, but containing AT180-immunoreactivity. Scale bar for **A**, **C**, **E** = 50 µm, Scale bar for **B**, **D**, **F** = 10 µm.

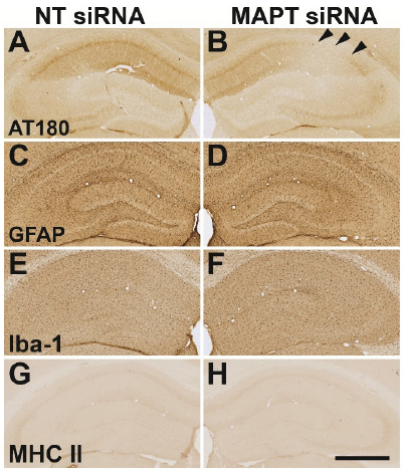

Fig. (7). Absence of inflammation after intracerebral injection of *MAPT* siRNA. P301S tau transgenic mice were treated with 0.4 nmol non-targeting (NT) and 0.4 nmol *MAPT* siRNA, and sacrifice 14 days later. The AT180 tau antibody was used to identify the area of effective tau silencing after injection of *MAPT* siRNA (**B**, black arrowheads) compared to the NT siRNA treated side (**A**). On adjacent sections, GFAP (**C, D**) and Iba-1 (**E, F**) antibodies revealed an unaltered morphology and density of astrocytes and microglia after injection of *MAPT* siRNA (**D, F**) compared to the NT siRNA treated side (**C, E**). In addition, no MHC II positive cells were presented within the region (**G, H**). Scale bar = 500 µm.

first introduction in *C. elegans in 1998* [21], siRNA techniques have been developed as a powerful tool for gene-specific knock-down [22]. The feasibility of retarding progressive neurodegeneration by siRNA-mediated knock-down of a pathogenic protein has been already demonstrated in an animal model of motor neuron disease [23]. However, the concern of the safety of siRNA delivery to treat diseases involving the central nervous system is still a matter of intense research [22, 24, 25]. There are several major obstacles to overcome before such a therapy might be considered as a

clinically relevant option. These issues include, apart from the necessity to overcome the blood-brain barrier, the risk of inflammation and neurotoxicity as well as the need for a reversible system to terminate the effect in case of adverse events. The effects of gene knock-down also need to be long-lasting for chronic neurodegenerative disorders. The latter can be achieved by viral based delivery systems using lentiviral or adeno-associated viral vectors [23, 26, 27]. Using this system, the siRNA sequences of interest are integrated in the cell genome or episomally expressed in a so-called short hairpin RNA (shRNA) [28]. These systems may have the advantage of long-lasting expression, however, they confer the risk of incontrollable and irreversible adverse effects. This is particularly true for lentiviral vectors, where the transgenic cDNA integrates into the cell genome. A non-viral based siRNA delivery, as evaluated in the present study, is therefore a safer system since it is reversible, if severe side effects including immunoresponse or off-target effects occur.

In order to deliver non-viral based siRNAs into the brain, also several obstacles have to be overcome. First, naked siRNA has a very short half-life *in vivo,* due to rapid degradation by nucleases and neutralization by the immune system [29, 30]. Consistently, we observed no silencing efficacy upon injection of chemically unmodified siRNA without transfection agent into the living brain (not shown). A former study using lipofectamine® Plus (Life Technologies) to deliver shRNA *in vitro* has achieved an allele specific suppression of Tau in Cos-7 and HeLa cells [31]. However, when we tested lipofectamine mixed with siRNA *in vivo*, this was in our hand both toxic to neurons and limited in distribution (not shown). We also tested a polyethylenimine (PEI)-based complexation of the siRNAs (1.5 μg/μL) [32] *in vivo* which showed high neurotoxicity in this experimental setting (not shown). G2-5 dendrimer [33] as transfection agent did not lead to a penetration into the brain parenchyma outside of the needle track and thus not to a meaningful silencing effect (not shown). Hence, the common transfection agents used *in vitro* did not prove to be properly working *in vivo* in our hands.

The Accell™ siRNAs have incorporated chemical modifications in siRNA molecules to facilitate penetration of cell membranes without additional transfection agents needed and have been widely used *in vitro* so far [34, 35]. A previous study has shown a good and widespread suppression of cyclophilin-B and GAPDH by a single intracerebroventricular injection of Accell™ siRNAs in the rat brain [36]. We also tested to inject Accell™ siRNA in the lateral ventricle of the P301S mice, however we could not observe any effect on tau expression in the hippocampus (not shown). The feasibility of intracerebroventricular injection of siRNA against tau might be evaluated in future studies using a higher continuously infused dose of siRNA. Nevertheless, following a single injection into the parenchyma of the hippocampus, there were a moderate distribution and a neuron-specific and siRNA-dependent knock-down, as investigated by GFP-coupled siRNAs molecules. Particularly, in the current study we provide evidence that the commercially available Accell™ siRNAs can also be administered *in vivo* to achieve a significant knock-down of the tau protein in a mouse model of tauopathies with good efficacy and safety. We found a concentration-dependent suppression of human tau by the *MAPT* siRNA *in vitro* and an effective dose to knock-down 45% of the tau expression in the hippocampus.

While the regional and temporal limitation of silencing efficacy after a single siRNA injection, as observed in our study, might be helpful in regionally and temporally confined neurological conditions (e.g. territorial infarction, focal epilepsy or a multiple sclerosis focus), the utility of the presently described approach is limited with regard to chronic and widespread brain disorders, such as most neurodegenerative disorders. These limitations might be overcome in a next step by chronic siRNA infusion. Supporting this idea, previous studies already demonstrated the feasibility of siRNA infusion *in vivo* for therapeutic purpose in neurological conditions. Infusion for 7 days of 16.6 μg/h siRNA against the P2X purinoceptor 3 relieved pathological pain in a rat model [11]. Infusion of siRNA over 4 weeks at 5 μg/h successfully knocked down alpha-synuclein expression in the substantia nigra in primates [37]. With regard to the molecular target of our study, previous work used antisense oligonucleotides to silence tau *in vivo* and demonstrated a beneficial effect in a mouse model of epilepsy [38], suggesting that a comparative study is needed to compare the relative efficacy and safety of tau silencing when using the siRNA and the oligonucleotide method. Together, these data suggest that siRNA-mediated tau-silencing should be further developed as therapeutic option for both acute and chronic neurological diseases.

CONCLUSION

The current data demonstrate the safety and provide a realistic delineation of the efficacy in the temporal and spatial dimension of a single injection of siRNA into the brain parenchyma. Thus, this work provides a stable basis for the further development of this method for therapeutic purposes in brain disorders.

CONFLICT OF INTEREST

The authors confirm that this article content has no conflict of interest.

ACKNOWLEDGEMENTS

This work was supported by the Deutsche Forschungsgemeinschaft (HO2402/6-1, HO2402/8-1), the German Ministry of Education and Research (BMBF GEF 10-54), the German Academic Exchange Service (DAAD to H.X., O.F. and A.D.A.), the seventh Framework Program (FP7/2007-2013) under grant agreement no. 220656 and Hjärnfonden (to T.C.). W.H.O. is Senior research Professor of the Charitable Hertie Foundation, Frankfurt/Main, Germany. We thank Robin Konhäuser for technical assistance.

PATIENT CONSENT

Declared none.

SUPPLEMENTARY MATERIAL

Supplementary material is available on the publishers web site along with the published article.

REFERENCES

[1] Spillantini MG, Goedert M. Tau pathology and neurodegeneration. Lancet Neurol 2013; 12: 609-22.

[2] Iba M, Guo JL, McBride JD, Zhang B, Trojanowski JQ, Lee VM. Synthetic tau fibrils mediate transmission of neurofibrillary tangles in a transgenic mouse model of Alzheimer's-like tauopathy. J Neurosci 2013; 33: 1024-37.

[3] Clavaguera F, Lavenir I, Falcon B, Frank S, Goedert M, Tolnay M. "Prion-like" templated misfolding in tauopathies. Brain Pathol 2013; 23: 342-9.

[4] SantaCruz K. Tau Suppression in a Neurodegenerative Mouse Model Improves Memory Function. Science 2005; 309: 476-481.

[5] Hochgrafe K, Sydow A, Mandelkow EM. Regulatable transgenic mouse models of Alzheimer disease: onset, reversibility and spreading of Tau pathology. FEBS J 2013; 280: 4371-81.

[6] Engel, T., F. Hernandez, J. Avila, and J.J. Lucas, Full reversal of Alzheimer's disease-like phenotype in a mouse model with conditional overexpression of glycogen synthase kinase-3. J Neurosci 2006; 26: 5083-90.

[7] Morris M, Hamto P, Adame A, Devidze N, Masliah E, Mucke L. Age-appropriate cognition and subtle dopamine-independent motor deficits in aged Tau knockout mice. Neurobiol Aging 2013; 34: 1523-9.

[8] Carrington JC, Ambros V. Role of microRNAs in plant and animal development. Science 2003; 301: 336-8.

[9] Krol J, Loedige I, Filipowicz W. The widespread regulation of microRNA biogenesis, function and decay. Nat Rev Genet 2010; 11: 597-610.

[10] Ramachandran PS, Keiser MS, Davidson BL. Recent advances in RNA interference therapeutics for CNS diseases. Neurotherapeutics 2013; 10: 473-85.

[11] Dorn, G, Patel S, Wotherspoon G, *et al.* siRNA relieves chronic neuropathic pain. Nucleic Acids Res 2004; 32: e49.

[12] Thakker DR, Natt F, Husken D, *et al.* Neurochemical and behavioral consequences of widespread gene knockdown in the adult mouse brain by using nonviral RNA interference. Proc Natl Acad Sci U S A 2004; 101: 17270-5.

[13] Piedrahita D, Hernandez I, Lopez-Tobon A, *et al.* Silencing of CDK5 reduces neurofibrillary tangles in transgenic alzheimer's mice. J Neurosci 2010; 30: 13966-76.

[14] Bellucci A, Westwood AJ, Ingram E, Casamenti F, Goedert M, Spillantini MG. Induction of inflammatory mediators and microglial activation in mice transgenic for mutant human P301S tau protein. Am J Pathol 2004; 165: 1643-52.

[15] Culmsee C, Gerling N, Lehmann M, *et al.* Nerve growth factor survival signaling in cultured hippocampal neurons is mediated through TrkA and requires the common neurotrophin receptor P75. Neuroscience 2002; 115: 1089-108.

[16] Hollerhage M, Goebel JN, de Andrade A, *et al.* Trifluoperazine rescues human dopaminergic cells from wild-type alpha-synuclein-induced toxicity. Neurobiol Aging 2014; 35: 1700-11.

[17] Franklin KBJ, P.G., The mouse brain in stereotaxic coordinates. 2nd ed. San Diego, CA: Academic Press; 1997.

[18] Sen N, Hara MR, Ahmad AS, *et al.* GOSPEL: a neuroprotective protein that binds to GAPDH upon S-nitrosylation. Neuron 2009; 63: 81-91.

[19] Allen B, Ingram E, Takao M, *et al.* Abundant tau filaments and nonapoptotic neurodegeneration in transgenic mice expressing human P301S tau protein. J Neurosci 2002; 22: 9340-51.

[20] Scattoni ML, Gasparini L, Alleva E, Goedert M, Calamandrei G, Spillantini MG. Early behavioural markers of disease in P301S tau transgenic mice. Behav Brain Res 2010; 208: 250-7.

[21] Fire A, Xu S, Montgomery MK, Kostas SA, Driver SE, Mello CC. Potent and specific genetic interference by double-stranded RNA in Caenorhabditis elegans. Nature 1998; 391: 806-11.

[22] Kim JW, Zhang YH, Zern MA, Rossi JJ, Wu J. Short hairpin RNA causes the methylation of transforming growth factor-beta receptor II promoter and silencing of the target gene in rat hepatic stellate cells. Biochem Biophys Res Commun 2007; 359: 292-7.

[23] Raoul C, Abbas-Terki T, Bensadoun JC, *et al.* Lentiviral-mediated silencing of SOD1 through RNA interference retards disease onset and progression in a mouse model of ALS. Nat Med 2005; 11: 423-8.

[24] Aigner A. Gene silencing through RNA interference (RNAi) *in vivo*: strategies based on the direct application of siRNAs. J Biotechnol 2006; 124: 12-25.

[25] Boudreau RL, Spengler RM, Davidson BL. Rational design of therapeutic siRNAs: minimizing off-targeting potential to improve the safety of RNAi therapy for Huntington's disease. Mol Ther 2011; 19: 2169-77.

[26] Vandenberghe LH, Xiao R, Lock M, Lin J, Korn M, Wilson JM. Efficient serotype-dependent release of functional vector into the culture medium during adeno-associated virus manufacturing. Hum Gene Ther 2010; 21: 1251-7.

[27] Anderson RD, Haskell RE, Xia H, Roessler BJ, BL Davidson. A simple method for the rapid generation of recombinant adenovirus vectors. Gene Ther 2000; 7: 1034-8.

[28] Deng Y, Wang CC, Choy KW, *et al.* Therapeutic potentials of gene silencing by RNA interference: Principles, challenges, and new strategies. Gene 2014.

[29] Musacchio T, Torchilin VP. siRNA delivery: from basics to therapeutic applications. Front Biosci (Landmark Ed) 2013; 18: 58-79.

[30] Kumari A, Kumar V, Yadav SK. Nanocarriers: a tool to overcome biological barriers in siRNA delivery. Expert Opin Biol Ther 2011; 11: 1327-39.

[31] Miller VM, Gouvion CM, Davidson BL, Paulson HL. Targeting Alzheimer's disease genes with RNA interference: an efficient strategy for silencing mutant alleles. Nucleic Acids Res 2004; 32: 661-8.

[32] Grzelinski M, Urban-Klein B, Martens T, *et al.* RNA interference-mediated gene silencing of pleiotrophin through polyethylenimine-complexed small interfering RNAs *in vivo* exerts antitumoral effects in glioblastoma xenografts. Hum Gene Ther 2006; 17: 751-66.

[33] Lim J, Simanek EE. Triazine dendrimers as drug delivery systems: from synthesis to therapy. Adv Drug Deliv Rev 2012; 64: 826-35.

[34] Gomez D, Kessler K, Michel JB, Vranckx R. Modifications of chromatin dynamics control Smad2 pathway activation in aneurysmal smooth muscle cells. Circ Res 2013; 113: 881-90.

[35] Jiang S, Park DW, Stigler WS, *et al.* Mitochondria and AMP-activated protein kinase-dependent mechanism of efferocytosis. J Biol Chem 2013; 288: 26013-26.

[36] Nakajima H, Kubo T, Semi Y, *et al.* A rapid, targeted, neuron-selective, *in vivo* knockdown following a single intracerebroventricular injection of a novel chemically modified siRNA in the adult rat brain. J Biotechnol 2012; 157: 326-33.

[37] McCormack AL, Mak SK, Henderson JM, Bumcrot D, Farrer MJ, di Monte DA. Alpha-synuclein suppression by targeted small interfering RNA in the primate substantia nigra. PLoS One 2010; 5: e12122.

[38] DeVos SL, Goncharoff DK, Chen G, *et al.* Antisense reduction of tau in adult mice protects against seizures. J Neurosci 2013; 33: 12887-97.

Received: April 01, 2014 Revised: June 15, 2014 Accepted: June 17, 2014

Supplementary Material

Tau Silencing by siRNA in the P301S Mouse Model of Tauopathy

Hong Xu[1,2], Thomas W. Rösler[2], Thomas Carlsson[3,4], Anderson de Andrade[2,4], Ondrej Fiala[4,5], Matthias Höllerhage[1,2,4], Wolfgang H. Oertel[4], Michel Goedert[6], Achim Aigner[7] and Günter U. Höglinger[1,2,4,*]

[1]Department of Neurology, Technical University Munich (TUM), Germany; [2]Department of Translational Neurodegeneration, German Center for Neurodegenerative Diseases (DZNE), Munich, Germany; [3]Department of Pharmacology, Institute of Neuroscience and Physiology, Sahlgrenska Academy, University of Gothenburg, Gothenburg, Sweden; [4]Department of Neurology, Philipps-University, Marburg, Germany; [5]Department of Neurology and Center of Clinical Neuroscience, Charles University, Prague, Czech Republic; [6]MRC Center for Brain Repair, University of Cambridge, UK; [7]Rudolf-Boehm-Institute for Pharmacology and Toxicology, Clinical Pharmacology, University of Leipzig, Germany

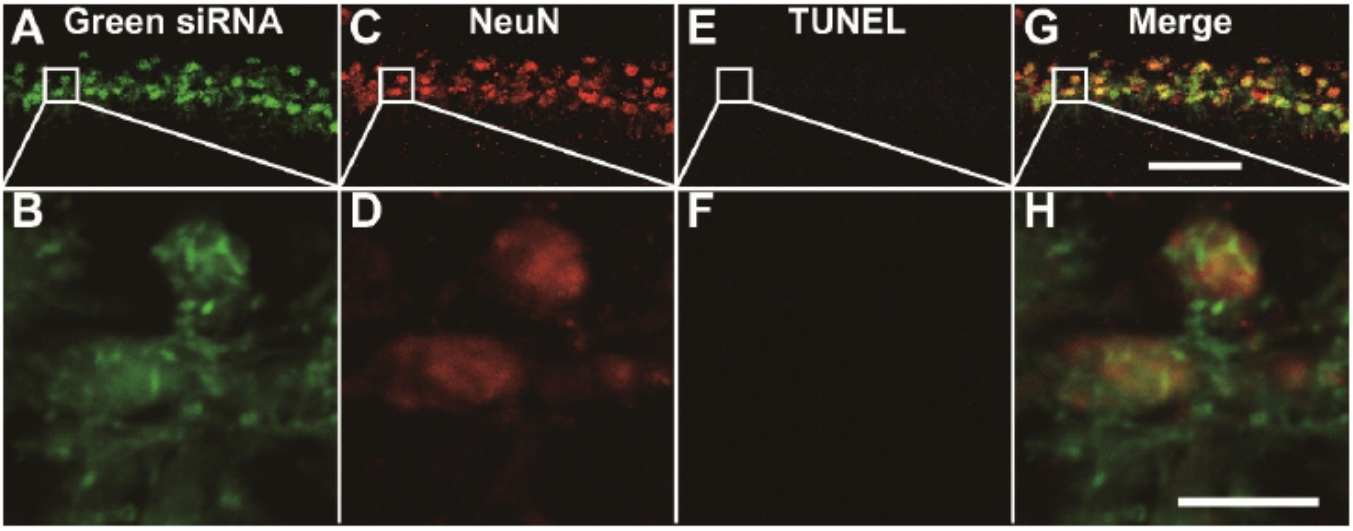

Supplementary Figure 1. The green siRNA signal (**A, B**) co-localizes with the immunoreactivity of the neuron-specific NeuN antibody (**C, D**) in absence of apoptosis-specific signal of the TUNEL assay (**E, F**). Merged images show the co-localization in yellow (**G, H**). Scale bar for A, C, E, G = 50 μm; Scale bar for B, D, F, H = 10 μm.

METHOD

TUNEL Assay: The TUNEL assay was performed using the Click-iT® TUNEL assay kit (Life Technologies). For the pretreatment, 4% paraformaldehyde-fixed sections first went through xylene and a series of ethanol solutions (100%-50%) following 10 min antigen retrieval at 99 °C in sodium citrate solution (10mM sodium citrate, 0.05% Tween 20, pH = 6.0). After cooling down, the sections were incubated with PBS containing 0.25% TritonX-100 for 20 min at room temperature and then washed twice with deionized water. The treatment was carried out following the user guideline of the kit. Control sections were treated with DNase I solution and showed positive TUNEL reactions.

OPEN ACCESS Freely available online

PLOS ONE

Mitochondrial Complex 1 Inhibition Increases 4-Repeat Isoform Tau by SRSF2 Upregulation

Julius Bruch[1,2☯], Hong Xu[1,2☯], Anderson De Andrade[1], Günter Höglinger[1,2]*

1 Department of Translational Neurodegeneration, German Centre for Neurodegenerative Diseases (DZNE), Munich, Germany, **2** Department of Neurology, Technische Universität München, Munich, Germany

Abstract

Progressive Supranuclear Palsy (PSP) is a neurodegenerative disorder characterised by intracellular aggregation of the microtubule-associated protein tau. The tau protein exists in 6 predominant isoforms. Depending on alternative splicing of exon 10, three of these isoforms have four microtubule-binding repeat domains (4R), whilst the others only have three (3R). In PSP there is an excess of the 4R tau isoforms, which are thought to contribute significantly to the pathological process. The cause of this 4R increase is so far unknown. Several lines of evidence link mitochondrial complex I inhibition to the pathogenesis of PSP. We demonstrate here for the first time that annonacin and MPP^+, two prototypical mitochondrial complex I inhibitors, increase the 4R isoforms of tau in human neurons. We show that the splicing factor SRSF2 is necessary to increase 4R tau with complex I inhibition. We also found SRSF2, as well as another tau splicing factor, TRA2B, to be increased in brains of PSP patients. Thereby, we provide new evidence that mitochondrial complex I inhibition may contribute as an upstream event to the pathogenesis of PSP and suggest that splicing factors may represent an attractive therapeutic target to intervene in the disease process.

Citation: Bruch J, Xu H, De Andrade A, Höglinger G (2014) Mitochondrial Complex 1 Inhibition Increases 4-Repeat Isoform Tau by SRSF2 Upregulation. PLoS ONE 9(11): e113070. doi:10.1371/journal.pone.0113070

Editor: Oscar Arias-Carrion, Hospital General Dr. Manuel Gea González, Mexico

Received July 11, 2014; **Accepted** October 23, 2014; **Published** November 17, 2014

Data Availability: The authors confirm that all data underlying the findings are fully available without restriction. All relevant data are within the paper.

Funding: J.B. was funded by the Bavarian Research Foundation (Bayerische Forschungsstiftung), H.X. by the DAAD (German Academic Exchange Service), G.U.H. by the DFG (Deutsche Forschungsgemeinschaft, HO2402/6-2). The funders had no role in study design, data collection and analysis, decision to publish, or preparation of the manuscript.

Competing Interests: The authors have declared that no competing interests exist.

* Email: hoeglinger@lrz.tum.de

☯ These authors contributed equally to this work.

Introduction

Tauopathies are a heterogeneous group of neurodegenerative diseases with the common feature of intracellular aggregation of the microtubule associated protein tau. They include, but are not limited to, Alzheimer's Disease, Progressive Supranuclear Palsy (PSP), Argyrophilic Grain Disease (AGD), Corticobasal Degeneration (CBD), Pick's Disease and some other forms of frontotemporal dementias. Different tauopathies vary significantly in their clinical and pathological phenotype [1].

In the human central nervous system there are six predominant splicing variants of the *MAPT* gene, encoding tau proteins. These depend on the exclusion or inclusion of exons 2, 3 and 10: 3R0N, 3R1N, 3R2N, 4R0N, 4R1N and 4R2N [2]. 0N signifies the inclusion of neither exon 2 or 3. 1N denotes the inclusion of exon 2 but not 3, whilst 2N denotes the inclusion of both exons 2 and 3. 3R denotes the absence of exon 10, 4R its presence. Exon 10 codes for an additional microtubule binding repeat, so that 4R isoforms have 4 binding repeats, whilst 3R isoforms have only 3.

Across different tauopathies the isoform constitution varies. A common classification of tauopathies, therefore, is between the 3R isoform and the 4R isoform tauopathies [3]. While in healthy adults and in Alzheimer's disease 3R and 4R isoforms are generally in balance, PSP, CBD and AGD feature a relative excess of 4R isoforms [4]. Pick's Disease, conversely, has a relative excess of 3R isoforms. This imbalance is thought to play a major role in the pathogenesis of these tauopathies [5]. 4R isoforms are more prone to aggregation than 3R isoforms [5]. A single mutation in the *MAPT* gene affecting the inclusion of exon 10 to favour generation of 4R tau appears to be sufficient to trigger a tauopathy [6]. This has led to the hypothesis that an excess of 4R tau may be significantly pathogenic. Therefore, reducing the relative amount of 4R may be a strategy for therapy in 4R tauopathies [5,7].

Alternative splicing of exon 10 is regulated by a combination of *cis*-elements in exon 10 and intron 10, as well as by *trans*-acting factors [2]. It is through these *trans*-acting factors that alternative splicing can be modified and regulated by the cell. They are divided into heterogeneous nuclear ribonucleoproteins (hnRNPs) and serine/arginine-rich (SR) proteins or SR-like proteins. The SR proteins participate in the spliceosome and are thus involved in both constitutive splicing and the regulation of alternative splicing [8]. They are controlled through phosphorylation and acetylation and have been discussed as a potential drug target in the context of cancer treatment [9,10]. However, so far, the molecular mechanisms leading to preferential generation of 4R tau by alternative splicing of wild-type tau in sporadic 4R tauopathies are not understood.

There are several lines of evidence suggesting a role for dysfunction of the mitochondrial respiratory chain, particularly

of mitochondrial complex I, in the pathogenesis of PSP. A study using transmitochondrial cytoplasmic hybrid (cybrid) cell lines expressing mitochondrial genes from persons with PSP found complex I activity to be reduced [11]. Dysfunctional complex I is a major emitter of reactive oxygen species [12] and evidence of oxidative stress has been found in autopsy material of PSP patients [13,14]. A study using combined phosphorus and proton magnetic resonance spectroscopy has identified evidence for cerebral depletion in high-energy phosphates and increased lactate levels in PSP, a pattern compatible with a primary failure of the mitochondrial respiratory chain [15]. Finally, there is also an epidemiological association between the consumption of soursop fruit containing the mitochondrial complex I inhibitor annonacin [16] and a PSP-like tauopathy on the island of Guadeloupe [17]. Annonacin has been shown to induce a tauopathy *in vitro* in cultured neurons [16,18], as well as *in vivo* [19]. So far described are four effects of annonacin that are typical features for tauopathies, namely increased tau protein levels, tau hyperphosphorylation, redistribution of tau from the axons to the somatodendritic compartment, and eventual cell death [18]. Here, we explore the effect of complex I inhibition on the alternative splicing of tau.

Materials and Methods

Cell Culture

Nunc Nunclon Delta 6-well (for protein and mRNA) or 48-well (for cell assays) plates (Thermo Fisher Scientific, Waltham, MA, USA) were coated with 100 μg/ml poly-L-lysine (Sigma-Aldrich, St. Louis, MO, USA) and 5 μg/ml fibronectin (Sigma-Aldrich). LUHMES (Lund Human Mesencephalic) cells, derived from female human embryonic ventral mesencephalic cells by conditional immortalization [20] (Tet-off v-myc over-expression) were seeded in a concentration of 130,000 cells/cm^2 to achieve a confluence of 50%. They were then differentiated for 8 days in a medium of DMEM/F12 (Sigma-Aldrich), 1 μg/ml Tetracycline, 2 mg/ml GDNF and 490 μg/ml dbcAMP into post-mitotic neurons [21] with a dopaminergic phenotype [20]. On day 8 post differentiation the cells were treated with 25 nM annonacin, 20 μM 6-OHDA or 10 μM MPP^+ for 48 h. For the intoxication period the medium was replaced with new medium containing glucose levels reduced to 250 μM, i.e. the physiological concentration in the human brain [22]. For the starving condition, cells were incubated for 24 hours in pure DMEM (Life Technologies, Grand Island, NY, USA) with no additives and no glucose.

Human Brain Tissue and Ethics Statement

Human fresh frozen brain sections of the *locus coeruleus* area were obtained from The Netherlands Brain Bank, Netherlands Institute for Neuroscience, Amsterdam (www.brainbank.nl). All Material has been collected from donors for or from whom written informed consent for a brain autopsy and the use of the material and clinical information for research purposes had been obtained by The Netherlands Brain Bank in accordance with the Declaration of Helsinki.

Quantitative Real-Time PCR

RNA from human tissue samples was extracted by grinding the tissue in liquid nitrogen to a powder and then dissolving it in the RA1 buffer supplied as part of the NucleoSpin RNA (Macherey Nagel, Düren, Germany) RNA extraction kit +1% (v/v) 2-Mercaptoethanol (Sigma-Aldrich). RNA from cells was extracted by scraping the cells from the culture plate with RA1 buffer +1% (v/v) 2-Mercaptoethanol. The remaining extraction procedure was according to the manufacturer's instructions for the NucleoSpin RNA kit. RNA concentrations were determined using the NanoDrop 2000c Spectrophotometer (Thermo Fisher Scientific). The RNA was then transcribed into cDNA with the iScript cDNA Synthesis Kit (BioRad, Berkeley, CA, USA) using the manufacturer's instructions. Real-Time PCR was performed on the Applied Biosystems StepOnePlus (Life Technologies) system using TaqMan Universal Master Mix II and TaqMan primers against total *MAPT, MAPT 0N, MAPT 1N, MAPT 2N, MAPT 3R, MAPT 4R, SRSF1, SRSF2, SRSF3, SRSF6, SRSF7, SRSF9, SRSF11* and *TRA2B*. *PSMC1* and *POL2A* were used as reference genes for relative quantification in all tau splicing factor experiments, while *PPIB* and *GAPDH* were used in all tau isoform experiments as they were determined to be the most stably expressed across the respective experimental conditions. All values are relative quantities compared to untreated (control) cells. Three biological repeats with three technical repeats each were analysed. Analysis was conducted with the Applied Biosystems StepOnePlus (Life Technologies) and Qbase+ (Biogazelle, Zwijnaarde, Belgium) software packages. Absolute quantification was performed by creating a standard curve with plasmids containing either the 2N3R or the 2N4R spliced variant of *MAPT* (obtained as a gift from Eva-Maria Mandelkow, DZNE Bonn, Germany). The absolute quantity was computed by deriving the relationship between CT values and absolute quantity with the StepOne Plus software.

Western Blotting

Protein was extracted from cells using the M-PER Mammalian Protein Extraction Reagent (Thermo Fisher Scientific). The protein solution was frozen at −80°C immediately after retrieval and for a minimum of two hours. The solution was then thawed on ice, vortexed, centrifuged at 5000 g for 15 minutes at 4°C and the supernatant retrieved. Total protein concentrations were determined using the BCA kit (Thermo Fisher Scientific) by heating the samples at 60°C for 30 minutes and measuring the absorption on the NanoDrop 2000c Spectrophotometer (Thermo Fisher Scientific). 20 μg of total protein were then adjusted to equal concentrations between samples by dilution with M-PER and subsequently heated at 95°C for 5 minutes with 1× Roti-Load loading buffer (Carl Roth, Karlsruhe, Germany). SDS-PAGE was performed using precast Gels (anyKD, Bio-Rad) in a tris-glycine running buffer (14.4% glycine, 3% Tris, 1% SDS w/v, Carl Roth). The protein was blotted onto PVDF membrane (Bio-Rad) at 70 V for 65 minutes. The membrane was blocked with 1× Roti-Block solution (Carl Roth) for 1h and then incubated at 4°C overnight under gentle shaking with the primary antibody (table 1) in TBS with 5% BSA (Cell Signaling, Danvers, MA, USA) and 0.05% TWEEN (Sigma-Aldrich). The membranes were then washed and incubated with the appropriate secondary antibody at 1:2500 (v/v) in 1× Roti-Block solution for 2 h, followed by further washing and exposure to Clarity Western ECL Substrate (Bio-Rad) or, in the case of 4-repeat tau, to **ECL solution** (General Electric, Fairfield, CT, USA). Chemiluminescence was detected with the Gel image System (Bio-Rad) and analysed by background subtracted optical density analysis with ImageLab software (Bio-Rad).

siRNA Silencing

LUHMES cells were seeded out and differentiated as described above and allowed to adhere to the plate floor for 4 h. siRNA (Sigma-Aldrich) targeted against SRSF2 (final concentration 200 nM) and Lipofectamine RNAiMAX (Life Technologies) (final concentration 1.2 μl/ml) were dissolved in separate aliquots of

Table 1. Primary Antibody Concentrations Used.

Antigen	Clone	Species	Concentration (v/v)	Company
Human tau	HT7	Mouse	1:1000	Pierce Antibodies, Thermo
3-repeat tau	8E6/C11	Mouse	1:500	Millipore
4-repeat tau	1E1/A6	Mouse	1:300	Millipore
Actin (I-19)	Polyclonal	Goat	1:2500	Santa Cruz Biotechnologies

doi:10.1371/journal.pone.0113070.t001

medium (OptiMEM, Life Technologies). The diluted siRNA was then added to the diluted Lipofectamine RNAiMAX. The combined solution was then allowed to incubate for 20 minutes before being added to the cells.

ATP Assay

ATP assays were conducted using the ATP test kit by Lonza according to the manufacturer's instructions. Luminescence was read with the FLUOstar Omega platereader (BMG Labtech). The data was analysed using the MARS Data Analysis Software (BMG Labtech).

MTT Assay

Thiazolyl Blue Tetrazolium Blue (MTT) (Sigma Aldrich) was dissolved in sterile PBS to a concentration of 5 mg/ml. This stock solution was added to the cells in culture medium to achieve a final concentration of 0.5 mg/ml. The 48-well culture plate was then incubated at 37°C for 1 h, the medium removed completely and frozen at −80°C for 1 h. The plate was then thawed, 300 µl DMSO (AppliChem, Darmstadt, Germany) was added per well and the plate was shaken to ensure complete dissolution of the violet crystals. 100 µl from each well were transferred to a new 96-well plate and the absorbance was read with the platereader at a wavelength of 590 nm (reference wave length 630 nm). The data was analysed using the MARS Data Analysis Software (BMG Labtech).

Statistics

Prism 6 (GraphPad Software, La Jolla, CA, USA) was used for statistical calculations and for the creation of line and bar graphs. Results were compared by 2-way ANOVA with Sidak post-hoc test, unless stated otherwise. Data are shown as mean ± SEM. $P < 0.05$ was considered significant.

Results

Annonacin Causes an Upregulation of the Tau 4-Repeat Isoform

We first characterized expression of tau isoforms in LUHMES cells, a cell culture line of human mesencephalic neurons, derived from female human embryonic ventral mesencephalic cells by conditional immortalization (Tet-off v-myc over-expression) [21]. These cells start expressing the 4-repeat (4R) isoform of tau from day 8 post differentiation into a neuronal phenotype. On day 10, 4R-spliced mRNA makes up 3.9% ±0.3 (n = 3) of the total MAPT mRNA. We used this human neuronal model for the present work as rodent cells express only 4R tau.

When treated with annonacin at a concentration of 25 nM for 48 h from days 8 to 10 post differentiation, LUHMES cells remain 60.7±0.4% viable (MTT assay) with an ATP concentration of 64±1% compared to that of untreated cells (figure 1A).

Under these conditions we observed the mRNA of the 4R isoforms of tau to be upregulated significantly (figure 1B) compared with untreated cells, as determined by quantitative PCR. There was no significant change in the relative quantity of 3R isoforms. The level of inclusion of exons 2 and 3 also did not change significantly, although there was a slight increase in the amount of 0N isoforms. This indicates that annonacin selectively increases inclusion of exon 10 with no or little relative effect on the alternative splicing of the other exons.

We also observed an upregulation of the 4R tau isoforms on the protein level by Western blot (figure 1C). 3R tau was again not significantly changed. The level of upregulation at the protein level is very similar to that on the mRNA level, suggesting a tight correlation between the regulation of alternative splicing and the isoform distribution seen at the protein level. There was no significant increase in the amount of total tau with annonacin, probably due to the greater proportion of 3R isoforms in LUHMES cells of this age.

The Splicing Factor SRSF2 Is Necessary for Annonacin-Mediated Alternative Splicing

We next explored the mechanism of how annonacin induces this isoform change. We tested 10 splicing factors known to influence the inclusion or exclusion of exon 10 in the MAPT gene [2] by quantitative PCR. An overview of the splicing factors tested is shown in table 2.

We found SRSF2 to be the only splicing factor significantly upregulated with annonacin treatment that is known to promote the inclusion of exon 10 (figure 2A). This prompted us to explore whether SRSF2 has a functional role to play in annonacin mediated 4R upregulation. We knocked down *SRSF2* with siRNA starting from 6 hours post differentiation in LUHMES cells and treated these cells with annonacin from days 8–10, as in the previous experiments. At day 10, *SRSF2* was reduced by half. In spite of this incomplete silencing efficiency, the 4R isoform of *MAPT* in annonacin treated cells was reduced dramatically compared to untreated cells (figure 2B). This suggests that SRSF2 plays a critical role in the upregulation of the 4R MAPT isoforms seen upon annonacin treatment.

More Splicing Factors Are Upregulated in Human PSP

We also tested splicing factor expression levels in human brain tissue of the *locus coeruleus* of 4 PSP patients and five control patients free of psychiatric or neurodegenerative diseases (table 3). This time, however, we limited our analysis to those splicing factors known to increase *MAPT* exon 10 inclusion. We confirmed the increase of the 4R isoform in the PSP patients compared to the controls (figure 2C). Expression of the splicing factors *SRSF2* and *TRA2B* was also increased significantly. This suggests that the increase in 4R isoforms seen with annonacin treatment may

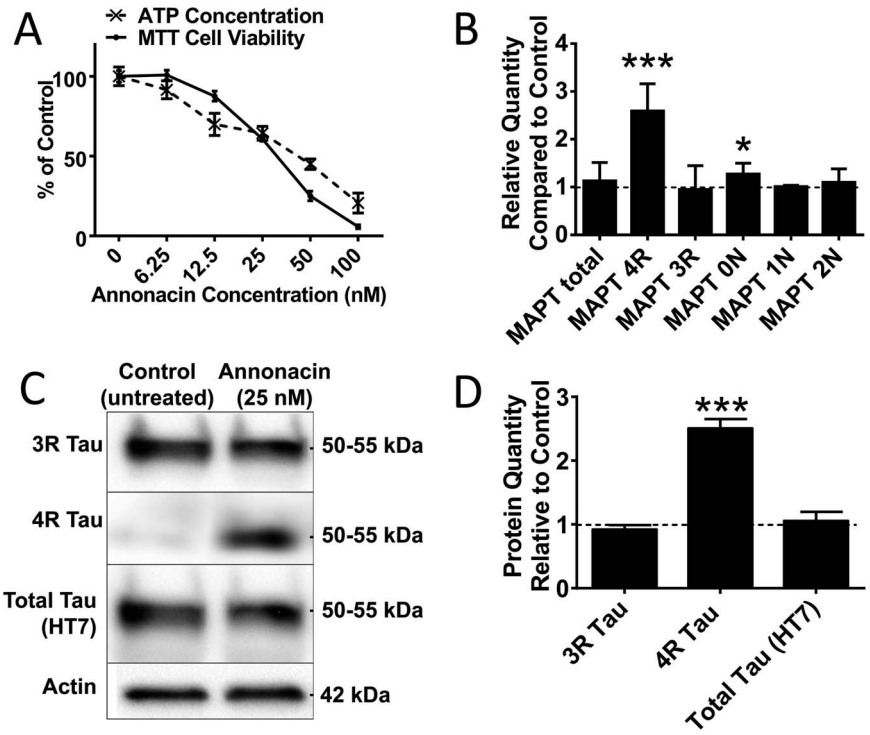

Figure 1. Annonacin Causes an Upregulation of the 4R Isoforms of Tau. A) LUHMES neurons were treated with different concentrations of annonacin for 48 h from day 8–10 post differentiation (n = 12). The MTT test, a measure for mitochondrial reducing function, and ATP concentration, are expressed as a relative percentage compared to untreated control cells. B) 4R isoform (exon 10) mRNA is upregulated with annonacin treatment. Quantitative PCR results showing the relative quantity of mRNA for different *MAPT* splicing variants in cells treated with 25 nM annonacin for 48 h from day 8–10 post differentiation compared to untreated cells (dotted line). 3 biological repeats with 3 technical repeats each. ***: $p<0.001$, *: $p<0.05$ vs. untreated cells (2-way ANOVA with Sidak's post-hoc test). C) 4R isoform protein is upregulated with annonacin treatment. Western blot for 3R and 4R isoforms of tau protein, as well as total tau (detected with the HT7 antibody). LUHMES cells were either left untreated or treated with 25 nM annonacin. Actin was used as loading control. D) Quantification of figure 1C. Results show the relative quantity (fold-change) compared to untreated control cells (relative quantity = 1, represented by dotted line). 3 biological repeats. ***: $p<0.001$ vs. untreated cells (2-way ANOVA with Sidak's post-hoc test).
doi:10.1371/journal.pone.0113070.g001

account partly for the mechanism by which 4R isoform tau is upregulated in PSP.

4R Tau Upregulation Occurs with Other Complex I Inhibitors but Not Oxidative Stress

We tested whether 4R isoform upregulation upon annonacin treatment is a non-specific consequence of neuronal injury, specific to mitochondrial complex I inhibition or even more specific to annonacin. We therefore repeated the experiment with 1-methyl-4-phenylpyridinium (MPP^+), another complex I inhibitor, 6-hydroxydopamine (6-OHDA), a neurotoxin known to be neurotoxic primarily through oxidative stress [23] and by starving the cells of glucose and nutrients. As shown in figures 3 A and B, a comparable level of toxicity and ATP reduction to

Table 2. Overview of the splicing factors known to influence MAPT exon 10 alternative splicing.

Splicing factor	Target *cis*-element	Effect on exon 10 splicing
SRSF1 (SRp30a, ASF)	PPE	Inclusion
SRSF2 (SRp30b, SC35)	SC35-like	Inclusion
SRSF3 (SRp20)	ND	Exclusion
SRSF4 (SRp75)	ND	Exclusion
SRSF6 (SRp55)	ND	Exclusion
SRSF7 (9G8)	ISS	Exclusion
SRSF9 (SRp30c)	ND	Inclusion
SRSF11 (SRp54)	PPE	Exclusion
TRA2B	PPE	Inclusion

Source: Adapted from [2].
doi:10.1371/journal.pone.0113070.t002

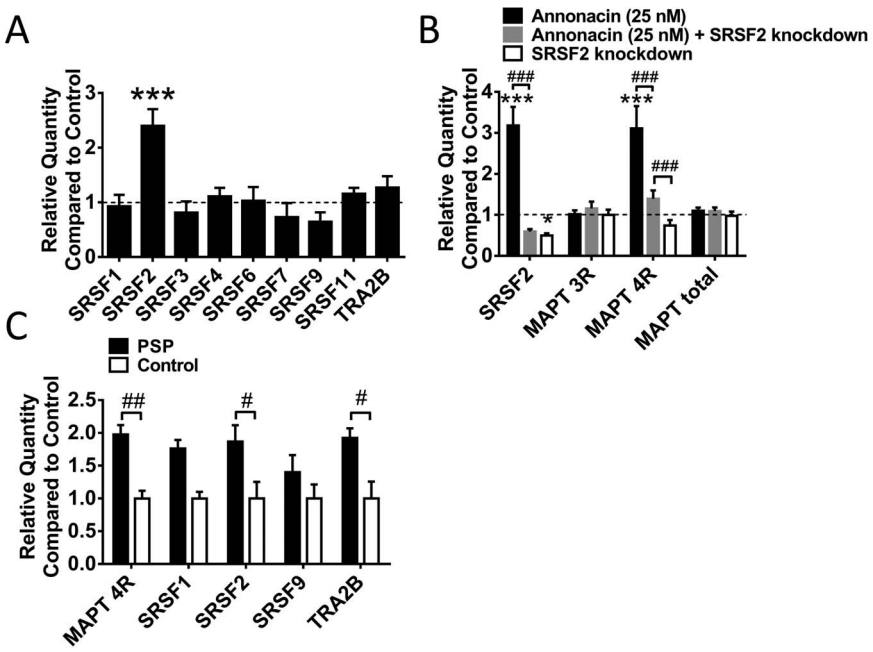

Figure 2. SRSF2 is a Critical Player in Annonacin Mediated Tau Alternative Splicing. A) Quantitative PCR results for 9 different splicing factors known to have an effect on exon 10 alternative splicing (table 2). Data shown are relative quantities compared to untreated cells (dotted line). Only SRSF2 was elevated significantly with annonacin treatment. All other splicing factors tested were not significantly elevated. 3 biological repeats with 3 technical repeats each. ***: $p<0.001$, *: $p<0.05$ vs. untreated control (2-way ANOVA with Sidak's post-hoc test). B) Quantitative PCR results for LUHMES cells on day 10 post differentiation treated with SRSF2 knockdown siRNA for 10 days and/or with annonacin for 48 h. 3 biological repeats with 3 technical repeats each. ***: $p<0.001$ vs. untreated control (dotted line); ###: $p<0.001$ (2-way ANOVA with Sidak's post-hoc test). C) Quantitative PCR results for the 4 splicing factors known to increase MAPT exon 10 inclusion in *locus coeruleus* tissue of four PSP patients and five controls without neurodegenerative diseases. 3 biological repeats with 3 technical repeats each. #: $p<0.05$, ##: $p<0.01$ (2-way ANOVA with Sidak's post-hoc test).
doi:10.1371/journal.pone.0113070.g002

that of 25 nM annonacin is achieved by 6-OHDA at a concentration of 20 μM (22% ATP reduction) and by MPP^+ at a concentration of 10 μM (37% ATP reduction). Therefore, we decided to use these concentrations to test the MAPT isoform changes with these toxins.

With MPP^+ treatment we observed a significant increase in exon 10 inclusion on the mRNA level by qPCR (figure 3C) and in the levels of 4R tau isoforms by Western blot (figure 4A, B) compared to controls, as with annonacin. With 6-OHDA treatment and with starvation we only observed a slight reduction in both 4R and 3R isoforms. In all three cases the inclusion of exons 2 and 3 did not increase (data not shown). This would suggest that complex I inhibition in general and not oxidative stress or neuronal suffering per se is responsible for the increased level of exon 10 inclusion observed with annonacin.

Finally, we explored the role of *SRSF2* in these observations. We found that MPP^+ also acts via SRSF2 upregulation and that there is no *SRSF2* upregulation with 6-OHDA treatment or starvation.

Table 3. Overview of Human Tissue Used.

Case Number	Diagnosis	Cause of Death	Age at death	Braak Stage	Sex	Postmortem delay (hours: minutes)
P1	PSP	"Natural death"	73	2C	Male	4:20
P2	PSP	Acute heart failure	70	3	Male	6:50
P3	PSP	Aspiration pneumonia	73	2	Male	6:15
P4	PSP	Urinary tract infection	70	1A	Male	5:20
C1	Non-demented control	Pancreas carcinoma	70	0	Male	7:30
C2	Non-demented control	Prostate cancer	69	0	Male	5:55
C3	Non-demented control	Lung emboli (clinical suspicion)	73	0	Male	24:45
C4	Non-demented control	Sepsis	71	1	Male	7:40
C5	Non-demented control	Myocardial infarction	67	1B	Male	18:35

doi:10.1371/journal.pone.0113070.t003

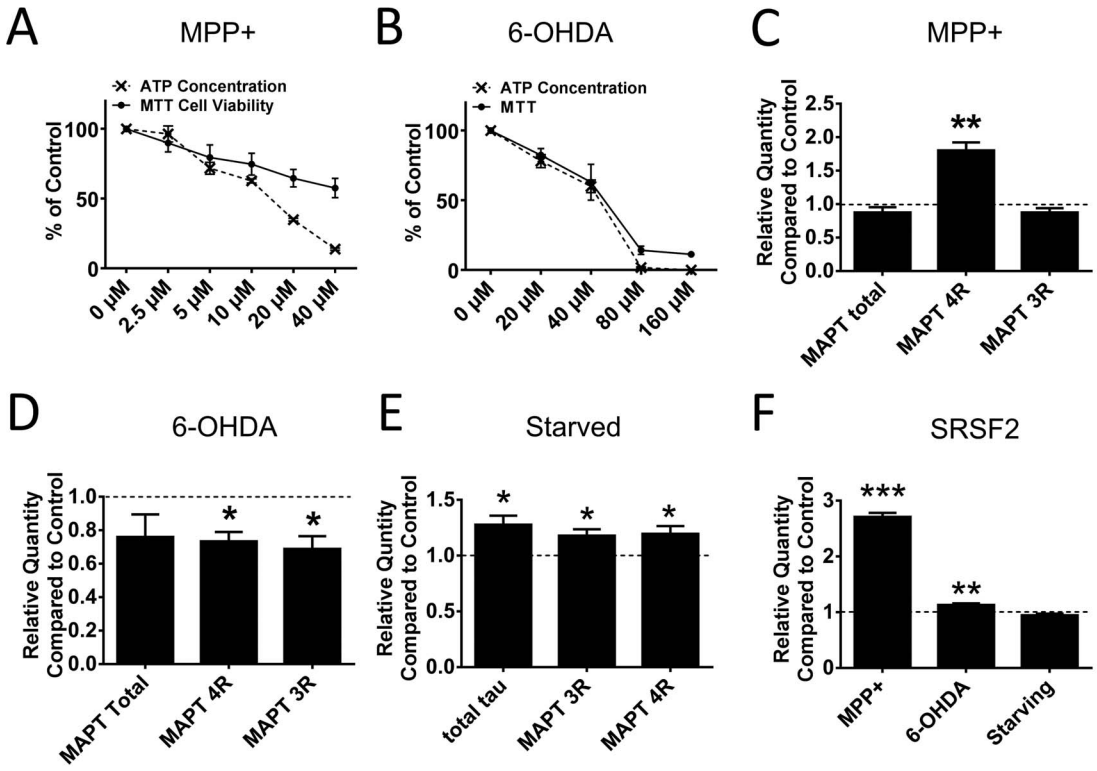

Figure 3. The 4R Isoform Shift Can Be Reproduced with Another Complex I Inhibitor but not with the Oxidative Stressor 6-OHDA. A) ATP concentration and MTT cell viability in LUHMES cells as measured by the MTT assay for different concentrations of 6-OHDA. Treatment was for 48 h from day 8–10 post differentiation. n = 12. B) ATP concentration and MTT cell viability in LUHMES cells as measured by the MTT assay for different concentrations of MPP+. Treatment was for 48 h from day 8–10 post differentiation. n = 12. C) Quantitative PCR results of MAPT splicing variants for LUHMES cells treated with 10 µM MPP^+ for 48 h from day 8–10 post differentiation. 3 biological repeats with 3 technical repeats each. **: $p<0.01$ vs. untreated cells (dotted line), (2-way ANOVA with Sidak's post-hoc test). D) Quantitative PCR results of MAPT splicing variants for LUHMES cells treated with 20 µM 6-OHDA for 48 h from day 8–10 post differentiation. 3 biological repeats with 3 technical repeats each. *: $p<0.05$ vs. untreated cells (dotted line), (2-way ANOVA with Sidak's post-hoc test). E) Quantitative PCR results of MAPT splicing variants for LUHMES cells starved of nutrients and glucose for 24 h from day 8–9 post differentiation. 3 biological repeats with 3 technical repeats each. *: $p<0.05$ vs. untreated cells (dotted line), (2-way ANOVA with Sidak's post-hoc test). F) Quantitative PCR results of SRSF2 for LUHMES cells treated with 10 µM MPP^+ or 20 µM 6-OHDA for 48 h from day 8–10 post differentiation or starved for 24 h from day 8–9 post differentiation. 3 biological repeats with 3 technical repeats each. *: $p<0.05$, **: $p<0.01$ vs. untreated cells (dotted line), (2-way ANOVA with Sidak's post-hoc test).
doi:10.1371/journal.pone.0113070.g003

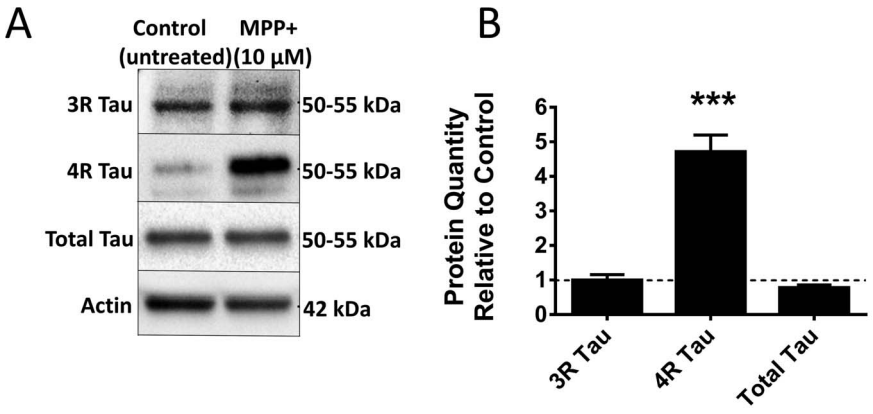

Figure 4. The 4R Isoform was upregulated in the protein level with MPP^+ treatment. A) 4R isoform protein is upregulated with MPP^+ treatment. Western blot for 3R and 4R isoforms of tau protein, as well as total tau (detected with the HT7 antibody). LUHMES cells were either left untreated or treated with 10 µM MPP^+. Actin was used as loading control. B) Quantification of figure 1G. Results show the relative quantity compared to the untreated control cells (dotted line). 3 biological repeats. ***: $p<0.001$ vs. untreated cells (2-way ANOVA with Sidak's post-hoc test).
doi:10.1371/journal.pone.0113070.g004

Discussion

Mitochondrial Complex I Inhibition Reproduces the 4R Isoform Shift Seen in Several Tauopathies

In this paper we have been able to add the increase in 4R tau isoforms as an additional feature to the list of characteristics of PSP that annonacin treatment reproduces in cell culture. This makes annonacin treated neurons a good model for PSP and potentially other sporadic 4R tauopathies. It is unique in the fact that it does not rely on any genetic modification of the *MAPT* gene or artificial overexpression. The fact that it reliably produces an increase in the 4R tau isoforms would also allow it to be used to screen, test and develop candidate drugs targeting tau alternative splicing – something that would not be possible with overexpression-based models of tauopathy.

However, the effect on alternative splicing is not specific to annonacin. Rather, it seems to be related to mitochondrial complex I inhibition more generally. This is suggested by the fact that we have observed the same increase in 4R tau isoforms with MPP^+, another complex I inhibitor. In fact, other features of tauopathy have also been reproduced by other complex I inhibitors [24,25]. However, due to the epidemiological evidence from Guadeloupe strongly linking annonacin consumption to a PSP-like tauopathy, annonacin makes a particularly convincing case as a cell culture based model for PSP. The only drawback of this model relying on immature human neurons is that despite the upregulation of 4R tau, after 10 days there still appears to be overall more 3R than 4R tau, whereas in adult human brain neurons, 3R and 4R are more or less balanced.

However, it is not yet fully understood to what extent the relative increase in the 4R tau isoform contributes to neurotoxicity or impairment of neural functioning. 4R tau isoform increases are only seen in a selection of tauopathies and are region specific. In Alzheimer's disease, there is no abnormal upregulation of 4R isoforms. In PSP, there is some evidence that the 4R isoform may not be upregulated in the frontal cortex, despite the existence of tau pathology in this region [26]. On the other hand, patients with FTDP-17 due to mutations that exclusively affect tau alternative splicing and result in an increase of 4R tau, are evidence that an upregulation of the 4R isoforms is sufficient to start tau aggregation [2,6].

SRSF2 Forms the Link Between Complex I Inhibitors and the Increase in 4R Isoforms

We have identified SRSF2 as a mediator essential for mitochondrial complex I inhibitor induced exon 10 inclusion. The fact that a knockdown of SRSF2 reverses the annonacin induced increase in 4R tau confirms that SRSF2 plays a necessary role for this isoform shift.

SRSF2 is controlled by several kinases including SRPK, AKT, topoisomerase I and CLK/STY family kinases, as well as lysine acetylation [27]. The histone deacetylase inhibitor sodium butyrate has already been demonstrated to increase SRSF2 levels [28], whilst the kinase activity of topoisomerase I can be inhibited with the antitumour drug NB-506 [9]. This suggests that, at least indirectly, SRSF2 is a potentially drugable target.

In our annonacin-treated cell cultures, which might be considered to be an acute model of a sporadic tauopathy, inhibition of SRS2 prevented the 4R isoform shift of tau but not the cell death induced by annonacin. This suggests that, in this model, the 4R tau is not necessary for cell death, since neurons might rather die from reduced energy production [18]. This does, however, not exclude that in a more chronic situation with even higher levels of 4R tau this isoform shift may become the predominant cause of neuronal dysfunction and death.

Complex I Inhibition Is Unlikely to Explain All of the Increase in 4R Isoforms in PSP

In human PSP patients both the SRSF2 and TRA2B splicing factors are upregulated. This suggests that the 4R upregulation is not exclusively due to complex I inhibition, as in that case we would have expected only SRSF2 to be upregulated. Therefore, exploring upstream events leading to TRA2B upregulation may lead to insights on further reasons for the increase in 4R tau isoforms in some tauopathies. It would also be interesting to compare the splicing factor expression levels in 3R tauopathies versus 4R tauopathies.

If SRSF2 is confirmed to be a key player in mediating the 4R isoform upregulation in PSP and other 4R tauopathies, this would make it a suitable drug target for reducing this isoform shift.

Conclusion

In summary, we can conclude that SRSF2 is a necessary mediator for mitochondrial complex I inhibitor induced tau 4R isoform upregulation. As SRSF2 is also increased in PSP patients this suggests mitochondrial complex I inhibition may play at least a partial role in the pathogenesis of 4R tauopathies such as PSP. However, other mechanisms are also likely to contribute.

Acknowledgments

Mr Robin Konhäuser and Ms Magda Baba were instrumental in maintaining the cell lines and cell culture. We would like to acknowledge the Netherlands Brain Bank for their generous contribution of the human brain tissue samples.

Author Contributions

Conceived and designed the experiments: JB HX GUH. Performed the experiments: JB HX. Analyzed the data: JB HX ADA. Contributed reagents/materials/analysis tools: ADA. Wrote the paper: JB HX GUH.

References

1. Williams DR (2006) Tauopathies: classification and clinical update on neurodegenerative diseases associated with microtubule-associated protein tau. Intern Med J 36: 652–660.
2. Liu F, Gong CX (2008) Tau exon 10 alternative splicing and tauopathies. Mol Neurodegener 3: 8.
3. Chen S, Townsend K, Goldberg TE, Davies P, Conejero-Goldberg C (2010) MAPT isoforms: differential transcriptional profiles related to 3R and 4R splice variants. J Alzheimers Dis 22: 1313–1329.
4. Buee L, Delacourte A (1999) Comparative biochemistry of tau in progressive supranuclear palsy, corticobasal degeneration, FTDP-17 and Pick's disease. Brain Pathol 9: 681–693.
5. Zhou J, Yu Q, Zou T (2008) Alternative splicing of exon 10 in the tau gene as a target for treatment of tauopathies. BMC Neurosci 9 Suppl 2: S10.
6. Spillantini MG, Murrell JR, Goedert M, Farlow MR, Klug A, et al. (1998) Mutation in the tau gene in familial multiple system tauopathy with presenile dementia. Proc Natl Acad Sci U S A 95: 7737–7741.
7. Avale ME, Rodriguez-Martin T, Gallo JM (2013) Trans-splicing correction of tau isoform imbalance in a mouse model of tau mis-splicing. Hum Mol Genet 22: 2603–2611.
8. Will CL, Luhrmann R (2011) Spliceosome structure and function. Cold Spring Harb Perspect Biol 3.
9. Pilch B, Allemand E, Facompre M, Bailly C, Riou JF, et al. (2001) Specific inhibition of serine- and arginine-rich splicing factors phosphorylation, spliceosome assembly, and splicing by the antitumor drug NB-506. Cancer Res 61: 6876–6884.

10. Zhong XY, Ding JH, Adams JA, Ghosh G, Fu XD (2009) Regulation of SR protein phosphorylation and alternative splicing by modulating kinetic interactions of SRPK1 with molecular chaperones. Genes Dev 23: 482–495.
11. Swerdlow RH, Golbe LI, Parks JK, Cassarino DS, Binder DR, et al. (2000) Mitochondrial dysfunction in cybrid lines expressing mitochondrial genes from patients with progressive supranuclear palsy. J Neurochem 75: 1681–1684.
12. Lenaz G, Baracca A, Fato R, Genova ML, Solaini G (2006) Mitochondrial Complex I: structure, function, and implications in neurodegeneration. Ital J Biochem 55: 232–253.
13. Stamelou M, de Silva R, Arias-Carrion O, Boura E, Hollerhage M, et al. (2010) Rational therapeutic approaches to progressive supranuclear palsy. Brain 133: 1578–1590.
14. Albers DS, Swerdlow RH, Manfredi G, Gajewski C, Yang L, et al. (2001) Further evidence for mitochondrial dysfunction in progressive supranuclear palsy. Exp Neurol 168: 196–198.
15. Stamelou M, Pilatus U, Reuss A, Magerkurth J, Eggert KM, et al. (2009) In vivo evidence for cerebral depletion in high-energy phosphates in progressive supranuclear palsy. J Cereb Blood Flow Metab 29: 861–870.
16. Lannuzel A, Michel PP, Hoglinger GU, Champy P, Jousset A, et al. (2003) The mitochondrial complex I inhibitor annonacin is toxic to mesencephalic dopaminergic neurons by impairment of energy metabolism. Neuroscience 121: 287–296.
17. Lannuzel A, Hoglinger GU, Verhaeghe S, Gire L, Belson S, et al. (2007) Atypical parkinsonism in Guadeloupe: a common risk factor for two closely related phenotypes? Brain 130: 816–827.
18. Escobar-Khondiker M, Hollerhage M, Muriel MP, Champy P, Bach A, et al. (2007) Annonacin, a natural mitochondrial complex I inhibitor, causes tau pathology in cultured neurons. J Neurosci 27: 7827–7837.
19. Yamada ES, Respondek G, Mussner S, de Andrade A, Hollerhage M, et al. (2014) Annonacin, a natural lipophilic mitochondrial complex I inhibitor, increases phosphorylation of tau in the brain of FTDP-17 transgenic mice. Exp Neurol 253C: 113–125.
20. Lotharius J, Falsig J, van Beek J, Payne S, Dringen R, et al. (2005) Progressive degeneration of human mesencephalic neuron-derived cells triggered by dopamine-dependent oxidative stress is dependent on the mixed-lineage kinase pathway. J Neurosci 25: 6329–6342.
21. Scholz D, Poltl D, Genewsky A, Weng M, Waldmann T, et al. (2011) Rapid, complete and large-scale generation of post-mitotic neurons from the human LUHMES cell line. J Neurochem 119: 957–971.
22. Silver IA, Erecinska M (1994) Extracellular glucose concentration in mammalian brain: continuous monitoring of changes during increased neuronal activity and upon limitation in oxygen supply in normo-, hypo-, and hyperglycemic animals. J Neurosci 14: 5068–5076.
23. Glinka Y, Gassen M, Youdim MB (1997) Mechanism of 6-hydroxydopamine neurotoxicity. J Neural Transm Suppl 50: 55–66.
24. Schapira AH (2010) Complex I: inhibitors, inhibition and neurodegeneration. Exp Neurol 224: 331–335.
25. Hoglinger GU, Lannuzel A, Khondiker ME, Michel PP, Duyckaerts C, et al. (2005) The mitochondrial complex I inhibitor rotenone triggers a cerebral tauopathy. J Neurochem 95: 930–939.
26. Chambers CB, Lee JM, Troncoso JC, Reich S, Muma NA (1999) Overexpression of four-repeat tau mRNA isoforms in progressive supranuclear palsy but not in Alzheimer's disease. Ann Neurol 46: 325–332.
27. Edmond V, Moysan E, Khochbin S, Matthias P, Brambilla C, et al. (2011) Acetylation and phosphorylation of SRSF2 control cell fate decision in response to cisplatin. EMBO J 30: 510–523.
28. Edmond V, Brambilla C, Brambilla E, Gazzeri S, Eymin B (2011) SRSF2 is required for sodium butyrate-mediated p21(WAF1) induction and premature senescence in human lung carcinoma cell lines. Cell Cycle 10: 1968–1977.

PLOS ONE

RESEARCH ARTICLE

Piericidin A Aggravates Tau Pathology in P301S Transgenic Mice

Matthias Höllerhage[1,2,3☯], Roman Deck[1☯], Anderson De Andrade[1,2], Gesine Respondek[1,2,3], Hong Xu[1,2], Thomas W. Rösler[1,2], Mohamed Salama[1,4], Thomas Carlsson[1,5], Elizabeth S. Yamada[1,6], Seham A. Gad El Hak[4], Michel Goedert[7], Wolfgang H. Oertel[1], Günter U. Höglinger[1,2,3]*

1. Dept. of Neurology, Philipps-Universität, Marburg, Germany, **2.** German Center for Neurodegenerative Diseases, Dept. for Translational Neurodegeneration, Munich, Germany, **3.** Department of Neurology, Technische Universität München, Munich, Germany, **4.** Department of Toxicology, Mansoura University, Mansoura, Egypt, **5.** Department of Pharmacology, Institute of Neuroscience and Physiology, Sahlgrenska Academy, University of Gothenburg, Gothenburg, Sweden, **6.** Experimental Neuropathology Laboratory, Federal University of Pará, Belém, Brazil, **7.** Division of Neurobiology, University of Cambridge, Cambridge, United Kingdom

*guenter.hoeglinger@dzne.de

☯ These authors contributed equally to this work.

OPEN ACCESS

Citation: Höllerhage M, Deck R, De Andrade A, Respondek G, Xu H, et al. (2014) Piericidin A Aggravates Tau Pathology in P301S Transgenic Mice. PLoS ONE 9(12): e113557. doi:10.1371/journal.pone.0113557

Editor: Emmanuel Planel, Centre Hospitalier de l'Université Laval, Canada

Received: May 14, 2014

Accepted: October 29, 2014

Published: December 1, 2014

Data Availability: The authors confirm that all data underlying the findings are fully available without restriction. All relevant data are within the paper.

Funding: This work was supported by the Deutsche Forschungsgemeinschaft (HO2402/6-1, HO2402/8-1), the German Ministry of Education and Research (BMBF GEF 10-54), Science and Technology Development Fund (Egypt, GEF 10-54), and the German Academic Exchange Service (DAAD to ACdA, HX, MS). Wolfgang H. Oertel is Senior research Professor of the Charitable Hertie Foundation, Frankfurt/Main, Germany. The funders had no role in study design, data collection and analysis, decision to publish, or preparation of the manuscript.

Competing Interests: The authors have declared that no competing interests exist.

Abstract

Objective: The P301S mutation in exon 10 of the tau gene causes a hereditary tauopathy. While mitochondrial complex I inhibition has been linked to sporadic tauopathies. Piericidin A is a prototypical member of the group of the piericidins, a class of biologically active natural complex I inhibitors, isolated from *streptomyces spp.* with global distribution in marine and agricultural habitats. The aim of this study was to determine whether there is a pathogenic interaction of the environmental toxin piericidin A and the P301S mutation.

Methods: Transgenic mice expressing human tau with the P301S-mutation ($P301S^{+/+}$) and wild-type mice at 12 weeks of age were treated subcutaneously with vehicle (N=10 $P301S^{+/+}$, N=7 wild-type) or piericidin A (N=9 $P301S^{+/+}$, N=9 wild-type mice) at a dose of 0.5 mg/kg/d for a period of 28 days via osmotic minipumps. Tau pathology was measured by stereological counts of cells immunoreative with antibodies against phosphorylated tau (AD2, AT8, AT180, and AT100) and corresponding Western blot analysis.

Results: Piericidin A significantly increased the number of phospho-tau immunoreactive cells in the cerebral cortex in $P301S^{+/+}$ mice, but only to a variable and mild extent in wild-type mice. Furthermore, piericidin A led to increased levels of pathologically phosphorylated tau only in $P301S^{+/+}$ mice. While we observed no apparent cell loss in the frontal cortex, the synaptic density was reduced by piericidin A treatment in $P301S^{+/+}$ mice.

Discussion: This study shows that exposure to piericidin A aggravates the course of genetically determined tau pathology, providing experimental support for the concept of gene-environment interaction in the etiology of tauopathies.

Introduction

Tau is a predominantly neuronal protein of which six major isoforms are generated by alternative splicing [1–4] from one gene *MAPT*, localized on the long arm of chromosome 17 (17q21) [5]. Tau is involved in the assembly and stabilization of microtubules [6]. Thus it plays an important role in axonal transport and neuronal viability. Intracellular aggregation of hyperphosphorylated tau protein is the histopathological hallmark of a group of neurodegenerative diseases, called tauopathies [7, 8]. The pathological hyperphosphorylation of tau-protein is considered as a possible early step in the formation of tau-aggregates in tauopathies [9].

The etiology of neurodegenerative tauopathies is multifactorial. Monogenetic *MAPT* mutations are responsible for some hereditary tauopathies, where so far, 51 disease-causing *MAPT* mutations are known [4]. One of these is the P301S mutation in exon 10, which leads to a substitution of the proline at position 301 by serine. The P301S mutation was first described in 1999 in families showing symptoms of corticobasal degeneration and frontotemporal dementia [10, 11]. Further work demonstrated, that there are two predominant clinical phenotypes in the patients carrying this mutation. Some show mainly parkinsonism similar to patients with progressive supranuclear palsy (PSP), while others show mainly symptoms of frontotemporal dementia [12]. This observation strongly suggests that independent genetic or environmental factors appear to shape the clinical phenotype of the disease caused by the P301S *MAPT* mutation.

In contrast to the purely genetically caused tauopathies described above, there are other tauopathies that appear to originate from exposure to a specific environmental factor. One prototypic example is the atypical Parkinson syndrome with tau pathology on the Caribbean island of Guadeloupe. Epidemiological studies have linked the disease to a high consumption of products from Annonaceae plants [13–15]. These plants contain high amounts of acetogenins, a class of lipophilic and potent inhibitors of complex I of the mitochondrial respiratory chain [16, 17]. The major representative of the annonaceous acetogenins is annonacin [18]. Systemic exposure to annonacin for 28 days induced neurodegeneration in rats *in vivo* [19]. Treatment of cultured striatal neurons from embryonic rats led to the accumulation of hyperphosphorylated tau in the cell soma of these cells [20]. These data strongly suggest that an environmental factor can trigger a tauopathy.

Between these two extremes of tauopathies, with solely monogenetic or environmental causes, the vast majority of sporadic cases are considered to result

from an interaction of genetic predispositions (e.g. [21]) and environmental triggers or modifiers.

However, not much is known about environmental factors that could either trigger or modify the course of a genetically determined tauopathy. Since the consumption of products from Annonaceae plants is uncommon in North America or Europe, the question arises, which other environmental factors could be relevant in the etiology of tauopathies. A previous *in vitro* study showed, that a broad spectrum of natural complex I inhibitors can induce tau pathology and cell death in cultured neurons [22]. One of the most potent natural neurotoxins to induce somatodendritic accumulation of phosphorylated tau and cell death in nanomolar concentrations is piericidin A [22]. Piericidin A, is the most common member of the family of piericidins, a class of potent complex I inhibitors synthesized by *streptomyces spp.* [23, 24]. These bacteria are ubiquitously present in marine and agricultural habitats [25].

The present study aimed to investigate the potential of piericidin A to trigger a tauopathy *in vivo* in wild type mice or to modify the course of a genetically caused tauopathy in transgenic mice overexpressing human P301S mutant tau [26]. Therefore, we treated P301S tau transgenic mice and wild-type mice with Piericidin A or vehicle by subcutaneous infusion over a period of 28 days and analyzed their brains for the presence and severity of tau-pathology.

Methods

Animals

P301S transgenic mice were developed by Prof. Michel Goedert, Division of Neurobiology, University of Cambridge (Cambridge, UK). The detailed description of the animal model can be found elsewhere [26]. Briefly, the P301S tau mutation - position counted in the longest human isoform, with 441 amino acids (aa) - was cloned into the cDNA of the shortest four-repeat tau isoform (383 aa, in comparison to the 441 aa isoform, this isoform lacks in exons 2 and 3). This construct was then cloned into a murine thy1.2 expression vector at the XhoI site. After removal of the vector sequences, transgenic animals were generated by pronuclear microinjection of F1 embryos of mixed C57BL/6J × CBA/ca mice. Founder animals, identified by PCR analysis were intercrossed with C57BL/6J mice to establish lines [26]. Homozygous $P301S^{+/+}$ and non-transgenic wild-type mice used for the study were kept in the same C57BL/6J background. All animals were 12 weeks of age at the beginning of the treatment period.

Preparation of the minipumps

Piericidin A (Figure 1; Santa Cruz Biotechnology, Inc., Santa Cruz, CA, USA), was diluted in equal volumes of dimethyl sulfoxide (DMSO, Sigma-Aldrich, St. Louis, MO, USA) and polyethylene glycol 400 (PEG). Osmotic minipumps (ALZET model 2ML4, DURECT Corporation, ALZET Osmotic Pumps, Cupertino, CA,

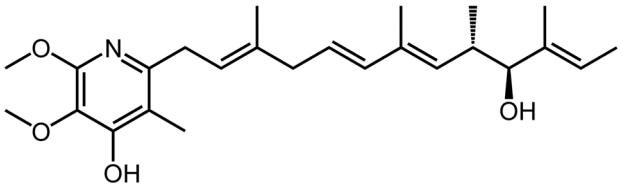

Figure 1. Chemical structure of piericidin A.

doi:10.1371/journal.pone.0113557.g001

USA) were either filled with solutions containing piericidin A or vehicle (50% DMSO and 50% PEG) and were incubated in sterile NaCl (0.9% wt/vol) for 4 h prior to implantation.

Surgery

The animal work was approved by the appropriate governmental authority (Regierungspräsidium Giessen, Germany), and conducted in accordance to the European Community Council Directive 86/609/EEC. For the experiments only male animals were used. In total, 19 transgenic animals ($P301S^{+/+}$) and 16 wild-type animals were operated. The average weight of the animals was 28 g. For the surgical procedure, the animals were anaesthetized by intraperitoneal (i.p.) injection of ketamine (10 mg/kg) and xylazine (20 mg/kg) diluted in saline. Then a small skin cut was made in the neck region of the animals and anatomical forceps were used to open a subcutaneous pocket in the back of the animals. Osmotic minipumps were placed in this skin pocket and the skin was sutured.

Infusion of piericidin A or vehicle

$P301S^{+/+}$ and non-transgenic wild-type mice were exposed to piericidin A or vehicle for 28 consecutive days via permanent subcutaneous infusion. The infusion rate of piericidin A was 0.014 mg/d (equivalent to a daily dose of 0.5 mg/kg) in a volume of 7 μL buffer per day, summing up to a total amount of 0.392 mg piericidin A per animal, infused over the whole experimental period of 28 days. Vehicle treated animals were infused with the same volume of buffer solution as vehicle. Of the 19 $P301S^{+/+}$ mice, 9 were exposed to piericidin A and 10 to the vehicle. Of the 16 wild-type animals, 9 were exposed to piericidin A and 7 to the vehicle. During the exposure period the animals were kept at a temperature of 21℃ at a humidity of 55% under a 12 h/12 h light/dark cycle with free access to food and water.

Tissue preparation

After the 28 days infusion period, the mice were deeply anaesthetized as described above and transcardially perfused with ice-cold 0.1 M phosphate buffered saline (PBS) for 2 minutes. Thereafter, the brains were quickly removed. The hemispheres were separated by a mid-sagittal cut. One hemisphere was post-fixed

in 4% (wt/vol) paraformaldehyde in 0.1 M PBS for 24 h, cryoprotected in 10% (wt/vol) sucrose in 0.1 M PBS for 48 h, frozen in isopentane at −30℃ for 2 min and stored at −80℃ for histological analysis. The other hemisphere was immediately dissected, frozen in −30℃ isopentane and stored at −80℃ for Western blotting.

Western blotting

Small pieces of frontal cortex where cut from the frozen brains and lysed using the T-PER protein extraction buffer (Thermo Scientific Pierce Protein Research Products, Rockford, IL, USA), supplemented with protease inhibitor (cOmplete Protease Inhibitor Cocktail, F. Hoffmann-La Roche Ltd., Basel, Switzerland) and phosphatase inhibitor (PhosSTOP Phosphatase Inhibitor Cocktail, F. Hoffmann-La Roche Ltd.), followed by centrifugation at 13,000 g for 15 min. Supernatants were loaded with Laemmli sample buffer (Bio-Rad, Laboratories, Hercules, CA, USA) to 12.5% SDS gels containing 10 μg protein per lane, separated by electrophoresis, and blotted to polyvinylidene difluoride membranes. These were blocked with 0.1 M tris buffered saline containing 0.1% (vol/vol) Tween (TBST, Sigma-Aldrich) and 5% (wt/vol) of skim milk powder (Sigma-Aldrich) for the HT7 blot or 10% (vol/vol) Roti-Block (Carl Roth, Karlsruhe, Germany) for the phospho tau blots for at least 1 h at room temperature and incubated overnight at 4℃ with TBST, 5% (vol/vol) bovine serum albumin (BSA, Cell Signaling Technology, Inc., MA, USA), and the following primary antibodies: tau monoclonal antibody clone HT7 (MN1000, Thermo Scientific Pierce Protein Research Products; 1:1000), AD2 anti-tau protein mouse monoclonal antibody against tau phosphorylated at serine 396 and serine 404 (mA #56484, Bio-Rad Laboratories, 1:2000), mouse monoclonal phospho-PHF-tau pThr231 antibody (AT180) against tau phosphorylated at threonine 231 (MN1040, Thermo Scientific, Rockford, IL, USA, 1:500), mouse monoclonal phospho-PHF-tau pSer202/Thr205 antibody (AT8) against tau phosphorylated at serine 202 and threonine 205 (MN1020, Thermo Scientific, 1:1000), anti-phospho-PHF tau pThr212/Ser214 antibody (AT100) against tau phosphorylated at threonine 212 and serine 214 (MN1060, Thermo Scientific, 1:1000). After three washes with TBST, the membranes were incubated for 2 h at room temperature with a horseradish peroxidase-conjugated secondary antibody (anti-mouse IgG, PI-2000, Vector Laboratories, Burlingame, CA, USA; 1:3000). Protein loading was controlled for by reprobing the membranes with a chicken anti-glyceraldehyde-3-phosphate dehydrogenase (GAPDH) antibody (AB2302; EMD Millipore, Billerica, MA, USA; 1:2000) and a horseradish peroxidase-conjugated secondary antibody (goat anti chicken IgY-HRP, sc-2428, Santa Cruz Biotechnology, Inc, 1:5000). For visualization, membranes were incubated with Pierce ECL Western blotting substrate (Thermo Scientific Pierce Protein Research Products). Signals were detected using the ChemiDoc-XRS system (Bio-Rad Laboratories). For quantification all Western blot results were normalized to GAPDH as control protein.

Immunohistochemistry

Brains were cut into 40 μm thick sections with a cryostat (Leica Biosystems, Wetzlar, Germany), collected in 10 regularly spaced series, and stored in 0.1 M phosphate buffer (PB) containing 0.01% (wt/vol) sodium azide at 4℃. Free floating sections were incubated subsequently for 15 min with 0.1% (vol/vol) H_2O_2 in 0.1 M PB to block endogenous peroxidase activity, for 1 h with 5% (vol/vol) normal donkey serum (NDS, Vector Laboratories) in 0.1 M PB and 0.2% Triton X-100 (Sigma-Aldrich) to inhibit non-specific binding sites, and for 24 h at 4℃ with the following primary antibodies: AD2 anti-tau protein mouse monoclonal antibody (mA #56484, Bio-Rad Laboratories, 1:1000), mouse monoclonal phospho-PHF-tau pThr231 antibody (AT180, MN1040, Thermo Scientific, 1:1000), mouse monoclonal phospho-PHF-tau pSer202/Thr205 antibody (AT8, MN1020, Thermo Scientific, 1:100), anti-phospho-PHF tau pThr212/Ser214 antibody (AT100, MN1060, Thermo Scientific, 1:100), anti-NeuN mouse monoclonal antibody, clone A60 (MAB377, EMD Millipore, 1:1000), anti-synaptophysin mouse monoclonal antibody, clone SY38 (MAB5258, EMD Millipore, 1:2000). All primary antibodies were diluted in 0.1 M PBS with 5% (vol/vol) NDS and 0.2% (vol/vol) Triton X-100. After incubation with the primary antibody the sections were rinsed three times with 0.1 M PB. Sections were then incubated for 2 h at room temperature with the appropriate biotinylated secondary antibody (anti-mouse IgG, Jackson ImmunoResearch, West Grove, PA, USA, 1:200) in 0.1 M PB with 5% NDS. The signal was amplified with the avidin–biotin method (VECTASTAIN Elite ABC Kit, Vector Laboratories, 1:200). Bound antibodies were visualized with 0.5 mg/mL of 3,3′-diaminobenzidine tetrachloride (DAB, Sigma-Aldrich). A positive signal was obtained by oxidation of the dye by adding 1% H_2O_2 (vol/vol) in water which led to a brownish color. After 2 min of incubation with H_2O_2 the sections were rinsed three times with PB 0.1 M. To exclude non-specific labeling, sections were incubated as described above with the respective primary antibody omitted.

Stereology

The cell numbers of phospho-tau (AD2, AT180, AT8, AT100) and NeuN-labeled neurons were estimated stereologically in the frontal cortex of one hemisphere by an observer blinded to the animals' identity, on regularly spaced (1/10) sections (average post-processing thickness 20 μm) under a 40× objective on an Olympus Microphot with the optical fractionator method, using the Stereo Investigator software (MicroBrightField, Inc., Williston, VT, USA). The frontal cortex was analyzed between 1.94 and 0.86 mm anterior and 0 to 2.0 mm lateral from the bregma. Coordinates were based on Paxinos and Franklin [27].

The criterion for counting a neuron was the presence of its nucleus either within the counting frame, or touching its right or top limit, but not touching its left or bottom limit. Total cell numbers were estimated by integration along the rostrocaudal extent of the structures. This sampling strategy gave a Schäfer coefficient of error ≤ 0.09.

Optical density measurement

To quantify synaptic density, the immunoreactivity for the synaptic vesicle protein synaptophysin was measured. Therefore images of the whole section were taken with an Olympus-E330 camera with a Componon-S 2.8/50 magnification lens, attached to a light table (Copylizer eVision exe.cutive, Kaiser Fototechnik, Buchen, Germany). Color images were then converted to monochrome images and inverted using ImageJ software (National Institute of Health, USA). The frontal cortex and corpus callosum region were delineated on three consecutive sections per animal and the average grey values were measured. Because of the lack of synapses in the corpus callosum, the value obtained in this region was considered as background and subtracted of the values obtained in the frontal cortex to correct for non-specific background staining.

Statistical analysis

Statistical analysis was done, using GraphPad Prism 6.0 (GraphPad Software, La Jolla, CA, USA). Results were expressed as mean $\pm$ SEM. The experimental groups were compared with a two-way analysis of variance (ANOVA) with the Fisher's LSD post-hoc test. A p-value <0.05 was assumed to be statistically significant.

Results

Low mortality due to experimental procedures

Altogether, 35 animals were used for this study. They were distributed in four groups: 10 P301S$^{+/+}$ mice with vehicle treatment, 9 P301S$^{+/+}$ mice with piericidin A treatment (0.5 mg/kg/d), 7 wild-type mice with vehicle treatment, and 9 wild-type mice with piericidin A treatment (0.5 mg/kg/d). All 35 animals survived anesthesia and the surgical procedure. In the group of wild-type mice treated with piericidin A, two died before the end of the 28 days infusion period and were excluded from further analysis. In the other three groups, all animals survived.

Piericidin A exposure led to reduced cortical synaptic density in P301S$^{+/+}$ mice, but not to cell death

To evaluate, whether piericidin A induced neurodegeneration, the total number of cells in the frontal cortex showing immunoreactivity against neuronal nuclei (NeuN) was counted stereologically. Since the reduction of synaptic density is considered to be an early sign of neurodegeneration [28], we also quantified the synaptic density in the frontal cortex by optical density measurement of immunoreactivity against the synaptic marker synaptophysin.

After 28 days of treatment with piericidin A or vehicle, we did not observe any significant difference in the NeuN counts in the frontal cortex between the four groups (Figure 2 A). In wild-type mice there was also no significant difference in

the synaptic density between vehicle treated (100 ± 7.8%) and piericidin A treated mice (91.9 ± 2.7%, Figure 2 B, empty bars). However, the synaptophysin immunoreactivity, likely to reflect synaptic density, was significantly reduced in piericidin A treated P301S$^{+/+}$ mice (83.7 ± 2.5% of vehicle treated non-transgenic mice) compared to vehicle treated P301S$^{+/+}$ mice (104.5 ± 6.8%, p=0.008, Figure 2 B).

Piericidin A exposure increased cortical tau-pathology in P301S$^{+/+}$ mice, but not in wild-type mice

To measure tau-pathology in the frontal cortex, brain sections were stained immunohistochemically with four different antibodies against tau, phosphorylated at different sites (AD2: pSer396/Ser404, AT8: pSer202/Thr205, AT180: pThr231, AT100: pThr212/Ser214). Immunoreactive cells were counted stereologically. After 28 days, vehicle treated wild-type mice showed only very little immunoreactivity against AD2, AT8, and AT180 and no immunoreactivity against AT100. Interestingly, treatment with piericidin A did not lead to a significant increase in the number of cells immunoreactive for AD2, AT8 or AT180 in wild-type animals (Figure 3 A, B, C, images on the left sides in the upper panels and white bars in the lower panels). In contrast, vehicle treated P301S$^{+/+}$ mice already showed a considerably large number of cells with AD2, AT8 and AT180 immunoreactivity. (Figure 3 A, B, C, images on the right sides in the upper panels and black bars in the lower panels) However, in vehicle treated P301S$^{+/+}$ mice, no AT100 immunoreactivity was detected (Figure 3 D). Treatment of P301S$^{+/+}$ mice with piericidin A further increased the number of cells immunoreactive for AD2 (12,300 ± 969 vs. 7,986 ± 720, p=0.0003) and AT180 (14,607 ± 692 vs. 9,207 ± 718, p<0.0001) compared to P301S$^{+/+}$ mice treated with vehicle. (Figure 3 A, C, images on the right sides in the upper panels and black bars in the lower panels). With AT8 immunoreactivity, there was the same tendency, but the differences were not significant (p=0.18, Figure 3 C, images on the right side in the upper panel and filled columns in the lower panel). Notably, piericidin A treated P301S$^{+/+}$ mice showed a considerable number of AT100^{+} neurons (770 ± 226), while vehicle treated P301S$^{+/+}$ mice showed no AT100 immunoreactivity (p<0.01, Figure 3 D).

Piericidin A exposure increased cortical levels of human tau in P301S$^{+/+}$ mice

To investigate whether treatment of P301S$^{+/+}$ mice with piericidin A over a period of 28 days also led to increased levels of transgenic tau, we conducted Western blots analysis using an antibody specific for human tau (HT7). Therefore, we took tissue samples from eight animals of each group. We observed a 2.1 ± 0.5-fold increase of human tau levels in P301S$^{+/+}$ mice exposed to piericidin A compared to vehicle treated P301S$^{+/+}$ mice (p=0.01, Figure 4A).

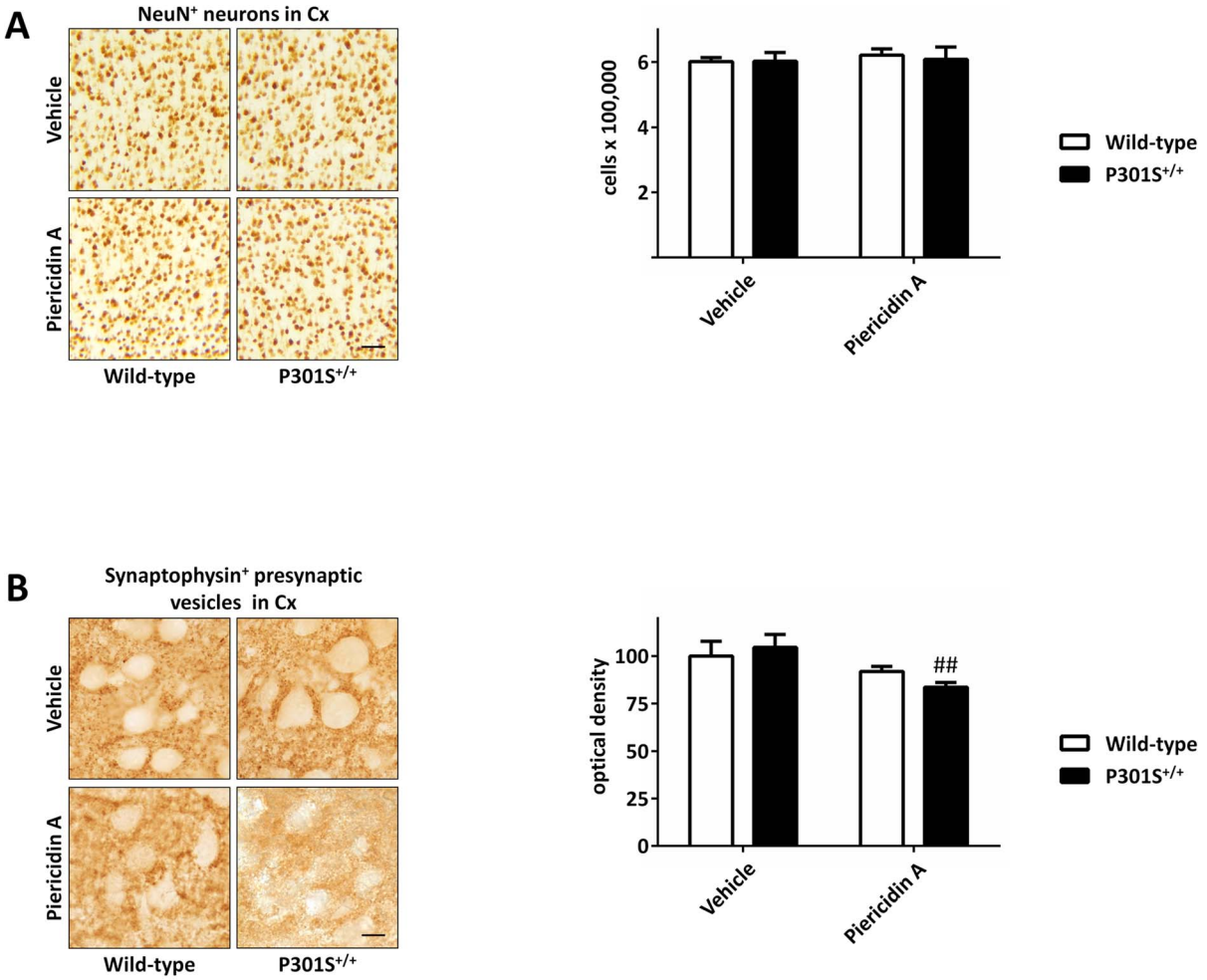

Figure 2. Effects of piericidin A treatment on neuronal cell count and synaptic density. A: Neuronal nuclei (NeuN)-stained sections of the frontal cortex (Cx) of wild-type and P301S$^{+/+}$ mice treated with vehicle or piericidin A (left panel). Quantification of NeuN immunoreactive cells in the cortex showed no difference in the four animal groups (right panel). Scale bar 50 μm. B: Sections of the frontal cortex stained with an antibody against synaptophysin as marker for the synaptic density (left panel). The immunoreactivity quantified by optical density measurement was significantly reduced in piericidin A treated P301S$^{+/+}$ mice compared to vehicle treated P301S$^{+/+}$ (right panel). Scale bar: 10 μm. ## $p < 0.01$, piericidin A treatment vs vehicle treatment at the same genotype. Two-way ANOVA with Fisher LSD post-hoc test.

doi:10.1371/journal.pone.0113557.g002

Piericidin A exposure led to increased cortical levels of pathologically phosphorylated tau in P301S$^{+/+}$ mice

Wild-type animals did not show immunoreactivity for phosphorylated tau with any of the four tested phospho-tau antibodies in Western blot analysis (AD2, AT180, AT8, AT100), regardless of treatment with piericidin A or vehicle (Figure 4 A–E). In vehicle and piericidin treated P301S$^{+/+}$ mice, AD2 and AT180 antibodies labeled a band of phopsphorylated tau at approximately 62 kDa (Figure 4 B and C). When staining with AD2, this band did not show significant alterations in intensity upon piericidin A treatment. With AT180, a decrease in intensity of this band was observed in piericidin A treated P301S$^{+/+}$ mice compared to vehicle treated P301S$^{+/+}$ mice (Figure 4 C). However, with AT180 we

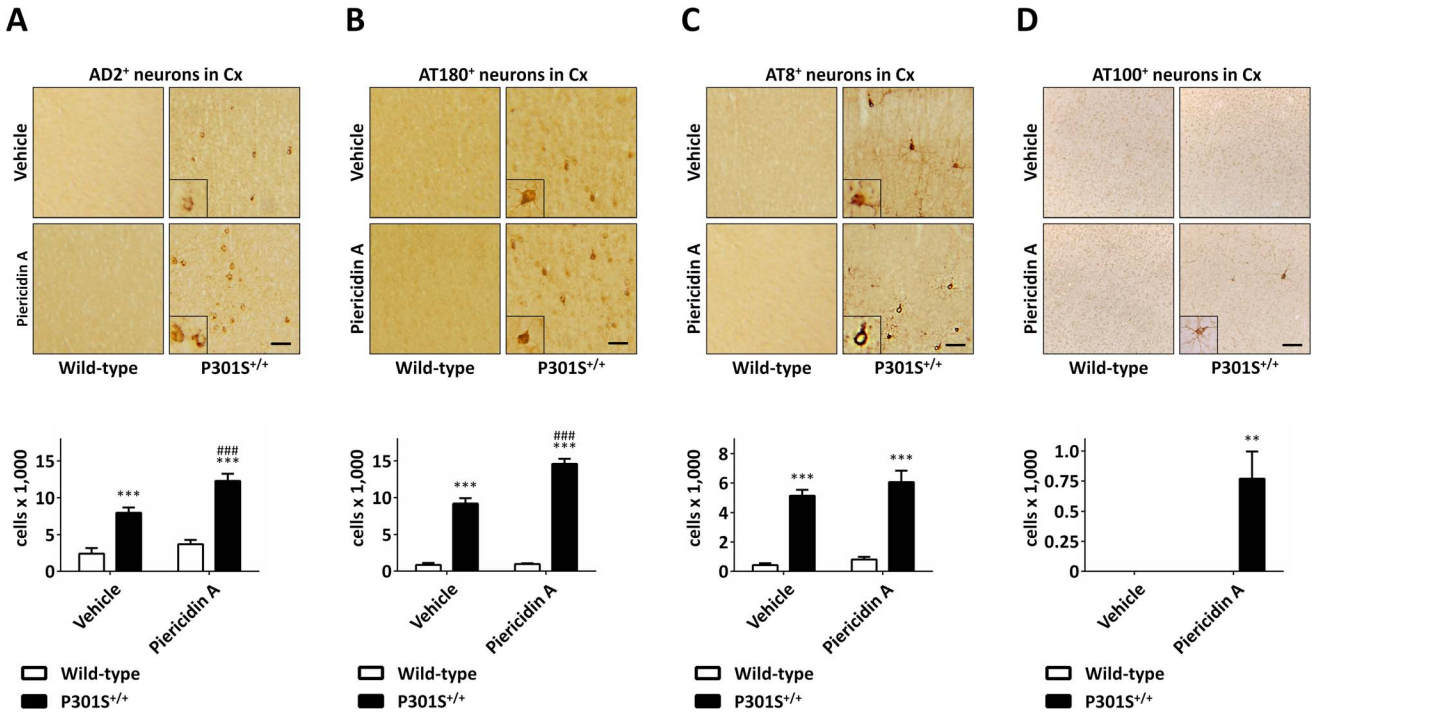

Figure 3. Histological sections showing the effect of piericidin A treatment on tau pathology. Frontal cortex (Cx) of wild-type and P301S$^{+/+}$ mice treated with vehicle or piericidin A. Sections were stained separately with the antibodies AD2 (A), AT 180 (B), AT8 (C), and AT100 (D). The inserts are 2.5-times magnified compared to the overview images. P301S$^{+/+}$ mice had significant higher numbers of phospho-tau positive cells in the frontal cortex compared to wild-type animals with the same treatment (lower panels, filled bars). Treatment with piericidin A further increased the number of AD2 immunoreactive cells (A, lower panel) and AT180 immunoreactive cells (B, lower panel). With AT8 immunoreactivity there was the same tendency, however, the difference was not significant (C, lower panel). With the AT100 antibody we only observed immunoreactive cells in piericidin A treated P301S$^{+/+}$ mice (D). Scale bars: 20 μm. * $p<0.05$, ** $p<0.01$, *** $p<0.001$, P301S$^{+/+}$ vs. wild-type at the same treatment. # $p<0.05$, ## $p<0.01$, ### $p<0.001$, piericidin A treatment vs. vehicle treatment at the same genotype. Two-way ANOVA with Fisher LSD post-hoc test.

doi:10.1371/journal.pone.0113557.g003

observed a second, higher molecular phospho-tau band at approximately 68 kDa, which was only detected in the piericidin A treated P301S$^{+/+}$ mice (Figure 4 C). The total level of AT180-reactive phospho-tau did not show a significant increase after treatment with piericidin A. Interestingly, AT8 and AT100 antibodies only detected this higher molecular weight band at 68 kDa. AT8 labeling revealed this band exclusively in the piericidin A treated P301S$^{+/+}$ mice (Figure 4 D). AT100 labeling revealed the 68 kDa band in both, piericidin A and vehicle treated P301S$^{+/+}$ mice, but its intensity was significantly increased upon piericidin A treatment (Figure 4E).

To investigate whether increased tau levels per se were responsible for the increased levels of phosphorylated tau, we measured the ratio of phosphorylated tau to total human tau. There was no significant difference in the AD2/HT7 ratio between P301S$^{+/+}$ mice treated with piericidin A or vehicle. There was 11.6 ± 4.3 fold increase ($p=0.04$) of AT180/HT7 in piericidin A treated P301S$^{+/+}$ mice compared to vehicle treated P301S$^{+/+}$ mice, when quantifying the 68 kDa phospho-tau bands. AT8/HT7 was also significantly increased by 4.2 ± 1.1 ($p=0.008$) and AT100/HT7 was increased by 10.1 ± 5.3 ($p=0.12$), ranging from

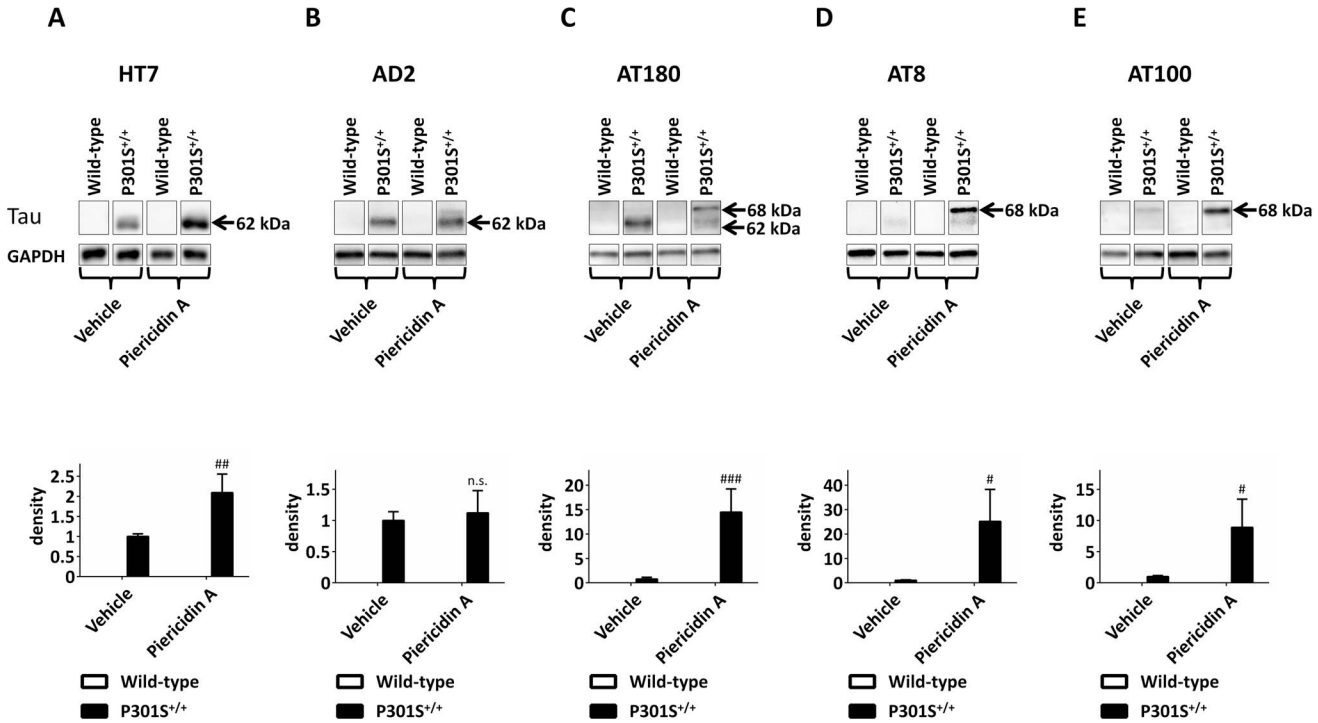

Figure 4. Western blots showing the effect of piericidin A treatment on total tau and phospho-tau levels. Upper panels: Western blots of wild-type and P301S$^{+/+}$ mice, exposed to Piericidin A or vehicle over a period of 28 days, stained with an antibody specific for human tau (HT7, A), an antibody against pSer396/Ser404 (AD2) phosphorylated tau (B), an antibody against pSer202/Thr205 (AT8) phosphorylated tau, an antibody against pThr231 (AT180) phosphorylated tau (C), and an antibody against pThr212/Ser214 (AT100) phosphorylated tau (E). Below the tau Western blots the glyceraldehyde 3-phosphate dehydrogenase (GAPDH) loading control is shown. Lower panels: Quantification of the Western blots after normalization to loading control (GAPDH). In the HT7 and AD2 Western blots, the whole visible band was quantified, whereas in AT180, AT8 and AT100 the 68 kDa band was quantified. # $p<0.05$, ## $p<0.01$, ### $p<0.001$, n.s. not significant, piericidin A treatment vs. vehicle treatment at the same genotype. Two-way ANOVA with Fisher LSD post-hoc test.

doi:10.1371/journal.pone.0113557.g004

1.2-fold to 23.6-fold in piericidin A treated P301S$^{+/+}$ mice, compared to vehicle treated P301S$^{+/+}$ mice. Most likely due to this high range, the increase of AT100/HT7 did not reach significance, even though it was seen in all P301S$^{+/+}$ mice upon piericidin A treatment. Altogether, these data suggest, that the observed increase of the levels of pathologically phosphorylated tau at the AT180, AT8, and AT100 epitopes in P301S$^{+/+}$ mice treated with piericidin A compared to vehicle treated P301S$^{+/+}$ mice was an effect independent of a mere increase of total human tau.

Discussion

The aim of the present study was to investigate, if a synergistic interaction between a genetic predisposition and the exposure to an environmental factor may be relevant for the etiology of neurodegenerative tauopathies.

Therefore, we treated P301S tau transgenic mice and wild-type mice with piericidin A, an inhibitor of the mitochondrial complex I of microbial origin or vehicle, respectively, via subcutaneous pump infusion for a period of 28 days.

Whereas we did not observe any neuronal cell loss, piericidin A led to a reduced immunoreactivity for synaptophysin and aggravated tau pathology in $P301S^{+/+}$ mice, but not in wild-type mice.

Because the $P301S^{+/+}$ mice develop typical histopathological features of tauopathies, which can also be found in post mortem tissue from patients [26], they are very suitable to study different aspects of the etiology and pathophysiology of neurodegenerative tauopathies.

Piericidin A, a very lipophilic inhibitor of mitochondrial complex I, was used, because the bacteria *(streptomyces spp.)* which synthesize piericidins, are living ubiquitously in normal soils, forest soils, or compost all over the world [25]. Therefore a contamination of fruits and vegetables with metabolic products of *streptomyces spp.* or the syntheses of these toxins within the human body appear to be possible ways of chronic exposure to bacterial toxins like piericidin A. Moreover, reports of *streptomyces spp.* causing diseases in patients show that a contamination of the human body with these bacteria is possible [29, 30].

In the present study, we did not observe cortical cell loss after a 28 days treatment period in the four animal groups. Since there were no data available about the bioavailability or efficacy of piericidin A *in vivo*, we chose the treatment doses on the basis of previous studies with lipophilic complex I inhibitors [19, 31, 22].

In two previous *in vivo* studies neurodegeneration was observed in rats after exposure to rotenone [31] or annonacin [19]. In the latter study annonacin was administered at doses of 3.8 mg/kg bodyweight or 7.6 mg/kg bodyweight of annonacine per day for a period of 28 days [19]. In a cell free assay, the potency of piericidin A to inhibit mitochondrial complex I was ~2 fold smaller than the one of annonacin. In cultured neurons, the potency of piericidin A to induce the redistribution of phosphorylated tau from the dendrites into the cell soma and to induce cell death of piericidin A was ~30-fold higher than that of annonacin [22]. In consideration of these data, a dose of 0.5 mg/kg body weight of piericidin A, which is ~15-fold smaller than 7.6 mg/kg dose of annonacin, seemed to be an appropriate dose to investigate effects of piericidin A *in vivo*. Possible reasons, why we did not observe cell loss, could be the different mode of application (subcutaneously, not intravenously) as well as the different species (mice, not rats), used here in comparison to the previous rotenone and annonacin work. This subcutaneous way of application was chosen, because it appeared to be more physiological than an intravenous application. A further reason, why we did not observe cell loss, might be the relatively young age of the mice at the beginning of the treatment period. Allen et al. observed spinal cord neurodegeneration and a severe clinical phenotype with paraparesis and general weakness in these mice at an age of 6 months [26]. In the present study, we treated mice with an age of 12 weeks at the beginning of the treatment period. This age was chosen, because we wanted to observe effects that precede severe neurodegeneration. It is likely that young mice have more efficient compensatory mechanisms than old mice to prevent neurons from dying. Accordingly, in patients carrying a P301S mutation there was also no cell loss observed in early stages of the disease [32].

Even though there was no cell loss in the four animal groups, we observed a significant reduction of synaptophysin immunoreactivity in P301S$^{+/+}$ mice that were treated with piericidin A. Because the immunoreactivity for this synaptic marker presumably reflects synaptic density, our observation corresponds to a reduction of synaptic density in P301S$^{+/+}$ mice with piericidin A treatment. This can be considered as an early sign of neurodegeneration and was also observed by others in a different P301S tau transgenic mouse line [33] as well as in patients [34], where it is considered to contribute to cognitive impairment [35]. Neither the toxin alone nor the transgene alone had a significant influence on the cortical synaptic density. The fact, that piericidin A led to a reduced synaptic density only in P301S$^{+/+}$ mice, suggests that there was a synergistic effect between the exposure to the toxin and the genotype of the mice.

As expected, we observed tau pathology in P301S$^{+/+}$ mice. Both groups of tau transgenic animals, vehicle or piericidin A treated, showed a significant number of neurons with immunoreactivity for phosphorylated tau. Piericidin A treatment however, led to a marked increase in the number of phospho-tau positive neurons in P301S$^{+/+}$ mice. Moreover, we only observed AT100^{+} neurons in piericidin A treated P301S$^{+/+}$ mice, but not in vehicle treated P301S$^{+/+}$ mice. In wild-type mice, on the other hand, neither the group of vehicle treated nor the group of piericidin A treated animals showed substantial signs of tau pathology. A similar observation was made in a recently published study, where mice, expressing human tau with the R406W mutation, which also belongs to the FTDP-17 mutations [36], were treated with annonacin subcutaneously for three days. There was also an increase in tau pathology only in the transgenic mice, while no tau pathology was observed in wild-type mice [37]. These observations further emphasize that there is a synergistic effect between the genotype and the exposure to an environmental toxin.

In accordance with the data from annonacin [37], piericidin A led to an increase in the levels of human tau in P301S$^{+/+}$ mice, as confirmed by Western blot analysis in the present study. Moreover, piericidin A treatment led to increased levels of pathologically phosphorylated tau in P301S$^{+/+}$ mice as shown by the formation of a higher molecular weight phospho-tau band at 68 kDa, which was either completely absent (AT8, AT180), or present only to a much lower extent (AT100) in the vehicle treated P301S$^{+/+}$ mice. This shift to higher molecular weight phospho-tau bands was previously described and associated with pathological tau phosphorylation [38]. Moreover, a recent work showed, that bands with a lower molecular weight can appear as unspecific bands with some commercially available tau antibodies [39]. Thus, the higher molecular band we observed in piericidin A treated P301S$^{+/+}$ mice might be the true correlate for pathologically phosphorylated tau, while the lower bands seen in AD2 and AT180 appearing at 62 kDa, might be non-specific.

The fact, that we observed a reduced synaptic density with piericidin A treatment in P301S$^{+/+}$ mice as well as an increase in tau pathology after subcutaneous administration shows, that the compound was able to pass multiple biological membranes and penetrated to the brain of the mice. Likewise, it should

be possible that piericidin A enters the brain after oral ingestion of contaminated food products. Admittedly, it is yet unknown, in what scale, fruits or vegetables are contaminated with bacterial toxins like piericidin A or the synthesizing bacteria themselves. However, because of the ubiquitary presence of these bacteria and the possibility that these very lipophilic toxins could accumulate in the brain over years, it seems worthwhile to further investigate, if the bacteria of their metabolites could be found in samples from patients suffering from a neurodegenerative tauopathy. This would provide further insight in the etiopathology of these diseases.

In summary, we showed for the first time, that piericidin A, a metabolic product of ubiquitously abundant bacteria, led to a loss of synaptophysin immunoreactivity and aggravation of tau pathology of P301S tau transgenic mice. We could show, that there was a synergistic interaction between the toxin and the genotype. Our results therefore provide further evidence that environmental toxins like piericidin A, rotenone or annonacin could be important factors in the etiology of tauopathies. This might be particularly the case in individuals at risk, having a specific genetic predisposition. Hence, avoiding the exposure to certain environmental toxins could be a way to prevent the development of neurodegenerative tauopathies or to slow the progress of these diseases.

Author Contributions

Conceived and designed the experiments: MH RD ADA GR HX TWR MS TC ESY SAGEH WHO GUH. Performed the experiments: MH RD ADA GR TC. Analyzed the data: MH RD ADA TC GUH. Contributed reagents/materials/analysis tools: MG. Wrote the paper: MH RD ADA GR HX TWR MS TC ESY SAGEH MG WHO GUH.

References

1. **Goedert M, Spillantini MG, Jakes R, Rutherford D, Crowther RA** (1989) Multiple isoforms of human microtubule-associated protein tau: sequences and localization in neurofibrillary tangles of Alzheimer's disease. Neuron 3 (4): 519–526.
2. **Andreadis A, Brown WM, Kosik KS** (1992) Structure and novel exons of the human tau gene. Biochemistry 31 (43): 10626–10633.
3. **Buée L, Bussière T, Buée-Scherrer V, Delacourte A, Hof PR** (2000) Tau protein isoforms, phosphorylation and role in neurodegenerative disorders. Brain Res. Rev. 33 (1): 95–130.
4. **Spillantini MG, Goedert M** (2013) Tau pathology and neurodegeneration. Lancet Neurol 12 (6): 609–622.
5. **Neve RL, Harris P, Kosik KS, Kurnit DM, Donlon TA** (1986) Identification of cDNA clones for the human microtubule-associated protein tau and chromosomal localization of the genes for tau and microtubule-associated protein 2. Brain Res. 387 (3): 271–280.
6. **Weingarten MD, Lockwood AH, Hwo SY, Kirschner MW** (1975) A protein factor essential for microtubule assembly. Proc. Natl. Acad. Sci. U.S.A. 72 (5): 1858–1862.
7. **Hernández F, Avila J** (2007) Tauopathies. Cell. Mol. Life Sci. 64 (17): 2219–2233.
8. **Goedert M, Spillantini MG** (2011) Pathogenesis of the tauopathies. J. Mol. Neurosci. 45 (3): 425–431.

9. **Mandelkow EM, Mandelkow E** (2012) Biochemistry and cell biology of tau protein in neurofibrillary degeneration. Cold Spring Harb Perspect Med 2 (7): a006247.

10. **Bugiani O, Murrell JR, Giaccone G, Hasegawa M, Ghigo G, et al.** (1999) Frontotemporal dementia and corticobasal degeneration in a family with a P301S mutation in tau. J. Neuropathol. Exp. Neurol. 58 (6): 667–677.

11. **Sperfeld AD, Collatz MB, Baier H, Palmbach M, Storch A, et al.** (1999) FTDP-17: an early-onset phenotype with parkinsonism and epileptic seizures caused by a novel mutation. Ann. Neurol. 46 (5): 708–715.

12. **Baba Y, Baker MC, Le Ber I, Brice A, Maeck L, et al.** (2007) Clinical and genetic features of families with frontotemporal dementia and parkinsonism linked to chromosome 17 with a P301S tau mutation. J Neural Transm 114 (7): 947–950.

13. **Caparros-Lefebvre D, Elbaz A** (1999) Possible relation of atypical parkinsonism in the French West Indies with consumption of tropical plants: a case-control study. Caribbean Parkinsonism Study Group. Lancet 354 (9175): 281–286.

14. **Caparros-Lefebvre D, Lees AJ** (2005) Atypical unclassifiable parkinsonism on Guadeloupe: an environmental toxic hypothesis. Mov. Disord. 20 Suppl 12: S114–8.

15. **Lannuzel A, Höglinger GU, Verhaeghe S, Gire L, Belson S, et al.** (2007) Atypical parkinsonism in Guadeloupe: a common risk factor for two closely related phenotypes. Brain 130 (Pt 3): 816–827.

16. **Cavé A, Figadère B, Laurens A, Cortes D** (1997) Acetogenins from Annonaceae. Fortschr Chem Org Naturst 70: 81–288.

17. **Zafra-Polo MC, González MC, Estornell E, Sahpaz S, Cortes D** (1996) Acetogenins from Annonaceae, inhibitors of mitochondrial complex I. Phytochemistry 42 (2): 253–271.

18. **Champy P, Melot A, Guérineau Eng V, Gleye C, Fall D, et al.** (2005) Quantification of acetogenins in Annona muricata linked to atypical parkinsonism in guadeloupe. Mov. Disord. 20 (12): 1629–1633.

19. **Champy P, Höglinger GU, Féger J, Gleye C, Hocquemiller R, et al.** (2004) Annonacin, a lipophilic inhibitor of mitochondrial complex I, induces nigral and striatal neurodegeneration in rats: possible relevance for atypical parkinsonism in Guadeloupe. J. Neurochem. 88 (1): 63–69.

20. **Escobar-Khondiker M, Höllerhage M, Muriel M, Champy P, Bach A, et al.** (2007) Annonacin, a natural mitochondrial complex I inhibitor, causes tau pathology in cultured neurons. J. Neurosci. 27 (29): 7827–7837.

21. **Höglinger GU, Melhem NM, Dickson DW, Sleiman, Patrick MA, Wang L, et al.** (2011) Identification of common variants influencing risk of the tauopathy progressive supranuclear palsy. Nat. Genet. 43 (7): 699–705.

22. **Höllerhage M, Matusch A, Champy P, Lombès A, Ruberg M, et al.** (2009) Natural lipophilic inhibitors of mitochondrial complex I are candidate toxins for sporadic neurodegenerative tau pathologies. Exp. Neurol. 220 (1): 133–142.

23. **Jeng M, Hall C, Crane FL, Takahashi N, Tamura S, et al.** (1968) Inhibition of mitochondrial electron transport by piericidin A and related compounds. Biochemistry 7 (4): 1311–1322.

24. **Takahashi N, Suzuki A, Tamura S** (1965) Structure of Piericidin A. J. Am. Chem. Soc. 87: 2066–2068.

25. **Chater KF, Chandra G** (2006) The evolution of development in Streptomyces analysed by genome comparisons. FEMS Microbiol. Rev. 30 (5): 651–672.

26. **Allen B, Ingram E, Takao M, Smith MJ, Jakes R, et al.** (2002) Abundant tau filaments and nonapoptotic neurodegeneration in transgenic mice expressing human P301S tau protein. J. Neurosci. 22 (21): 9340–9351.

27. **Paxinos G, Franklin KB** (2004) The Mouse Brain in Stereotaxic Coordinates. San Diego, CA: Elsevier.

28. **Mandelkow EM, Stamer K, Vogel R, Thies E, Mandelkow E** (2003) Clogging of axons by tau, inhibition of axonal traffic and starvation of synapses. Neurobiol. Aging 24 (8): 1079–1085.

29. **Dunne EF, Burman WJ, Wilson ML** (1998) Streptomyces pneumonia in a patient with human immunodeficiency virus infection: case report and review of the literature on invasive streptomyces infections. Clin. Infect. Dis. 27 (1): 93–96.

30. **Kofteridis DP, Maraki S, Scoulica E, Tsioutis C, Maltezakis G, et al.** (2007) Streptomyces pneumonia in an immunocompetent patient: a case report and literature review. Diagn. Microbiol. Infect. Dis. 59 (4): 459–462.

31. **Höglinger GU, Lannuzel A, Khondiker ME, Michel PP, Duyckaerts C, et al.** (2005) The mitochondrial complex I inhibitor rotenone triggers a cerebral tauopathy. J. Neurochem. 95 (4): 930–939.

32. **Lossos A, Reches A, Gal A, Newman JP, Soffer D, et al.** (2003) Frontotemporal dementia and parkinsonism with the P301S tau gene mutation in a Jewish family. J. Neurol. 250 (6): 733–740.

33. **Yoshiyama Y, Higuchi M, Zhang B, Huang S, Iwata N, et al.** (2007) Synapse loss and microglial activation precede tangles in a P301S tauopathy mouse model. Neuron 53 (3): 337–351.

34. **Bigio EH, Vono MB, Satumtira S, Adamson J, Sontag E, et al.** (2001) Cortical synapse loss in progressive supranuclear palsy. J. Neuropathol. Exp. Neurol. 60 (5): 403–410.

35. **Bigio EH, Brown DF, White CL** (1999) Progressive supranuclear palsy with dementia: cortical pathology. J. Neuropathol. Exp. Neurol. 58 (4): 359–364.

36. **Ostojic J, Elfgren C, Passant U, Nilsson K, Gustafson L, et al.** (2004) The tau R406W mutation causes progressive presenile dementia with bitemporal atrophy. Dement Geriatr Cogn Disord 17 (4): 298–301.

37. **Yamada ES, Respondek G, Müssner S, Andrade A de, Höllerhage M, et al.** (2014) Annonacin, a natural lipophilic mitochondrial complex I inhibitor, increases phosphorylation of tau in the brain of FTDP-17 transgenic mice. Exp. Neurol. 253: 113–125.

38. **Han D, Qureshi HY, Lu Y, Paudel HK** (2009) Familial FTDP-17 missense mutations inhibit microtubule assembly-promoting activity of tau by increasing phosphorylation at Ser202 in vitro. J. Biol. Chem. 284 (20): 13422–13433.

39. **Petry FR, Pelletier J, Bretteville A, Morin F, Calon F, et al.** (2014) Specificity of anti-tau antibodies when analyzing mice models of Alzheimer's disease: problems and solutions. PLoS ONE 9 (5): e94251.